Fabrication of 3D printed Gelatin-Hyaluronic Acid hydrogels based on enzyme-mediated tyramine conjugates and other derivatives

Miranda Morata Martínez

BSc (Hons) Biomedical Engineering

Submitted in fullfilment of the requirements for the Degree of Master in Research

Supervisors: Manuel Salmerón-Sánchez, Gloria Gallego Ferrer

Centro de Biomateriales e Ingeniería Tisular
Universidad Politécnica de Valencia

ciber-bbn
Centro Investigación Biomédica en Red
Bioingeniería, Biomateriales y Nanomedicina

School of Science and Engineering

College of Engineering

University of Glasgow

March 2021

Table of contents

List of figures

List of tables

Acknowledgements

I would first like to thank my supervisor Dr. Manuel Salmerón-Sánchez and my co-supervisor Dra. Gloria Gallego Ferrer, both very involved in all this process, for letting me work in this wonderful field, and for their immense support. I´m grateful for having such two excellent examples of effort and endeavour.

I also wanted to thank the people in the CBIT and CeMi teams for their support during this project, from whom I can only say it is been a pleasure to meet you, in good times and in bad. Álvaro, Mark, Alex, Oana, Matt, Vini, Mariana, ..., Thank you a lot.

Thanks to my family, the biological and the chosen one, and my friends, to the ones I made on the way and the ones who waited, for their constant mocking about never coming back from Scotland, you were almost right.

To Gary and Rachel, for opening their door and making me feel at home for the last 2 years we have spent living together. Needless to say, they are already part of my family as well.

To the IT services and administrators of the University of Glasgow, for their appreciated and constant feedback and who helped me with all my enquiries and problems on the way.

To Scotland, my lovely home for a short time, but which I will always keep deep in my heart and all that it represents.

And of course to Carlos, who always encouraged me to go on no matter what, even when that meant waiting for me to come home for a wee longer.

Author´s declaration

The material protocols presented in Section 3, which included the hydrogel synthesis, their formation and the quantification of their degree of substitution (3.1 – 3.5), were previously developed, studied and published by the Center of Biomaterials and Tisular Engineering (CBIT) of the Polytechnical University of Valencia (UPV) of Spain, with the collaboration of the Center for the Cellular Microenvironment (CeMi) of the University of Glasgow. Both of my supervisors, Gloria Gallego Ferrer (CBIT) and Manuel Salmerón-Sánchez (CeMi) were directy involved in this research.

Publications

Poveda-Reyes, S., Moulisova, V., Sanmartín-Masiá, E., Quintanilla-Sierra, L., Salmerón-Sánchez, M., & Ferrer, G. G. (2016). Gelatin-Hyaluronic Acid Hydrogels with Tuned Stiffness to Counterbalance Cellular Forces and Promote Cell Differentiation. *Macromolecular Bioscience, 16(9), 1311–1324*

Sanmartín-Masiá, E., Poveda-Reyes, S., & Gallego Ferrer, G. (2017). Extracellular matrix–inspired gelatin/hyaluronic acid injectable hydrogels. *International Journal of Polymeric Materials and Polymeric Biomaterials, 66(6), 280–288.*

Moulisová, V., Poveda-Reyes, S., Sanmartín-Masiá, E., Quintanilla-Sierra, L., Salmerón-Sánchez, M., & Gallego Ferrer, G. (2017). Hybrid Protein–Glycosaminoglycan Hydrogels Promote Chondrogenic Stem Cell Differentiation. *ACS Omega, 2(11), 7609–7620.*

Master thesis

Sanmartín Masiá, EDR. (2016). *Síntesis y caracterización de hidrogeles injectables inspirados en la matriz extracelular para la regeneración de tejidos blandos.*

Šandrk, N. (2016). *Preparation of bioactive composite material for bone tissue repair*.

I declare that this thesis is an original report of my research, has been written by me and has not been submitted for any previous degree. The experimental work is almost entirely mine; the collaborative contributions have been indicated clearly and acknowledged. Due references have been provided on all supporting literature and resources.

List of abbreviations

% w/v……..…Weight volume percentage
µL…….……Microlitre
µm……..……Micrometre
µM……..…...Micromolar
3D……...Three-dimensional
AM……...…Additive manufacturing or Acetoxymethyl
BB…….…..Blocking buffer
CAD……Computer-aided design
cc……..cubic centilitre
CF-KRB……... Calcium Free Krebs Ringer Buffer
COOH……. Carboxylic acid or group
DAPI……... 4 ',6-diamidino-2-fenilindol
DBB……...Droplet-based brioprinting
DMEM……...Dulbecco's Modified Eagle Medium
DOD……..Drop on demand
DPBS……Dulbecco's phosphate buffered saline
ECM…….Extracellular matrix
EDC……... .N-(3-Dimethylaminopropyl)-N'-ethylcarbodiimide hydrochloride
EDTA……Ethylenediaminetetraacetic acid
EthD-1……Ethidium homodimer-1
FBS……Fetal bovine serum
FDM…… Fused deposition modelling
G……Gauge
g……..Gram or gravity
GAG……... Glycosaminoglycans
Gel……Gelatin
GM…….Growth medium
HA …….Hyaluronic acid
HEPES……4-(2-hydroxyethyl)piperazine-1-ethane-sulfonic acid
H_L……...Lift nozzle
HMW-HA……..High molecular weight hyaluronic acid
H_n, L_n……Needle length

HRP…… Peroxidase from horseradish Type VI

H_S……Safe position

ITS-X…….. Insulin-Transferring-Selenium-X

kPa……...Kilopascal

kV……Kilovolt

LMW-HA……...Low molecular weight hyaluronic acid

M…… Molar

MES…… .2-(N-Morpholino)ethanesulfonic acid

mg…….Milligram

mL……..Millilitre

mM……..Millimolar

mPa…….Millipascal

ms……..Millisecond

MWCO…….Molecular weight cut-off

N…….Newton

NHS……...N-Hydroxysuccinimide

nm……..Nanometre

P/S…….. Penicillin/Streptomycin

Pa……Pascal

PBS…….Phosphate buffered saline

PCL…….. Polycaprolactone

PEA……Poly ethyl acrylate

PEG……. Polyethylene glycol

PGA……. Polyglycolic acid

PLLA……... Poly(L-lactide)

RGD…… Arginine-glycine-aspartic acid

rpm……..Revolutions per minute

s……Second

Sd…….Standoff distance

Tyr…… Tyramine hydrochloride

WB……..Washing Buffer

Abstract

Extracellular matrices (ECMs) in soft tissues are highly hydrated structures mainly composed of glycoproteins (such as collagen or fibronectin) and glycosaminoglycans (such as hyaluronic acid (HA) or keratan sulfate), each one with a tissue-specific composition (1). Many of these tissues are unable to regenerate themselves or can only repair minor injuries, as is the case of skin (2), heart (3) and cartilage (4).

Hydrogels are hydrophilic polymeric networks with high water retention capability which have been frequently proposed as potential candidates for soft tissues regeneration due to their tunable physical, chemical and biological properties, biocompatibility and their ability to mimic the native ECMs (5-7). Besides, they promote phenotype maintenance and induce re-differentiation of different cells such as cardiomyocytes (8), chondrocytes (9) and hepatoblast (10).

Most hydrogels need to be chemically cross-linked to not dissolve at body temperature. Conventional cross-linking methods involving chemical reactions are generally cytotoxic. Solvents, initiators or unreacted substances are left behind, often resulting in inflammation and cell death (11-13). In order to prevent any harmful effect on cells, they must be therefore pre-formed under safe lab conditions, thoroughly washed and sterilised before implantation.

Cross-linking reactions mediated by enzymes (14-16), also known as enzyme-mediated or enzyme-catalysed cross-linking, have been proposed relatively recently as a less problematic alternative for hydrogel scaffolding. In these systems, aqueous hydrogel precursor solutions are mixed with cellular components and/or desired bioactive agents prior to injection into the defect area. Enzymes, included or subsequently added to the precursor solutions, catalyse the cross-linking reaction immediately upon injection, generating covalent bonds between specific functional groups found within the polymer side chains.

These mild in situ reactions, which can take place in a matter of seconds or minutes, do not produce any cytotoxic effects (17,18) and present several advantages (19-21) over pre-created hydrogels: adaptation to the shape of the defect, lower risk of implant migration, easy and effective cell encapsulation and deliverability, and minimally invasive surgical interventions that improve patient compliance and recovery (18,22-27).

Gelatin (Gel) is a natural polymer derived from the partial denaturation of collagen that has attracted attention as a hydrogel scaffold into which cells can be embedded. It has accessible functional groups that can react with other molecules and different integrin-binding sites for

cell adhesion and differentiation (28). However, its poor mechanical properties limit its applications. This lack of mechanical strength can be overcome by preparing blends of gelatin with other polymers (29) by enzyme-mediated reactions such as hyaluronic acid (HA). HA is well known for its high hydrophilicity, good lubrication, biocompatibility, and low cell and protein adhesive properties (30). Gel-HA hydrogels enzymatically cross-linked by horseradish peroxidase (HRP) and hydrogen peroxide (H_20_2) through the covalent bonding of tyramine (Tyr) have demonstrated their non-cytotoxicity and potential for cell adhesion and spreading (33-35). HA concentration in this system can be modified according to the required stiffness, water sorption, pore size and gelation time (18, 31, 32), which gives rise to potential candidates for several types of soft tissue models, regeneration strategies and applications in minimally invasive procedures.

Traditional approaches based on hydrogel or other soft materials for scaffolding are limited in their capacity of producing complex microstructures with accurate biomimetic properties. Three-dimensional (3D) bioprinting technologies to the contrary, offer a novel versatility to co-deliver cells and biomaterials with precise control over their configurations, spatial distributions and pattern exactitude, achieving personalized constructs that mimic the functionality of target tissues and organs (22, 36-42). One of the most appealing applications of 3D bioprinting nowadays is the development of functional 3D tissue models. Current 2D cell cultures, particularly the animal models employed for *in vitro* drug testing, are shown to respond differently to drug candidates compared to humans, and hence their use as models of human diseases or medical conditions result ineffective and futile (163).

However, like any other new and complex technology, the process towards its complete implementation still has a long way to go. The determination and understanding of the parameters involved in a process of hydrogel printing as well as the effects of their combination are paramount for the success of the scaffold and can present a challenge even to the most veteran researchers.

In this work, we propose a viable and reproducible cell encapsulation protocol of Gel-Tyr/HA-Tyr hydrogels by means of 3D bioprinting for in vitro drug testing and further use in regenerative medicine, significantly reducing the worker's laboratory time and facilitating the completion of long laborious tasks in multi-sample hydrogel generation. We also provide an extensive and well-documented description of several parameters directly involved in every process of printing design and protocol optimisation as well as some of their common individual effects on printed scaffolds.

1. Introduction

Life in well developed, ageing, ever-growing populations results indubitably shaped by the advances in the medical field, and vice versa.

The rising prevalence of chronic musculoskeletal conditions, the non-stop global increase in prevailing causes of death (43), or the constant improvement in surgical techniques, not only have all contributed to the severe problem of organ shortage and scarcity of patient-compatible donors we face today (44, 45), but also to the driving force behind new tissue regenerative science, research, and development to overcome it.

Before the emergence of tissue engineering, strategies to deal with tissue losses were the exclusive domain of the surgery repertoire; options were restricted to the use of rudimentary artificial prosthetics, organ transplantation, or the autologous transfer of patients' tissue. Nowadays, the use of autografts, allografts, and xenografts continues to be the leading therapy solution for numerous damaged tissues (46-54); unfortunately, it is not exempt from shortcomings. It stands to reason that, from a biology perspective, there should be no better material to replace a living tissue than one of the same nature, and yet despite organ transplantation generally saves lives, prolongs lifespan and increases the quality of life of thousands of people every year (55), chances are that abnormal interaction, dislodgment, infection, eventual chronic rejection and failure (56-62), to name a few, still occur on a fairly regular basis. Ironically, it is all mostly due to the same reason why they are found so attractive for replacement, their peculiar subjection to the body´s response.

Biocompatibility is the primary requirement of an implantable material, unrelatedly to its origin. When a biomaterial comes into contact with a biological system, biocompatibility assures an appropriate host reaction with no immune, thrombogenic, toxic, or allergic inflammatory response. Tissue grafts are formed by a variety of cells contained in an organic matrix; glycoproteins, antigens present on the cell surface membrane, can be recognised by the human leukocytes and remain strongly immunogenic compared to the ones in the extracellular matrix (ECM) (63, 64). Even though some grafts are accepted in their entirety by the organism and can incorporate the own patient´s cells, as a general rule, tissues as is the case of heart valves, must dispose of all the foreign biological signalling before their clinical use, leaving exclusively the remaining acellular matrice but morphologically and mechanically similar to the original organ composition. Some chemical and physical processes used to suppress immunogenicity may interfere with cellular recolonization,

interaction, and remodelling of the cell environment, never integrating into the recipient tissue (65, 66). Nonetheless, albeit all the existing biological, economical, clinical, and ethical limitations associated with organ donation and/or their obtention, decellularized tissues today are mostly provided from bovine or porcine specimens, being currently and successfully used as implants for bone, tendons, ligaments, and heart valves, as well as providing less aggressive alternatives to organ transplantation.

Not surprisingly, the market has reflected an increasing demand for alternative high-performance biomaterials over the past few decades, where tissue engineering and regenerative medicine arenas have so far become a hallmark of state-of-art biomaterial research. It is no wonder either that, the global biomaterial market is becoming one of the most profitable markets in the coming years, with an estimated value of USD 121.1 billion in 2020 and a predicted value of over USD 300 billion by 2027 (67). Areas such as vascular therapy, cardiology, spine, trauma, orthopaedics, or wound care among others, raise real, unique challenges regarding the development of new assorted and functional replacement constructs as well as the procedures of their processing and assembly into implantable devices (68).

Available biomaterials currently on the market include a wide scope of materials of synthetic, natural, and hybrid nature (69-72). Metals and alloys, ceramics, polymers and composites, offer now the opportunity to select among very unique materials to meet the specific requirements of the anatomic location, the functionality of the tissue structure and pathobiology, healing process, and medical treatment. Examples of this selection include the use of high electroconductivity metals as electrodes in artificial organs, chemically inert materials for permanent replacement of lost function, or biodegradable materials as temporary constructs where regeneration and healing of lost tissue or function are still possible (73,74).

Concerning the latter, the most frequent strategy associated with tissue engineering is the use of natural or synthetic biodegradable matrices embedded with living cells and biomolecules of interest (75). Those matrices, in a way similar to decellularized tissues, are able to mimic the different biological ECMs due to their wide diversity of mechanical and chemical properties and, in turn, they renovate or restore tissue´s functionality, providing an improvement in the quality of life of those who receive them. In regenerative medicine and tissue engineering, those matrices or constructs are commonly known as *scaffolds* given their similar role to the support structures in the building industry.

Scaffolds can be described as three-dimensional, porous, solid biomaterials designed to perform some or all of the following functions: (a) promote cell-material interactions, cell adhesion, and extracellular matrix (ECM) deposition; (b) allow sufficient diffusion of gases, nutrients, and regulatory factors to permit cell survival, expansion and differentiation; (c) possess a degradation rate similar to the regeneration rate of the replaced tissue, and (d) cause minimal inflammation or toxicity to the organism (76).

The criteria for selecting suitable scaffold biomaterials is therefore based on their mechanical strength, surface energy and chemistry, porosity and interconnectivity, molecular weight, solubility, shape and structure, hydrophilicity, water absorption, degradation and erosion mechanism (77). To date, polymer and polymer composites have been widely studied and used in several engineering disciplines including biomaterial research, since their optimal characteristics tend to be more easily and reproducibly controlled, especially when compared to other typical materials (78).

1.1. Polymers for scaffolding

Polymers are by far the largest and more versatile class of biomaterials regarding their variety of physical, biological and mechanical properties. They have been thoroughly studied and used for the manufacture of medical devices as well as for tissue-engineering scaffolds (79,80) as a result of their chemical tunability, biocompatibility, high porosity with very small pore size, high surface-to-volume ratio, and an extensive selection of fabrication techniques and final forms. The similarities between the long-chain architectures of biological tissues and natural polymers such as proteins or polysaccharides, or synthetic polymers, have motivated researchers to successfully attempt to grow skin and cartilage (81), bone and cartilage (82), heart valves and arteries (83), nerves (84), and other various soft tissues (85).

They can be categorised based on their origin, structure, properties, and molecular arrangement of their repeating units. Depending on their origin, polymeric scaffolds are principally classified into synthetic or biologic, degradable or non-degradable (77).

1.1.1. Natural polymers

Natural and naturally-derived polymers were the first group of biodegradable biomaterials used for clinical applications (86). These materials, some of them after a process of derivatization, are effortlessly recognised and accepted by biological systems due to their

native bioactive properties and superior cell-material interactions, as well as metabolically processed through established pathways in the organism (87). As a result of their similarities with the native ECM, natural polymers have been frequently used as skin substitutes where some of them are well-known for their hemostatic properties, antimicrobial properties, or encouraging reepithelization when seeded with skin cells (88).

However, naturally-occurred polymers lead sometimes to immunogenic reactions or pathogens transmission, becoming difficult to purify and sterilise (89). In other cases, they can be very costly and complex if resource availability is limited or present batch-to-batch variations in their final properties, transforming them into a challenge to reproduce with accuracy. Compared to their synthetic counterparts, natural polymers generally exhibit a narrow and scarce range of mechanical properties (87), compromising their use in hard tissue applications; current developments in nanocomposite technology offer the chance of enhancing this rigidity, mechanical strength and other properties by blending processes and composite preparation, combining the properties and the synergetic effects of their components (90).

The most predominant natural polymers used in biomedical applications are protein-based (e.g., collagen, gelatin, silk, fibrinogen, elastin, keratin) and polysaccharide-based (e.g., cellulose, amylose, dextran, chitin, hyaluronic acid).

Proteins or peptides, well-known for their controlled natural degradability, are the major component in natural ECMs and most probably present the key to a new generation of biomaterials. Proteins properties are inherently connected to their composition and chemical structure, formed by repeated short amino acid sequences; recent studies show that not only will be possible in a near future to tune properties of specific proteins by changing these sequences organisation but also to combine appealing qualities of different proteins by fusing their complete sequences altogether, giving rise to a new series of proteins with novel enhanced properties (91-96).

Polysaccharides, on the other hand, consist of long-chain carbohydrate molecules composed of individual monosaccharide units bound together by glycosidic linkages. Their molecular formula is $C_X (H_2O)_y$ where *x* can be from 200 to 2500 (87). Polysaccharides are often isolated and purified from renewable resources (e.g., plants, animals, microorganisms), broadly distributed in nature and thus further away from scarcity. Similarly, this peculiar group of polymers has structural resemblances, chemical versatilities as well as comparable biological functionalities to the organic ECM components, which mitigates the immune

response of the organism (97). Polysaccharides are rather heterogeneous molecules, they can contain small variations in their repeating units and, as a result, own dissimilar properties to molecules from another batch (98). The most exploitable and attractive advantage of these polymers relies on their freely available hydroxyl and amine domains along with their structures, becoming possible to bind synthetic monomers or other bioactive molecules to their structures and hence to alter their physicochemical properties. This possibility offers the best features of both worlds, natural and synthetic, opening the door to a new collection of natural polymer-based semi-synthetic biomaterials alongside the development of new methodologies and modelling tools to predict their optimal properties (97).

1.1.2. Synthetic polymers

Synthetic polymers, regarding their non-natural derived origin, are free from immunogenicity (66) but lack chemical and biological signalling, something that, from a cellular perspective, makes them less recognisable and attractive for cell attachment. Many synthetic polymers need to be functionalised before their use to acquire specific binding domains, responsible for cell attachment and spreading on the biomaterial surface. Common functionalisation techniques include mixing, surface coating or surface grafting polymerization (66, 99). Notwithstanding, their benefits far outweigh any possible drawback: synthetic polymers can be designed, synthesized and tailored in large uniform quantities; they possess predictable and reproducible physical and mechanical properties, including elastic modulus, tensile strength, degradation rate or degree of porosity; compared to natural polymers, their synthesis and processing are generally easier and cheaper; and since they do not include any biological material that may be compromised, they can also be kept for longer shelf times. Some synthetic polymers examples are polyesters (e.g., polyglycolic acid (PGA), poly(L-lactide) (PLLA), polycaprolactone PCL), polyacrylates as PEA, polyurethanes or poly(ethylene glycol) (PEG).

1.2. Hydrogels

Hydrogels are three-dimensional hydrated networks based on the cross-linking of natural or synthetic polymers. They can be tuned to obtain favourable physical, chemical and biological scaffold properties (5-7) with the intention to emulate their native ECM counterparts. Hydrogels scaffolds share biochemical similarities with the highly hydrated glycosaminoglycans (GAGs) components of connective tissues, which are very elastic, flexible, and possess highly viscous properties (100).

Given their structure, hydrogels are eligible for perfusing with hydrophilic nutrients and growth factors (66). They are highly biocompatible and biodegradable, with the ability to encapsulate cells in 3D microenvironments during and after the cross-linking process (100, 118, 119) without undermining cell´s natural behaviour (8-10), cell-substrate interactions, or cell-to-cell interactions (120), making them perfect for bioinks and 3D biofabrication techniques. They have been extensively explored so far for many biomedical applications including cell culture substrates and scaffolds for tissue regeneration (101-107), cell encapsulation and delivery (102, 104, 108-111), drug and protein delivery (112-115), and biomedical devices involving microfluidics or responsive materials (115-117).

Based on the polymers that comprise them, hydrogels can be classified into synthetic or natural. Synthetic hydrogels are hydrophobic with strong chemical bonds, resulting in materials with low degradation rates and excellent mechanical strength, however, due to their poor number of binding domains, cells cannot often attach to them (66). Hydrogels based on natural polymers on the contrary are inherently biodegradable and biocompatible, but present similar issues to the rest of polymers from biological origin. Although a great number of organs exhibit very soft consistencies, no more than a few tissues possess mechanical properties akin to natural hydrogels; indeed, the main drawback of hydrogels is their inherent weakness, which limits their application in medium-hard tissues. Hydrogels lacking mechanical integrity often suffer from the loss of their designed shape, providing insufficient mechanical strength in weight-bearing actions such as in bone and joints (78). In terms of fabrication and processing, they are also strongly subjected to stresses such as compression or sheering (66), breaking apart without difficulty. Various methods have been applied to improve the mechanical properties of polymer-based hydrogels, such as chemical cross-linking, physical treatments and blending with other natural or synthetic polymers (126-128).

Hydrogels are cross-linked networks produced by covalent or noncovalent bonds that do not dissolve at physiological temperature. The generation of cross-linking bonds can be induced by several mechanisms such as physical processes, by applying heat or cold, chemical processes by the addition of chemical cross-linkers, photochemical processes by the activation of photo-reactive chemical groups, and enzymatic processes by enzyme catalysis. Chemical, physical and photochemical cross-linking are well-known strategies that usually rely on incompatible external stimuli or cytotoxic reactions, where some initiators or unreacted intermediate substances remain after the gelation process. Many of these reactions, performed under lab conditions, often produce inflammation and cell death (11-13), restricting hydrogel applications cross-linked by these methodologies.

1.2.1. Enzymatically crosslinked Gel-Tyr/HA-Tyr hydrogels

Recently, increasing interest has been focused on enzymatically cross-linked hydrogels (1921), also known as enzyme-mediated or enzyme-catalysed, where covalent cross-links are generated by mimicking the biological cross-linking methods of the organism using enzymes, always occurring under mild, physiological conditions. The ability of enzymes to form cross-linked protein networks has been exploited to alter the appearance and the texture of food products, to strengthen protein-based fibres for textile manufacturing, or to develop new biomimetic tissue scaffolds. The majority of the enzymes involved in the cross-linking can be commonly found in catalysing reactions naturally occurring inside biological organisms (242-246). Enzymatic reactions are catalysed by most enzymes at neutral pH and moderate temperatures, which facilitates the *in situ* formation of hydrogels as well as the cross-linking of natural polymers that cannot resist harsh chemical conditions. Another major advantage relates to the substrate specificity of the enzyme. Enzymes have usually evolved to catalyse one reaction, or a particular type of reaction, where the level of specificity depends on the function of the particular enzyme. Unwanted side reactions or toxicity are, therefore, avoided since reactions do not randomly occur in undesired locations of the hydrogel (247). Cell encapsulation and deliverability result uniform, easy and effective given the poor requirements of temperature, toxic chemicals or light radiation (17,18), presenting a simple mechanism for the generation of cross-linked constructs and improving the mechanical strength of peptide/polysaccharide hydrogels in applications where material robustness is essential.

Minimally invasive procedures are highly advantageous in tissue engineering therapies, presenting an innovative alternative for the replacement of tissues. In situ cross-linkable gels are based on aqueous precursor solutions with cellular components and/or bioactive agents that can be administrated via injection. Injectable scaffolds eliminate the need for complicated surgical interventions improving patients' compliance and recovery (18,22-27) at the same time that they overcome the risk of implant migration and infection. Most importantly, integration within wounds and tissue defects is permitted by the in situ cross-linking, being possible to apply during endoscopic or arthroscopic procedures thanks to the initial viscosity of the precursor solution before gelation.

Gelatin (Gel) protein is one of the main integral components of skin, bone, cartilage, and connective tissues. It has superior advantages like biocompatibility, biodegradability and the absence of harmful byproducts (121-123). It is less immunogenic than collagen, relatively cheap, and has great potential for promoting cell attachment, differentiation, and proliferation (124,125). Gelatin naturally contains various available integrin-binding domains like arginine-glycine-aspartic acid (RGD), domains that are recognised by cells and used to attach to the material surface and spread.

Gelatin hydrogels have been studied for some time, gaining significant attention in arenas like drug delivery and regenerative medicine thanks to their solubility in water and various organic solvents and therefore their facility for being processed and used along with a wide selection of natural and synthetic polymers (126-128). Due to their potential porosity, gelatin hydrogels can absorb until 45 times their weight in liquid, capable of being totally reabsorbed into the system in 4 to 6 weeks (129).

Gel is derived from the partial denaturation of collagen. Depending on how hydrolysis is catalysed, either under acidic (Type A) or basic (Type B) conditions, gel can be obtained in two different forms and present slight variations in some of their properties. One of gel's peculiar properties lies in its isoelectric point. The isoelectric point indicates the pH value at which a molecule carries no net electrical charge, a value that in the case of gelatin is altered depending on how collagen is extracted. This property allows gelatin to bind with either positively or negatively charged molecules, including therapeutic agents or growth factors. Based on this, both acidic and basic gelatin molecules with isoelectric points of 5.0 and 9.0 respectively, can be used in hydrogel form as controlled release devices under physiological conditions (130). Type A gelatin presents more carboxylic groups, making it preferable for scaffolds over type B (131). Research conducted by *Lee et al. (2016)* assessed the influence

of both types in GelMa properties, finding a higher degree of methacrylation in type B, whereas type A presented a higher resolution after extrusion printing (132).

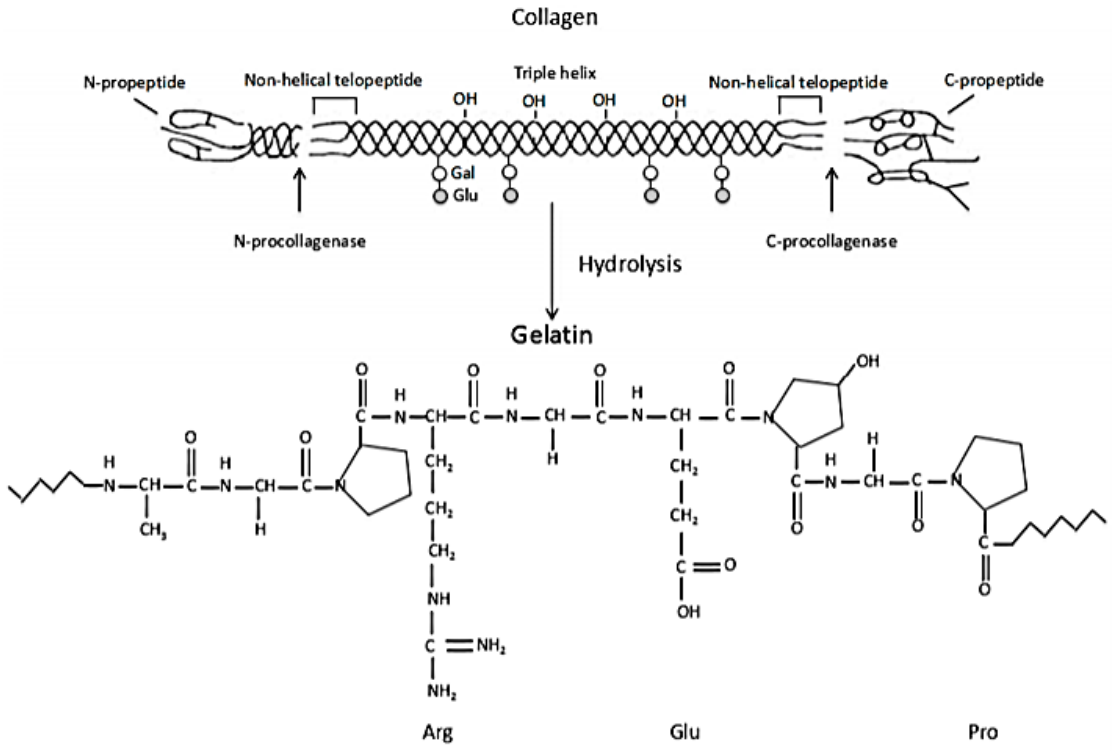

Figure 1. Schematic description of collagen hydrolysis to gelatin (249).

Gelatin-based hydrogels have been investigated as potential bioinks for 3D printing, due to their easy, flexible and smooth deposition and tunable shape by mechanical means. Gelatin physically cross-links below its sol-gel transition temperature (≈ 35°C), where the protein chains partially aggregate and attempt to regain their original triple helical structure observed in collagen; regions where the helical structure is reformed and stabilized by intramolecular bonds act as cross-linking points (133). Above gelatin´s gelation point, these regions are no longer stable and gelatin loses its semi-solid state, becoming soluble in water again. Due to this dependency effect on temperature, gel´s viscosity becomes inversely proportional to temperature, where bioink solutions can be adjusted at the moment of deposition and acquire specific thickness levels, according to the requirements of the printing method employed.

Like other natural polymers, gelatin possesses low mechanical strength, limiting its application in some tissues such as in muscle or cartilage. This problem can be overcome by the preparation of gelatin blends with other natural or synthetic polymers (134), which benefits from gelatin´s natural adhesion and cell signalling properties in exchange for increasing the mechanical properties of the whole mixture.

Hyaluronic acid (HA) is a naturally occurring polysaccharide of alternating N-acetyl-D-glucosamine and D-glucuronic acid (135). It has been successfully used in scaffolds for neural (136), bone (137), cartilage (138), and corneal (139) tissue regeneration applications. HA, like gel, is ubiquitously present in human ECMs and other vertebrates, found in locations that include synovial fluid, vitreous humour, skin, and other many tissues where friction occurs, including joints, tendons, and pericardium (140, 141). HA participates in many key processes, including tissue regeneration, wound healing, morphogenesis, matrix organisation and cell signalling (142-144). It has many important physiological and biological functions; some clinical applications include regulation of inflammation, enhanced cell migration, proliferation and differentiation, angiogenesis, osteoconduction, healing with less scarring or the treatment of rheumatoid arthritis and knee osteoarthritis (145).

HA is well known for its high hydrophilicity, good lubrication, and biocompatibility, as well as for its low cell and protein adhesive properties (30). HA-based hydrogels are only formed when chemically cross-linked through the esterification of the carboxyl or hydroxyl groups (146). They contain functional binding groups, making them easily coss-linkable with peptide polymers. Besides, due to HA high molecular weight, aqueous solutions are highly viscous (147), making it a great candidate for bioprinting applications where good rheological properties are required. Sufficiently viscous HA solutions have also been demonstrated to have shear-thinning properties under certain shear levels (147), decreasing momentarily their apparent viscosity when they are extruded.

In summary, the addition of HA appears to be an excellent option for increasing the mechanical properties of Gel hydrogels by different cross-linking methods (148-151), especially including the ones enzymatically cross-linked in situ by tyramine (Tyr) conjugates (18, 31, 32) using HRP (horseradish peroxidase) and H_20_2 as catalysers.

HRP enzyme occurs in horseradish roots and catalyses the oxidative coupling of phenols in the presence of hydrogen peroxide (H_20_2). Although several functional groups, such as aromatic phenols, amines, and phenolic acids can be used for the oxidative coupling, all polymers currently used for HRP-catalysed cross-linking utilise phenol as reducing substrate, because the cross-linking reaction between phenol groups happens to be much faster than other phenol derivatives (248).

Promising studies show the great tunability potential of Gel-Tyr/HA-Tyr hydrogels where HA concentration can be modified according to the required stiffness, water sorption, pore size and gelation time (18, 31, 32), turning out particularly versatile and useful for many surgical applications and soft tissue models, including skeletal muscle and chondrogenic differentiation (33-35).

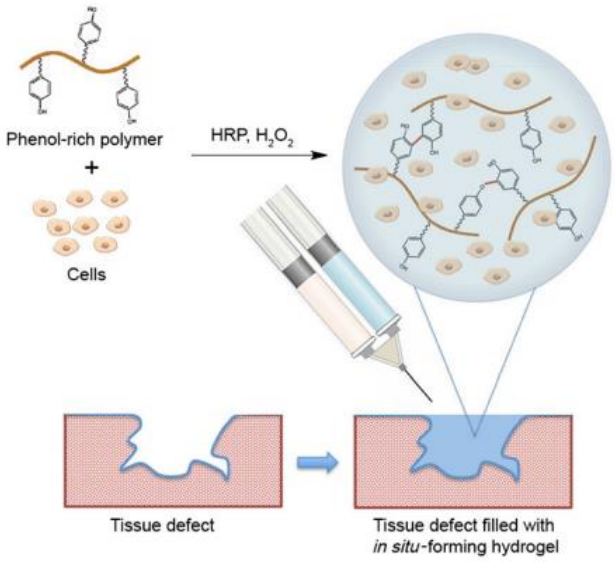

Figure 2. Filling of tissue defects by HRP-catalysed in situ-forming hydrogels using a dual-syringe for surgical applications (248). The syringe is loaded with a different phenol-rich polymer solution in each barrel, either containing HRP alongside cells or H_20_2. When both solutions mix and exit from the syringe needle, the ultimate solution results in the in situ formation of hydrogels via HRP-catalysed cross-linking (248).

1.2.2. Hydrogels in biofabrication

Even though a collection of encapsulated cells and matrices inside a 3D scaffold is considerably closer to becoming a functional tissue, three-dimensional platforms have proven to be necessary but not always sufficient for the success of fabricated tissues. This is mainly due to the low level of biomimetic organisation of the heterocellular environment, as well as instability and low repeatability of current 3D scaffold fabrication techniques.

Results from several 3D studies evince the strong existing cause-effect relationship between the increase in dimensionality and a significant positive impact on cell proliferation, differentiation, response to mechanical stimuli, and cell survival in cellular microenvironments (152-154). Despite this fact, human tissue is anything but a simple and homogeneous structure. It consists of several, functional cell types and a vascularized,

hierarchical architecture dependent on the tissue type. Proper tissue development, function, and adaptation to the environment are all equally triggered by the ECM architecture and the populating cells (66). For successful tissue replacement, any fabricated tissue should recreate the complexity and heterocellularity of native tissue at different scales (155), as well as lead the cells employing chemical and mechanical cues, promoting specific behaviours and proliferation rates (66). When the scaffold architecture fails to retain the different cell populations, biological response is followed by the formation of thrombi, cysts, or even tumours. Similar occurs with mechanical failure, where cells negatively react with inflammation or fibrosis that may destroy the scaffold's integrity. When a scaffold fails to provide proper signals for its recognition, cells do not attach to the material surface and their health starts to deteriorate as a whole, often ending up in necrosis and/or apoptosis (66). Mimicking the biological and functional organization and complexity of native tissues by means of biofabrication is now therefore regarded as the next challenge in the complete regeneration of tissues in the human body (156).

Research has repeatedly shown how extracellular matrix deposition and remodelling are not only significant steps in functional tissue formation but also decisive in the ultimate result of the scaffold. Conventional biofabrication approaches in tissue engineering are typically based on scaffold-based or scaffold-guided constructs with a random distribution of cells, matrix, and bioactive cues, where their manufacturing does not allow the control of specific spatial distribution (157). Vascularisation in 3D models remains an unsolved problem, which plays a vital role in tissue growth and survival, and drug delivery. In addition, techniques including particulate leaching, freeze-drying, electrospinning, and microengineering, typically possess limited reproducibility and versatility in their fabrication procedures, generally involving the use of organic solvents, high temperatures or cross-linking agents not compatible with living organisms (157).

The development of new deposition and fabrication technologies allow researchers nowadays to design and generate scaffolds with more complex architectures, without either compromising the biological components or the clinical outcome of the constructs.

On that note, hydrogels offer the superior advantage of being processed under more cell-friendly conditions. Often classified in the biofabrication field as 'bioinks', their precursor solutions are held together by weak physical interactions that initially enable good deposition or printability in the company of biological compounds, followed by chemical or enzyme-mediated cross-linking stabilisation (156). Hydrogels with high water contents are excellent

for the incorporation of cells and bioactive compounds, providing an instructive, aqueous 3D environment that simulates the native extracellular matrix (156). All these reasons make hydrogels particularly attractive for biofabrication.

1.3. 3D printing in biofabrication

The term biofabrication commonly refers to the full process of assembly of biomaterials, cells, and biochemical agents to produce an organ (158), regardless of the moment of introduction of cellular components. The vast compendium of current biofabrication techniques provides the organ designer with additional designing options to generate singular scaffold configurations.

The reality is, however, that the promise of three-dimensional organ systems presents to the designer today not one but a few intricate puzzles when building even the simplest of tissues. The material, with its properties, cellular affinity, and evolution over time; the conditions in which the material is handled and assembled, and its integration with the biofabrication process, are all interconnected degrees of freedom that require particular setting and optimisation to answer a specific medical application. As Burg and Burg (2014) well described, the creation of 3D scaffolds that support tissue and organ fabrication ultimately relies on the 'basic' task of correctly defining "the right process to place the right biomaterials with the right characteristics at the right place at the right time" (p.221) (158).

3D printing, a technique at the cutting edge of the biofabrication field, promises higher shape fidelity, lower fabrication times and minimum dependence on the human factor, and even in some cases, the simultaneous inclusion of embedded cells throughout the process without negatively affecting their survival.

3D bioprinting is a rapidly expanding field that combines the disciplines of developmental biology, stem cells, and computer and materials science (159). 3D bioprinting was first demonstrated by Klebe (160) in 1988, using the term "cytoscribing" to refer to the technique of positioning cells in a precise way on a 2D surface using a computer-control inkjet printer or graphics plotter. The technique started evolving as more research groups joined in, taking place approximately twenty years later the first international workshop on bioprinting and biopatterning at the University of Manchester (161). In the last decade, interest in the discipline dramatically escalated, becoming an emerging technology with many applications and providing high reproducibility and precise control over fabricated constructs in an automated manner (162). Particularly in the biomedical field, 3D bioprinting refers to several

different additive manufacturing (AM) techniques based on different physical principles, which can print not only materials but also living cells in a specific location (68).

Overall, 3D bioprinting aims to construct anatomically accurate tissues, organs and other biological systems *in vitro* to mimic their analogous parts within the human body (155) through layer-by-layer material deposition and accordingly to anatomical 3D image analysis and computed tomography techniques (163, 164). Other applications include the development of 3D tissue models that may eventually replace current 2D cell cultures and animal models for *in vitro* drug testing since animals are shown to respond differently to drug candidates compared to humans, and hence result ineffective as models of human diseases or medical conditions (163). Altogether, this biofabrication technique offers more efficient and less time-consuming processes to create unique, customized products for tissue modelling and replacement, becoming one of the greatest highlights in modern medicine nowadays.

However, 3D bioprinting is yet at an early stage and as with any other new, complex system, the process towards its complete realization can be rather laborious, iterative and often gradual. Whether a bioink is suited or not for 3D bioprinting is mainly defined by the material´s rheological properties and the cross-linking method. We also find several system properties that influence hydrogel printability and cell viability, including gelation, nozzle gauge, shear stress, network properties, and fabrication time (157), all deeply interconnected as it will be later described.

One of the most important components of a 3D bioprinting system is the bioink. Bioinks are a mixture of cells, biomaterials and bioactive molecules which compose the substrate of the final scaffold during the printing process (163, 100). The four principal types of bioink materials are hydrogels, microcarriers, cell aggregates, and decellularized matrix components (165, 166). Bioinks are generally required to be biocompatible, biodegradable, and should not have any toxic effect on the body, including their waste and intermediates compounds. Also, they should enable rapid cell growth and proliferation to start the regeneration process. There is a wide-ranging selection of materials that can be used for scaffolds; however, due to the cell and material heterogeneity found in the different tissue types, the use of several bioinks will be sometimes needed, which have to be optimised for precise control over cellular and matrix deposition (68, 165).

Bioinks most importantly, compared to conventional fabrication techniques, need to preserve and assure cell viability of the embedded cells during the printing process, while meeting all the printing requirements, in other words, they must be bioprintable.

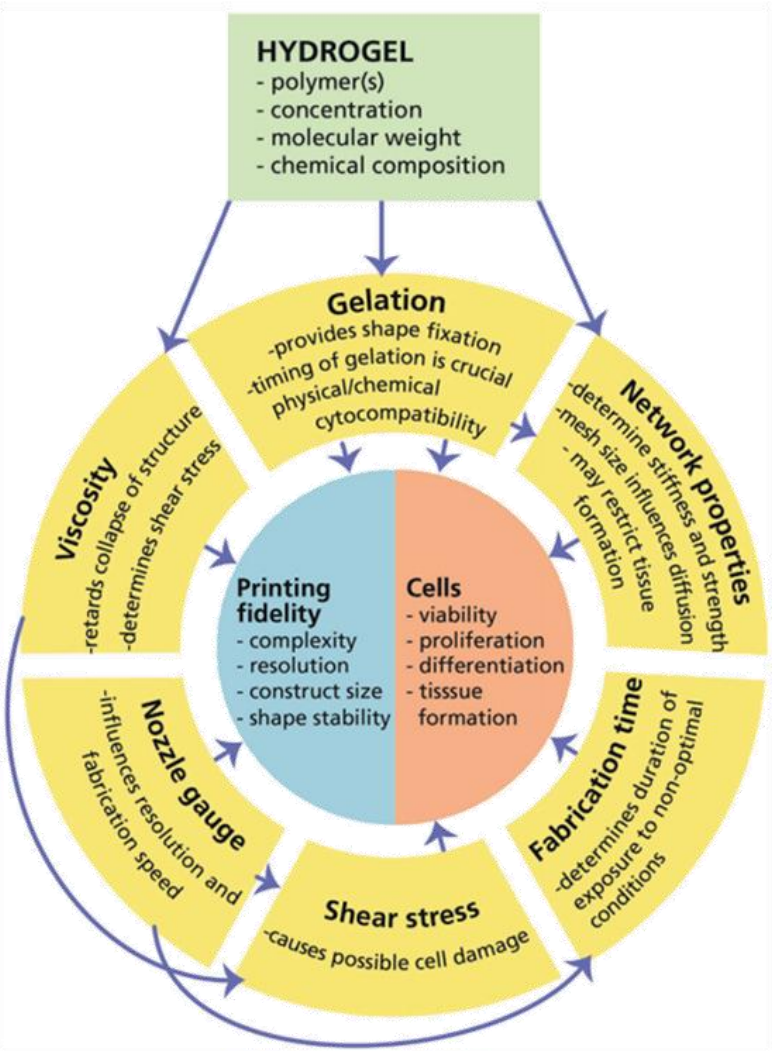

Figure 3. Concept map of parameters and relations critical to 3D bioprinting technologies. The hydrogel (polymer type(s), concentration, molecular weight and chemical composition and cross-linking approach) directly determines the viscosity, gelation mechanism and speed, and mechanical properties of the final scaffold. This, in combination with processing parameters, such as nozzle gauge and fabrication time influence the main outcomes: printing fidelity, cell viability and tissue function (157).

The bioprinter itself also plays a pivotal role in the fabrication process. Since tissues and organs are highly complex, bioprinter should be able to print the different cell types in the company of the biomaterials at a time (165) to assure cellular components reach the centre of the scaffold, a task that not all the techniques are capable of. The printed structure should

be of a minimum resolution which is dependent on the accuracy of the system, the printing method, and the material properties. Other requirements include: sufficient build speed to retain the scaffold shape and structural integrity, material and printing versatility, full automation capability and user-friendliness, affordability, and ease of sterilization techniques to avoid possible infections in surgery or cell studies (167).

1.4 3D bioprinting technologies

Most of the fabrication approaches reported in literature possess a common limitation and is their poor working versatility in cases where the required operational parameters (e.g., rheology, pressure, temperature, voltage) are relatively different from the ones established by their own working mechanism (168). In other words, each biofabrication technique is applicable only in a particular range of the material properties (e.g., viscosity, surface tension, cell concentrations, melting point, solvent evaporation), restricting the choice of materials.

1.4.1 Fused deposition modelling (FDM)

Several additive manufacturing (AM) technologies, which could be potentially used in bioprinting applications, work with conditions that often exceed the physiological range, becoming incapable of working with cellular components. These techniques lack the flexibility to mimic cell distributions in native tissues, especially when strategies for the regeneration of multiple tissue interfaces or organs are desirable (168); however, they have shown different degrees of success in 3D fabricated scaffolds by adding posterior steps of indirect AM to the process.

The most popular technique in AM is fused deposition modelling (FDM), also known as 3D fibre deposition (3DF) or bioextrusion. FDM is based on the hot-extrusion and deposition of thermoplastic materials, like synthetic polymers, which are generally provided in filaments or pellets shape (168).

These filaments are melted and deposited layer-by-layer by a heated nozzle on a build platform, on which a 3D structure is eventually built. In some cases, a second printhead is used to deposit temporary supporting material, or scaffolds can be generated by the simultaneous work of multiple printheads. FDM possess the ability to print objects with excellent mechanical properties and high porosity. Besides, geometry is precisely controlled by horizontal and vertical movement (x,y,z) of the printheads or the platform, depending on

the system. It benefits from low-cost materials, fast fabrication speed, and is easy to operate. In terms of bio-applications, FDM shows limitations of material selection compared to other conventional methods, where only a few thermoplastic materials are biocompatible enough for its use in scaffolds. Moreover, high temperatures employed with these molten polymers limit the direct incorporation of biological factors or high water contents, causing natural polymers and hydrogels to be completely impractical.

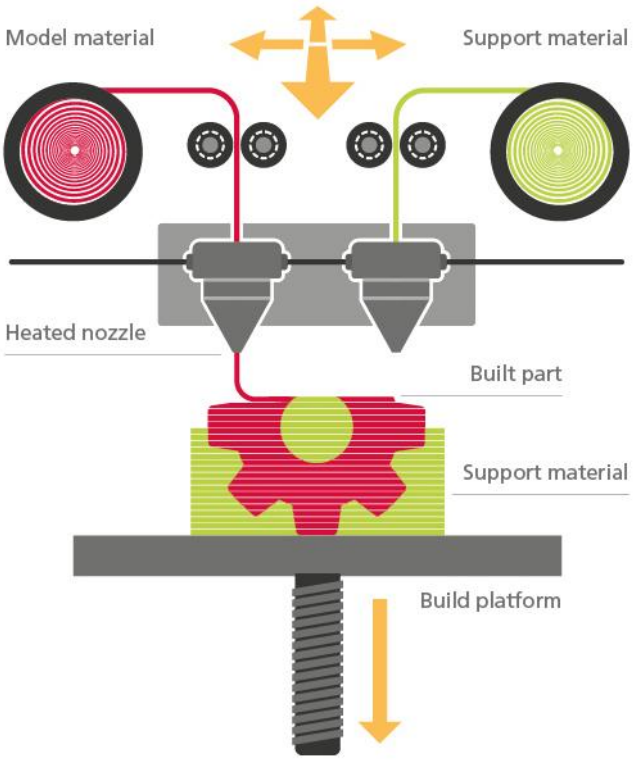

Figure 4. Diagram of FDM process (159)

Nonetheless, other techniques based on extrusion and droplet-based (168), allow the direct incorporation of cells into a biomaterial carrier or bioink during the process of AM.

1.4.2 Extrusion-based bioprinting

Another extrusion-based technique is bioplotting, also called extrusion bioprinting (not to be confused with bioextrusion, although their names may differ in each classification system found in literature). Extrusion bioprinting is the most affordable and common used technique in 3D bioprinting (165). Numerous types of tissue have already been studied, including neuronal tissue (169, 170), heart valves (171, 172) and cartilage (173, 174). Bioink dispensing, in a way similar to bioextrusion, is performed by the application of mechanical

or pneumatic pressure at the back of the dispenser (175), allowing the extrusion through a micro nozzle of a wide range of materials (176). It fabricates 3D constructs by stacking 2D layers (176) of very different materials, from highly viscous hydrogels (≤ 6 x 10^7 mPa s) (163, 177, 178) to cell pellets (169), tissue spheroids (179,180), and tissue strands (181).

Despite having a relatively low resolution (>100 µm) (68) and limited fabrication speed with complex shapes, extrusion bioprinting has a few important advantages like the implementation of high cell concentration bioinks with excellent cell survival (above 90%), scalable production and the ability to print natural polymers and synthetic polymers with low melting points or in hydrogel form (68).

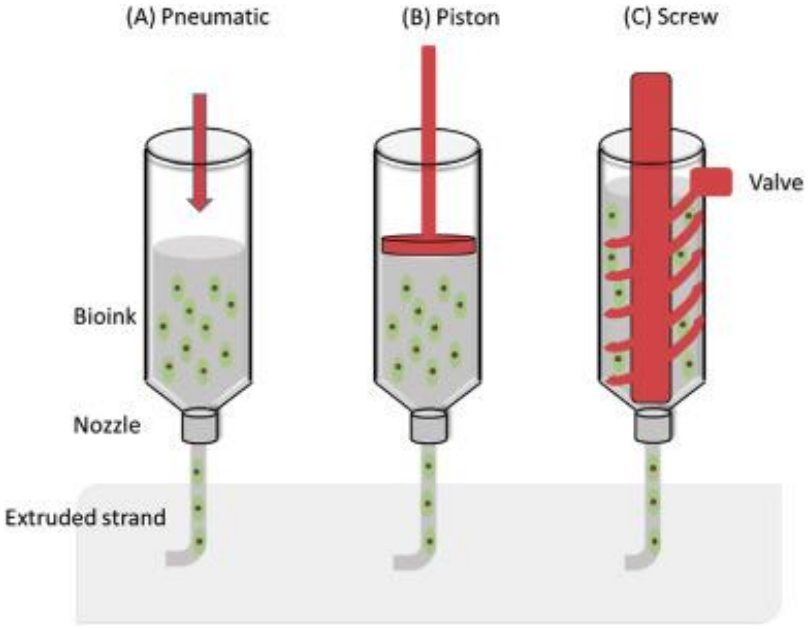

Figure 5. Extrusion-based bioprinting. (A) Pneumatic via pressurized air, (B) piston-driven mechanical or pneumatic extrusion, and (C) screw-driven extrusion (160).

Published results demonstrated its tremendous versatility in multi-material printing. *Ozbolat et al. (2014)* succeded in the creation of an extrusion '*Multi-arm*' system capable of processing the dispensing of different cell types and materials at the same time, reducing the fabrication time and enabling fabrication of more complex structures (182). Other promising projects as the one investigated by *Liu et al. (2017)*, alternatively developed a system capable of printing simultaneously with a multiple-channel single-printhead. Each channel was connected to its own bioink reservoir and computer-aid, devised to open the different valve mechanisms only at a required moment of the printing (183). Working with this technique

requires a minimum material viscosity to assure structure stability. Hydrogels with poor viscous properties although being printable, generally need the use of other structural bioinks, fugitive materials or plotting baths to prevent deformation of the construct after extrusion. Cell sedimentation and pressure influence are also enhanced, making difficult it to calibrate specific flow rates and homogeneous cell distributions.

1.4.3 Droplet-based bioprinting (DBB)

Droplet-based technologies are simple and agile techniques that deposit picoscale or nanoscale droplets on top of a substrate without any contact with the platform surface (176). They are highly versatile and able to print at high speed and high resolution, but mostly all working modes are only suitable for materials with low viscosities (163, 165), on the contrary to extrusion-based systems.

Due to the general low viscosity requirement (< 30 mPa·s) (184) and to avoid nozzle clogging, cell densities in these types of bioinks are generally lower than in other techniques (1-3 x 10^6 cells/mL) (68, 185). Printed constructs have poor mechanical and structural integrity (163), and there is a restriction of size in the constructs due to possible cross-contamination of the bioinks in simultaneous printing. Besides, the uniformity of the droplets and the control of vascularisation and porosity of the final constructs need to be improved (163, 165). DBB can be generally divided into different categories depending on the literature:

Inkjet bioprinting

- **Continuous-inkjet**

Based on the Rayleigh-Plateau instability principle (163), the bioink solution is ejected through a nozzle exit when pressure is applied, breaking up into individual droplets. Undesirable droplets are deflected by an electric field to a gutter, where the unused ink is recycled for many applications in other disciplines, somehow, for most applications in biomaterial science, especially the ones working with encapsulated cells, recycling after exposure to the environment is absolutely unviable due to the risk of contamination of the process and the bioink (186).

- **Drop-on-demand (DOD) inkjet**

Preferred over continuous-inkjet, DOD systems only generate droplets when desired and thus are more economical (163). Rather than an applied pressure, droplets in this inkjet type

are formed by breaking the fluid´s surface tension at the nozzle tip. Surface tension is broken by the propagation of a pressure pulse caused by different physical principles where if the pulse exceeds the pressure threshold at the nozzle, a drop is ejected. However, in the absence of pressure application, the liquid is held in place only by the surface tension. Consequently, this group of techniques only work with very low viscosity fluids. Although it has some advantages over other printing methods such as its low cost and high resolution (20-100 um) (176), due to the small size of the printed droplets, time of processing is considerably increased and final constructs lack mechanical strength (176). Based on their physical principle, we find:

- **Thermal-induced system.** The actuator is locally heated when applying a voltage pulse, creating a vapour bubble that rapidly expands and bursts (68, 163).
- **Piezoelectric-induced system.** When the voltage pulse is detected, the piezoelectric actuator suffers a physical deformation transferred to the fluid chamber, producing a pressure wave (68, 163).
- **Electrostatic forces.** Volume in the fluid chamber is increased by the action of an electrode and a pressure plate. The pressure plate deflects from its original position after a pulse is applied (68, 163).
- **Electrohydrodynamic jet.** This inkjet technique follows a slightly different approach compared to the rest of the DOD systems. In the resting phase, bioink is pushed to the orifice exit by back pressure, forming a rounded meniscus at the tip due to the surface tension. When a high voltage (0.5-20 kV) is applied between the nozzle and the surface substrate, the potential difference causes the mobile ions of the material to accumulate near the meniscus surface, overcoming the surface tension. Changing the applied voltage, bioink properties and flow rate, the system allows different jetting modes, from a dripping mode with low printing times to a continuous stream of droplets (68, 163).

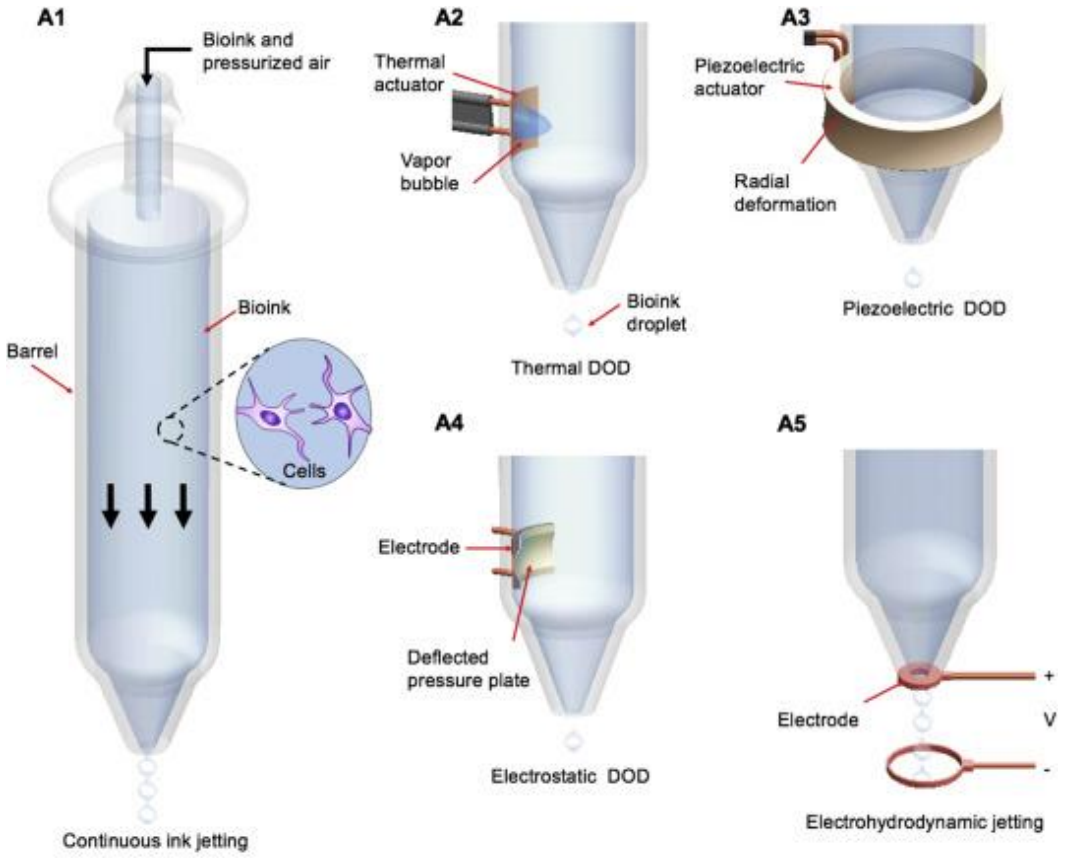

Figure 6. Inkjet bioprinting. (A1) Continous-inkjet, (A2) Thermal DOD inkjet, (A3) Piezoelectric DOD inkjet, (A4) Electrostatic DOD inkjet, and (A5) Electrohydrodynamic jetting (163).

Micro-valve bioprinting

This approach consists of the generation of droplets under pneumatic pressure (176), controlling the opening and closing of the nozzle gate by means of an electromagnetic microvalve. The microvalve contains a solenoid coil and a ferromagnetic plunger that blocks the exit in the absence of electricity. When the electromagnetic field is generated, the valve coil at top of the printhead attracts the plunger upwards, unblocking the orifice. If the pneumatic pressure is large enough, bioink is ejected (68, 176). Depending on the applied pressure and the valve opening times, this technique allows different modes, continuous or dripping dispensing. Longer valve-opening times and pressures facilitate the deposition of more viscous bioinks (1-70 mPa·s) (187, 188) compared to other droplet-based systems (inkjet-based: 3-30 mPa·s) (1184), but excessive pressure can generate undesired satellite droplets during deposition (187). Despite the micro-valve system can print even more high

viscous bioinks (up to 200 mPa), slow filament elongation is found in viscous properties above 70 mPa s (187, 189), which produces unstable flow rates.

As a rule, volume in droplets generated by micro-valve printers tends to be larger in comparison with other droplet-based techniques, regardless of the nozzle geometry, which substantially reduces resolution (176). However, printed cells with this approach are found to be highly viable, retaining their function, genotype and phenotype, and being able to proliferate (190-192).

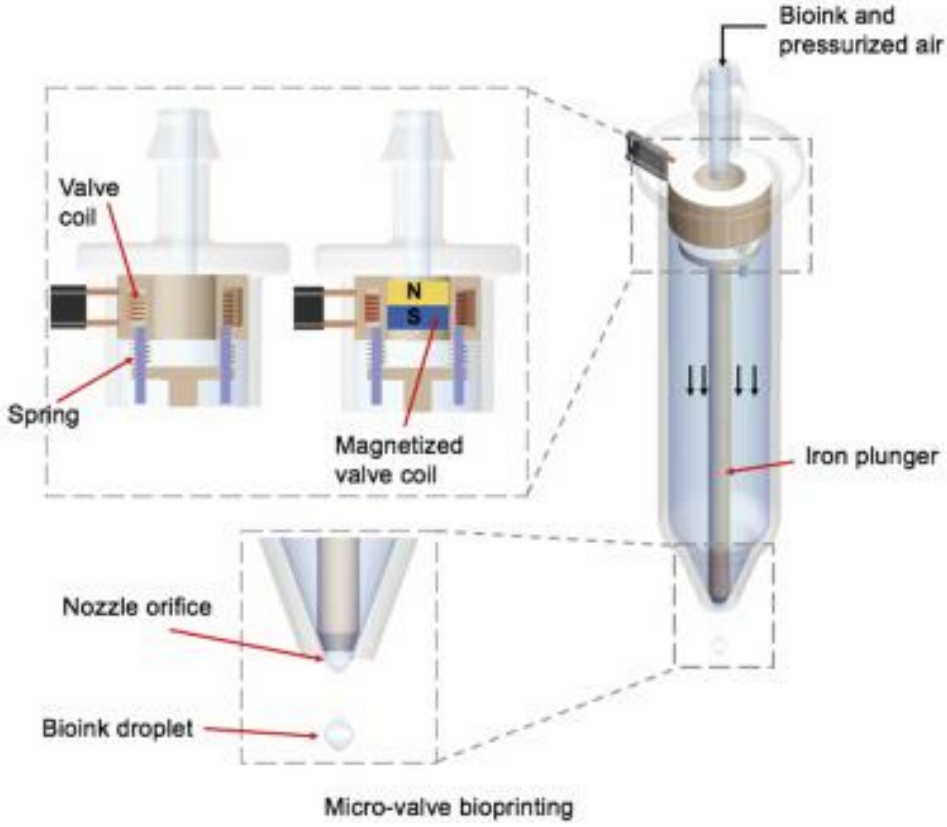

Figure 7. Micro-vale bioprinting (163).

Acoustic-droplet ejection bioprinting

Unlike the rest of inkjet systems, bioinks in this approach are well kept in an open reservoir held in place by the surface tension at small converged exit conduct, generating droplets on-demand employing acoustic waves. When voltage is applied, the acoustic actuators placed upon the exit create circular waves towards the acoustic focal point, exceeding the surface tension and ejecting the bioink (68). An important disadvantage of this technique is the loss of control over droplet ejection due to the possible disturbances when either the printhead or substrate are in movement. Another disadvantage includes the incapacity to print with

middle-high viscosity materials at high cell density ratios such as the case of some commonly used hydrogels (68, 163).

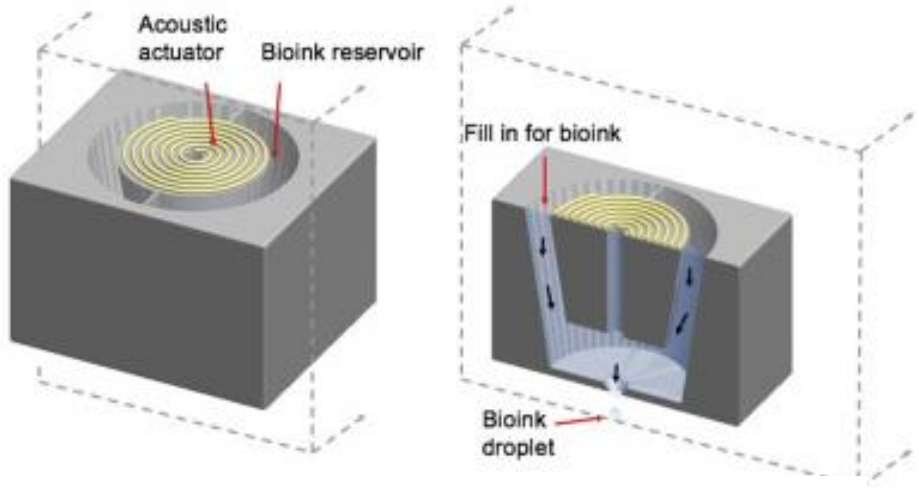

Figure 8. Acoustic-droplet-ejection bioprinting (163)

1.4.4 Hybrid bioprinting

Many research groups have started to develop what are called "hybrid" bioprinting systems (193-196), where grafts are constructed by alternate deposition of stiff thermoplastic polymers and cell-laden hydrogels. This approach allows the use of multiple hydrogels (and thus multiple cell types and bioactive factors), and since hydrogels are supported by the thermoplastic material, a broader range of hydrogel formulations can be exploited compared to bioprinting of hydrogels alone. Hydrogel requirements for viscosity and gelation speed are less restricted, therefore combination with technologies such as inkjet printing may be possible.

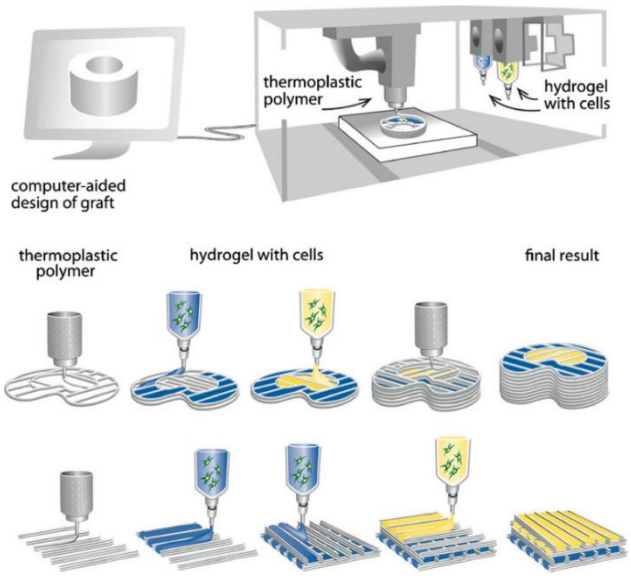

Figure 9. Schematic overview of a hybrid bioprinting process. Once the thermoplastic material is extruded and cooled, hydrogel bioprinting can be performed layer-by-layer by different approaches, generating a hybrid 3D structure (193).

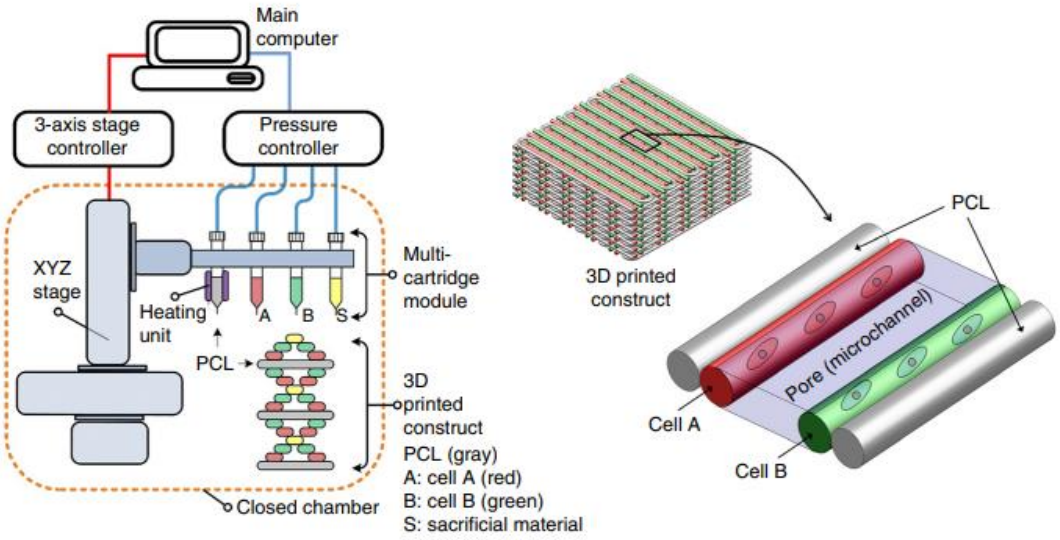

Figure 10. Another example of layer-by-layer multi-material 3D bioprinting process, where scaffolds can be fabricated using supporting materials such as PCL and sacrificial materials in company of cell-laden hydrogels with poor shape integrity (197).

1.5. Operational parameters in bioprinting

Adaptation of extrusion-based and droplet-based systems for very different scaffold applications instigate researchers to understand the fundamentals and interaction of the different working parameters, such as pressure, nozzle geometry, flow rate, or standoff distance (94, 198-200), which ultimately define the process and the scaffold success. However, factors influencing bioprinting are numerous and interrelated, and therefore they won´t be all mentioned in this introduction.

1.5.1. Parameters inside the nozzle tip

Flow rate and applied pressure

Flow rate (Q) is expressed as function a of several variables, including applied pressure ($P_{applied}$), material viscosity (η), nozzle geometry (Ø, L), and surface tension (σ) (95).

Fluid motion in a dispensing barrel is ideally controlled by a pressure balance between internal and external forces. Applied pressure ($P_{applied}$) and the weight of the ink inside the extruder (mg) are counterbalanced by the frictional resistance of the material viscosity (P_{η}) and wall-plunger parts (P_{fr}), as well as the atmospheric pressure (P_{atm}), which pushes the fluid upwards through the nozzle orifice due to the existing negative pressure inside the

barrel. When applied pressure exceeds the pressure delta (ΔP) at the nozzle tip, a minimal flow rate is obtained. Therefore, more viscous fluids extruded through smaller nozzle diameters (Ø) or longer needle length (L) will need higher levels of pressure to trigger similar flow rates.

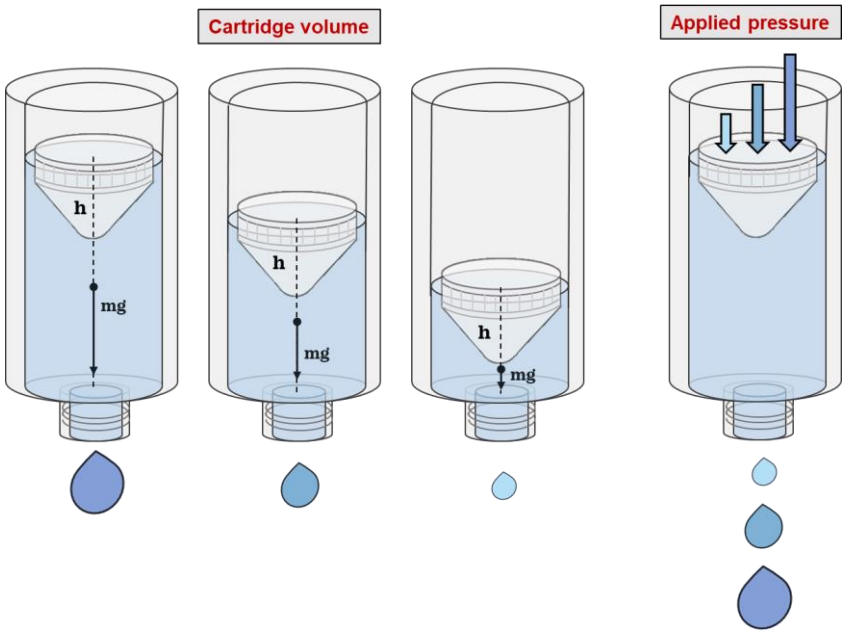

Figure 11. Illustration of flow dependence on cartridge volume and applied pressure.

Nozzle geometry

Nozzle geometry is normally divided into two popular types, cylindrical and tapered nozzles. Results show that under similar working conditions, tapered nozzles always trigger higher pressure gradients, and therefore higher flow rates, compared to cylindrical nozzles (201,202). Tapered nozzles typically have larger diameters at the entrance, and smaller ones at the tip bottom; a characteristic that provides a favourable pressure gradient, dictated by the cone-half angle (θ_c) and tip diameter (D_t) (202). n situations where the extrusion pressure is limited, a tapered nozzle will be the best option for achieving higher flow rates, especially with an increase in viscosity or/and a decrease in nozzle diameter (95).

Shear stress

Shear stress (τ) is of special interest in bioprinting since it is believed to be the main cause of cell damage and loss during printing (203, 204, 205). When a fluid is in motion, shear stress is developed due to its contained particles moving relative to one another. If we consider fluid motion inside a pipe, which has a similar geometric profile to any printing dispenser, fluid velocity will be zero at the surface wall, increasing towards the centre of the conduct and being maximum at the centre of the lumen. Shear forces will then occur between

adjacent layers of the fluid, which relatively move at a different speed, achieving the highest value at the edge of the wall. Another term considered of interest and closely related to shear stress is the shear rate (ϒ), which is defined as a measure of the rate of relative motion between adjacent layers, often expressed as a velocity gradient.

The level of shear stress is directly dependent on different parameters, such as nozzle geometry, printing pressure, and viscosity of the bioink (206, 207). Although blunt cylindrical nozzles are conventionally used to print with higher resolution, cells appear to be less affected by shear in tapered nozzle designs, generating an approximately 10-fold decrease in cell viability post-printing compared to cylindrical nozzles of identical gauge (68, 208). Changing the nozzle diameter will also affect cell printability, where the same number of cells in narrow versus large nozzle aperture will be differently affected by mechanical stressors by other cells and the contact with the nozzle walls (209). Medium nozzles sizes (250-800 µm) ensure optimal cell distribution and printing fidelity, consequently assuring high cell survival rates during hydrogel flow (209).

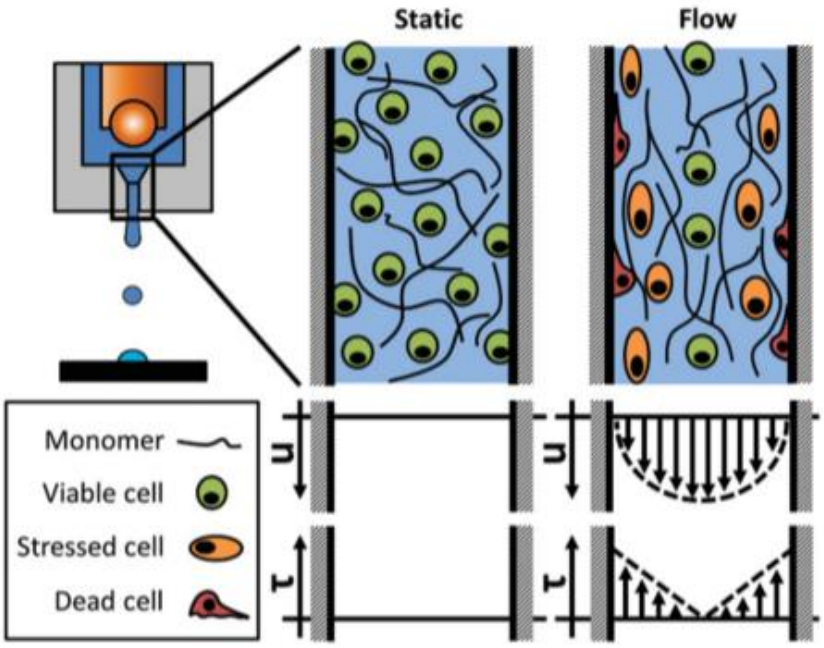

Figure 12. Schematic illustration of the velocity (u) and shear stress (τ) distribution on cells in at the nozzle during a dispensing process (203).

Excessive levels of printing-induced shear stress have shown to have not only an immediate impact on cell viability but in the long run also an alteration of cellular behaviour in the cells that survived the printing process. For the tested cell types, L929 mouse fibroblast and hMSC, *Blaeser et al.* found that the stress threshold was exceeded when reached 5 kPa (203).

Therefore, these phenomena become crucial where, in an attempt to improve the final printing resolution, hydrogels of high viscosity and small nozzle geometries are applied.

In extrusion-based printing, polymer bioinks rely on their viscoelastic characteristics, where shear-thinning and self-healing properties are paramount (175). A characteristic shear-thinning property is important for the extrusion process of bioinks which require high viscous formulations since it protects the embedded cells against mechanical stressors during flow. In rheology, the viscosity of a polymer is always larger than that of the corresponding monomer and increases hastily with higher molecular weight. This is due to entanglement and intramolecular forces between the randomly oriented polymer chains (210). Polymer solutions including hydrogels, as well as dispersions and melts, are in most cases non-Newtonian liquids.

To put it in a nutshell, non-Newtonian fluids possess an *apparent viscosity* (*η)* directly influenced by the application of different levels of shear rate. Shear-thinning behaviour, probably the simplest and most frequent rheological effect (211), occurs in polymers with a sufficiently high molecular weight, whose polymer chains begin to disentangle and to align under shear flow, which causes the apparent viscosity to drop (210).

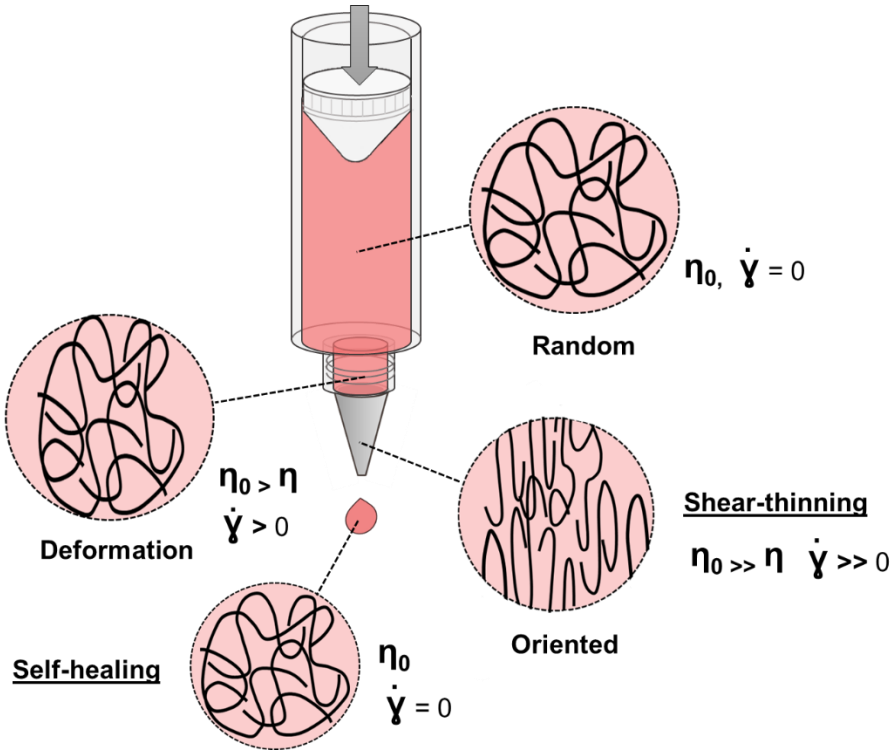

Figure 13. Shear-thinning and self-healing effects during polymer solution dispensing.

This degree of disentanglement depends on the applied shear rate, wherein theory at appropriately high shear regimes polymers should be completely unravelled and aligned, therefore behaving like Newtonian liquids, whereas for very low shear rates, polymer chains movement should not impede or modify shear flow due to the minimum extrusion speed, reaching the called *zero shear rate viscosity (*η_0) (210).

Apart from shear-thinning, bioink should then be able to self-heal quickly after removal of shear to keep structural and mechanical integrity. For this reason, the bioink should harden immediately after printing in a cytocompatible manner (175).

Cellular density

Cellular density plays a crucial role in the development and fabrication of specific constructs due to its direct influence on both cell fate and the physical properties of printed hydrogels. According to the tissue of interest, cell density can affect multiple outcomes post-printing. Printing low-density bioinks (< $1x10^6$ cells mL^{-1}), although relatively unaffected by shear forces, can result in poor tissue integration and ingrowth construct due to poor cell-cell interaction and proliferation (209). In contrast, when cell numbers are too high (> $5x10^6$ cells mL^{-1}), they can lead to undesired cell over-accumulation in the print head as well as in the scaffold, limiting available space to spread and proliferate. Overpopulated cell-laden hydrogels can also suffer from pronounced cell hypoxia, cell saturation and disruptive cell-to-cell interaction (209).

From gravity's perspective, higher cell densities in poorly viscous solutions may lead to additional sedimentation effects, increasing the chances of clogging events at the nozzle exit and density alterations in the desired final constructs.

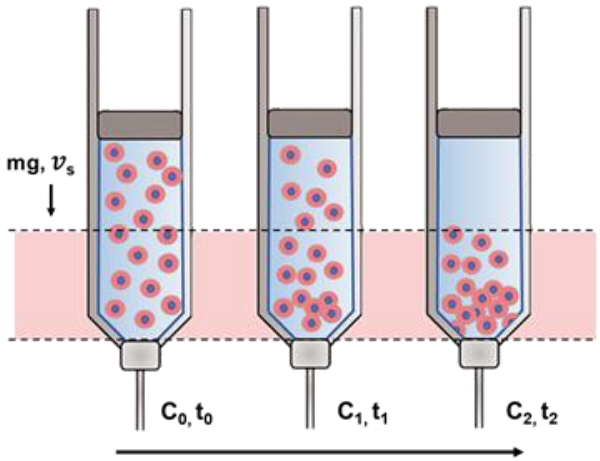

Figure 14. Cell sedimentation process in poor viscous solutions.

Despite this, high cell concentrations have been shown to increase both the overall bioink viscosity and its shear-thinning effect, due to the friction exerted by the bioink flow at the cell surface (203, 212). An increase in cell density also reduces the surface tension of the bioink, improving jet stability (satellite droplets) during droplet formation in droplet-based systems (212). However, evidence of a reduction in stiffness of finished cell-laden hydrogels has been recently reported with an increase of cell density (213,214), possibly resulting in swollen and unstable 3D printed strands.

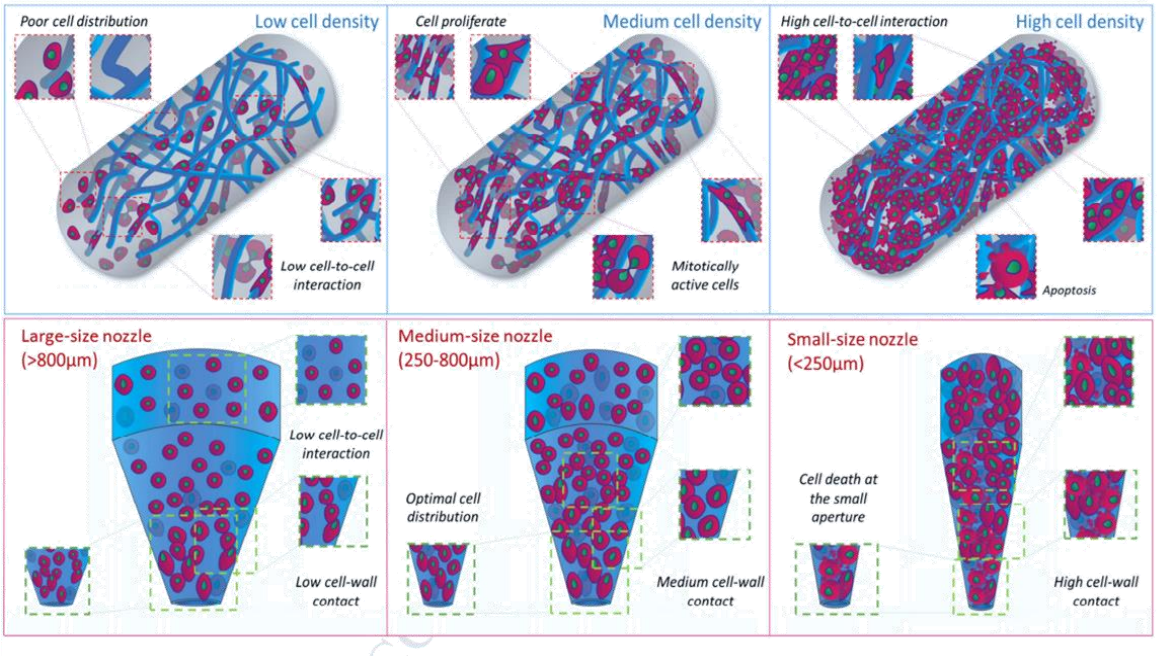

Figure 15. Cell seeding density influence on 3D cell-laden hydrogel's polymer strands and extrusion through large-size (>800 µm), medium-size (250-800 µm) and small-size (<250 µm) nozzles. Above, extruded filaments can retain a number of cells (pink) proportional to the cell seeding density. Polymeric chains (blue) concentration and distribution directly influence cell proliferation capability. Below, maintaining constant the number of cells loaded in a printing syringe but changing the nozzle aperture will affect cell printability and viability of the final construct (209).

Printing temperature

Last but not least important, to avoid the use of high-pressure levels and consequently suffer from high levels of shear stress, fluid viscosity sometimes can be decreased when decreasing or increasing the printing temperature (T). Printing temperature can also be altered sometimes to prevent cell sedimentation, by increasing fluid viscosity in fluids of low viscosity. Somehow, depending on the cell type and the fabrication time, extreme changes

in fluid temperature can decrease cell survival during and after printing. *Zhao et al* assessed the differences in cell viability at different temperatures and holding times in 5% gelatin 1% alginate hydrogels after printing, showing a significant decline of cell survival rate with the increase of holding times at any holding temperature as well as when decreasing holding temperature at any holding time (96).

In summary, the ink flow rate through the nozzle is: (a) inversely proportional to the viscosity (η), (b) directly proportional to the applied pressure ($P_{applied}$), (c) inversely proportional to the pipe length (L), and (d) directly proportional to the nozzle diameter (D) (95).

In the same way, shear stress (τ) during the printing process will generally be: (a) inversely proportional to cell viability, (b) directly proportional to the printing resolution, viscosity (η) and applied pressure ($P_{applied}$), (c) directly proportional to the pipe length (L), (c) inversely proportional to the nozzle diameter (D).

1.5.2. Parameters out of the nozzle tip

Capillary rise effect

Capillary rise effect refers to the upward rise of dispensed bioink around the nozzle tip (95), normally driven by two possible causes. Pneumatic dispensing systems suffer from a time lag between the end of pressure application and the end of material flow, producing a build-up at the nozzle tip during printhead movement from point to point. Second, the capillary rise is closely related to the degree of affinity between material and the nozzle surface (215), in other words, driven by the ink wettability, tending to increase in hydrophilic nozzle surfaces (216), and low viscosity inks. It is reasonable to think that hydrophobic substrates will also increase the capillary rise. The material build-up at the nozzle tip can impede smooth dispense and reduce the printing resolution.

Evaporation rate

Another important parameter is the evaporative effect of the bioink. Significant solvent loss can alter ink rheology, and flow rates by causing ink solidification at the tip of the nozzle (217-19). Under isothermal conditions, the rate of evaporation is intensified by the ambient condition as the degree of humidity and the boiling temperature of the solvent. In cases where a bioink has a high capillary rase, chances are it is due to the low viscosity of the material, and evaporation rates and material build-up may end in partial clogging of the nozzle. This

sometimes can be avoided by increasing flow velocity or by decreasing the standoff distance. On the other hand, in cases where the bioink viscosity is somewhat dependent on the printing temperature, material build-ups and partial clogging may be more regular. It is also important to maintain a uniform printing temperature around the nozzle, as well as prevent stops during printing if possible.

Standoff distance

The space between the nozzle and the substrate is commonly known in 3D printing as the *standoff distance (h, Sd, etc.,)*, which has been seen to have an important influence on deposit precision, resolution, and accuracy among the different bioprinting approaches.

Construct resolution in droplet-based systems results from the level of accuracy obtained in the droplet deposition, which is closely related to the important characteristic of droplet integrity. When droplet integrity is lost, depending on the droplet size, viscosity, density, and surface tension of the bioink selected (68, 163), the droplet may tend to splash or spread, either by disintegrating into secondary droplets (splashing), or expanding its surface area (spreading) through undesired areas, causing several distortions in the construct final shape or in the worst-case scenario, causing structural failure (68, 163).

The minimum standoff distance in noncontact fabrication methods, like droplet-based systems, is described as the distance in which a stretched liquid dispensed from the nozzle merges into a single droplet with possible satellite droplets (220). The droplet is formed from a single ejected liquid column that rapidly generates a leading drop followed by an elongated tail or ligament, that when it eventually breaks can lead to the formation of smaller satellite droplets (186). Normally, these drops reach and merge with the leading drop before impact on the substrate, making their presence irrelevant. In case they are still present at impact, they lead to noncircular impact footprints of the drop, degrading the quality of the printing result. To facilitate drop merging in flight, standoff distance in DOD systems is typically established approximately in 2-3 mm (186). At a longer standoff distance, droplets trajectory may be deviated by undesired airflow from the printing environment. In order to ensure stable single drops, it is also customary to set the standoff distance at a minimum.

Analogously, standoff distance has been demonstrated to have a certain influence on extrusion-based flow rates. It has been observed that if other printing parameters are held constant, decreasing the standoff distance to less than half the nozzle diameter, resistance to flow tends to increase due to the generation of back pressure (221-223). At a high standoff

distance ($h > \pi * D$) (222,224) otherwise, the bioink filament can become unstable, breaking up into discrete droplets due to the Plateau-Rayleigh instability (163). In general, research states a standoff distance of similar size as the nozzle diameter in use to achieve a stable and continuous filament (222, 225-227).

In conclusion and to avoid conceptual errors, waste of time and resources, and reiterated post-calibration processes, design and validation of efficient bioprinting protocols need to be fundamentally based on the biomaterials mechanical properties, rheology, and cell affinity; the appropriate implementation of functional bioinks; and the printing characteristics, selecting from the beginning the most suitable method for the particular scaffold application.

2. Aims and Objectives

Regarding all the positive results so far obtained with the group of gelatin-hyaluronic acid (Gel-HA) hydrogels enzymatically cross-linked by tyramine (Tyr) conjugates, this master project aims is to develop a simple, viable and reproducible 3D bioprinting protocol that provides an easier, faster and more automated cell encapsulation and complete hydrogel gelation for future drug screening and testing assays, compared to the already established manual protocol.

To do so, this dissertation addresses the following objectives:

- Literature review, study and selection of the different bioprinting approaches available in the workspace, for the set of Gel-Tyr/HA-Tyr.
- Learning and preparation of the tyramine conjugates (Gel-Tyr) and (HA-Tyr) and their blending compositions. Establish a manual gelation protocol for Gel-Tyr/HA-Tyr hydrogels with and without embedded cells, to use as controls.
- Assessment of the dispensing mechanism of the hydrogel precursor solutions and cross-linking solution in the bioprinting system. Acquisition of the necessary technical know-how in the selected bioprinting systems. Detection of the diverse working parameters that intervene in the printing process and design of a prior calibration protocol that ensures good reproducibility, and limited waste of material resources.
- Development of the bioprinting protocol. Evaluation of its cytocompatibility via the analysis of cell cultures assays. Implementation and adjustment of the culture multi-well plate in the protocol.

Likewise, this project also aspires to pave the way for colleague researchers in a first decision-making process concerning the application of fundamentals in bioprinting, where bioprinting physics and parameters, hydrogel/bioink properties, or even the selection of the correct technology, are necessary to avoid conceptual errors, waste of time and resources, and reiterated post-calibration procedures.

If the reader bears in mind questions such as the following ones:

Which technique of the ones available would be more suitable for my type of material?

Would technique 'X' be able to print this material without compromising mechanical integrity and cell viability? Would technique 'Y' be able to print this material in a reproducible way?

Would parameter 'Z' compromise my cell viability during printing? Given yes or no, in which interval?

If technique 'X' or 'Y' appeared to be suitable for hydrogel printing, to which degree its implementation would be worthwhile?

This project will try to answer them, or at least, lend the reader a hand in the process.

3. Materials and Methods

3.1. Materials

3.1.1. Hydrogel synthesis

- Gel from porcine skin (gel strength 300, Type A), Sigma Aldrich (USA)
- HA sodium salt from Streptococcus equi, Sigma Aldrich (USA)
- Tyramine hydrochloride (98%), Sigma Aldrich (USA)
- N-(3-Dimethylaminopropyl)-N'-ethylcarbodiimide hydrochloride (EDC), Iris Biotech GmbH (Germany)
- N-Hydroxysuccinimide (NHS, 98%), Sigma Aldrich (USA)
- 2-(N-Morpholino)ethanesulfonic acid (MES, >99%), Sigma Aldrich (USA)
- Dialysis tubing (3500 and 12400 MWCO), Sigma Aldrich (USA)

3.1.2. Hydrogel formation

- Dulbecco's phosphate buffered saline (DPBS), Sigma Aldrich (USA)
- 4-(2-hydroxyethyl)piperazine-1-ethane-sulfonic acid (HEPES), Sigma Aldrich (USA)
- Potassium dihydrogen phosphate (extra pure), Scharlab (Spain)
- Sodium chloride (synthesis grade), Scharlab (Spain)
- Potassium chloride (synthesis grade), Sigma Aldrich (USA)
- Peroxidase from horseradish Type VI (HRP), Sigma Aldrich (USA)
- Hydrogen peroxide solution (30% w/w in H_2O, with stabilizer), Sigma Aldrich (USA)

Calcium Free Krebs Ringer Buffer (CF-KRB) solution was prepared with 115 x 10^{-3} M sodium chloride, 5 x 10^{-3} M potassium chloride, 1 x 10^{-3} M potassium dihydrogen phosphate, and 25 x 10^{-3} M HEPES in mQ water.

3.2. Synthesis of Gel-Tyr

Gel-Tyr synthesis was carried out based on the protocol by *Sakai et al.* (228) with some modifications. The molar ratios used to obtain Gel-Tyr are:

Tyr:COOH	EDC:COOH	EDC:TYR	NHS:EDC
2:1	2:1	1:1	1:10

Table 1. Molar ratios used for tyramine graft reaction in gelatin.

When the tyramine graft reaction is carried out, a reaction is produced between the activated carboxyl groups of Gel and the free amine groups of tyramine, generating a 2° amine group and giving as result Gel molecules with phenol moieties as it is presented in ***Figure 16***.

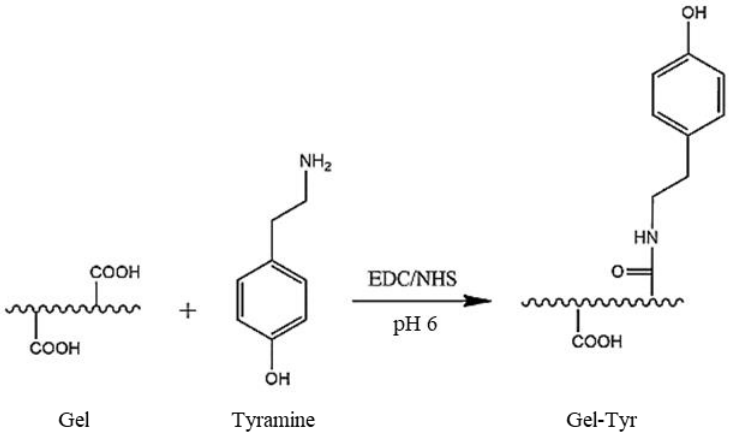

Figure 16. Tyramine graft chemical reaction in presence of Gel molecules. EDC and NHS are used as catalysers and activators of the reaction (32).

For Gel, 20 mg/mL of gelatine and 50 x 10^{-3} M MES was dissolved in 20mL of mQ water under stirrer at 60°C for 30 min. Then 0.111g of hydrochloride of tyramine was added and kept in agitation at room temperature for 20 min. Then pH was adjusted to 6 and 7 mg of NHS was added afterwards till complete dissolution for 30 min. 0.122 g of EDC was finally added to the solution and stirred at 37°C for 24h. Unreacted reagents were removed from the solution by means of dialysis against deionized water for 48h (using a dialysis tube of 12400 MWCO). To preserve the material integrity, Gel-Tyr was lyophilized in a LyoQuest (Telstar Life Science Solutions, Japan) at -80°C and sealed in Falcon tubes for any further use.

3.3. Synthesis of HA-Tyr

For the HA tyramine grafting, first, HA of low molecular weight (LMW-HA) (around 320 000 Da) needed to be obtained from acid degradation of the commercial high molecular weight HA (HMW-HA) (229). The selection of LMW-HA was determined by the impossibility of filtering HA solutions of high molecular weight for their sterilisation and later use in culture assays, even when employed at low densities. To do so, a solution of 500 mL was prepared at 0.1% (w/v) of HA of high molecular weight, reducing its pH to 0.5 with the addition of HCl and keeping in agitation for 24h at 37°C. Subsequently, pH was adjusted to 7 with NaOH and dialysed against distilled water for 3 days (using a dialysis tube of 3500 MWCO) to purify the solution. Finally, low molecular weight HA was lyophilized at -80°C for 4 days.

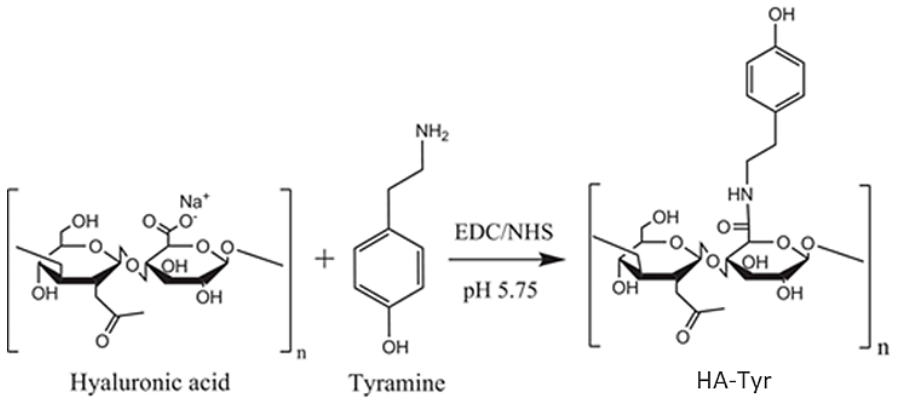

Figure 17. Tyramine graft chemical reaction in presence of HA chains. EDC and NHS are used as catalysers and activators of the reaction (32).

As in Gel, tyramine grafting in HA chains aims the obtention of molecules with phenol moieties capable of reticulating in the presence of HRP and H_20_2 to form injectable hydrogels. The chemical reaction follows the same path as with gelatin, generation of amine groups as a result of the reaction between carboxyl groups of hyaluronic acid and free amino groups of tyramine.

The synthesis of HA-Tyr was performed following the protocol described by *Darr and Calabro* (230), where the employed molar ratios were:

Tyr:COOH	EDC:COOH	EDC:TYR	NHS:EDC
2:1	1:1	1:2	1:10

Table 2. Molar ratios used for tyramine graft reaction in hyaluronic acid.

To obtain HA-Tyr, we prepared a solution of 20 mL at 150 x 10^{-3} M NaCl in mQ water, added 0.276 M MES and 75 x 10^{-3} M NaOH under stirrer until complete dissolution. Then, pH was adjusted to 5.75 and 0.1 g of low molecular weight HA was added to the solution and kept in agitation at 500 rpm for 2 hours at room temperature. Once LMW-HA was dissolved, 86.5 mg hydrochloride of tyramine was included and stirred for 20 min at room temperature. The pH was again adjusted to 5.75 and 47.77 mg EDC and 2.8 mg NHS were added to the solution, which was afterwards under stirrer at 37°C for 24h. For the next 2 days, the solution was dialysed against deionized water at 150 x 10^{-3} M NaCl for 24h and against distilled water for another 24h (using a dialysis tube of 3500 MWCO). To preserve the material integrity, HA-Tyr was finally lyophilized at -80°C and sealed in Falcon tubes for further use.

3.4. Gel/HA hydrogel formation

Gel-Tyr/HA-Tyr conjugates hydrogels reticulate through enzymatic oxidative reactions of the phenol moieties in the polymer's side chain, catalysed by HRP (horseradish peroxidase) and consuming H_2O_2 as co-substrate. The oxidative coupling of phenol moieties occurs via carbon-carbon bond at the ortho positions or via carbon-oxygen bond between the carbon at the ortho position and the phenoxy oxygen position, where the gelation time will be dependent on the concentration of both catalysts (231) (HRP and H_2O_2), the proportion Gel/HA (232), the degree of substitution of carboxyl groups obtained, and the concentration of polymer in solution (233).

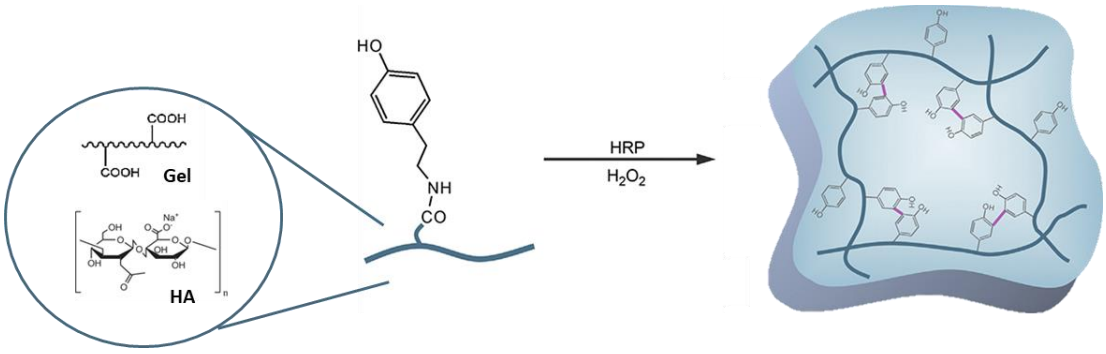

Figure 18. Hydrogel formation of Gel/HA conjugate hydrogels in the presence of HRP and H2O2 as catalysers (234).

First, 2 % w/v Gel-Tyr and 2 % w/v HA-Tyr solutions were prepared in CF-KRB, keeping HA tyramine conjugate at 4°C overnight and Gel-Tyr at 37°C for 30 min before use. Once they were fully dissolved, solutions with different proportions of Gel/HA were obtained

(100/0, 70/30, 50/50, 30/70, 0/100). Finally, 50 µL hydrogels were prepared by mixing 80 vol% of the Gel/HA mixtures with 10 vol% of 12.5 U mL^{-1} HRP (1.25 U mL^{-1} in the final volume) and 10 vol% of 20 x 10^{-3} M H_2O_2 (2 x 10^{-3} M in the final volume).

To check whether the droplets were completely gelified or not, samples were removed carefully from the parafilm with the help of a spatula.

3.5. Degree of substitution of the modified Gel-Tyr and HA-Tyr

The degree of substitution of tyramine may be explained in this case as the percentage of phenol moieties found in the polymer's side chains, replacing the activated carboxyl groups (COOH) after the tyramine graft chemical reaction. In Gel-Tyr and HA-Tyr hydrogels, the degree of substitution is considerably constant, providing a useful parameter for both grafting verification and reproducibility evaluation among different batches.

To determine the degree of substitution of the tyramine phenolic groups in Gel and HA, solutions of 0.1% (w/w) were prepared for each material, measuring their absorbances with a double beam UV spectrophotometer (CECIL CE9200 UV/VIS, Buck Scientific, Norwalk, CT, USA) at 275 nm and using as reference a calibration curve of known tyramine concentration solutions. At this wavelength, absorbance values for pure Gel and HA were 0 due to the negative presence of tyramine phenolic groups.

3.6. Gelation time

To ensure the cross-linking process was completely achieved, 50 µL hydrogels of each Gel/HA mixture (100/0, 70/30, 50/50, 30/70, 0/100) were prepared on a parafilm surface and cross-linked. Gelation time was taken as the time when the hydrogels could be detached as a unit from the surface.

$$\text{Substitution degree (\%)} = \frac{Tyr\ (mM)}{COOH\ (mM)} \cdot 100$$

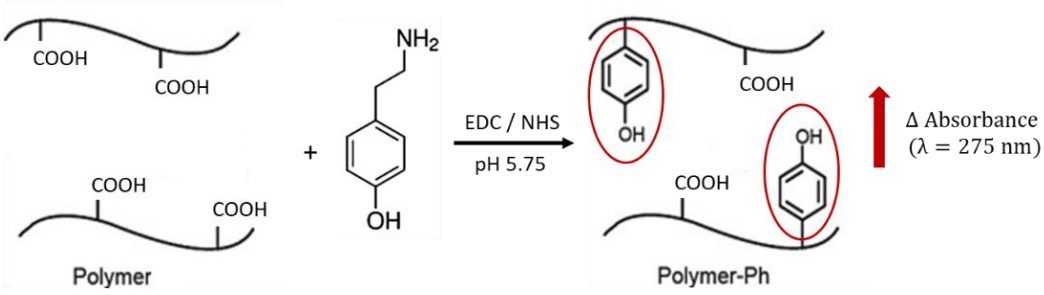

Figure 19. Analysis of the Gel-Tyr and HA-Tyr substitution degree after graft chemical reaction.

To assess the influence of both catalysts, HRP and H_2O_2, over the gelation process, gelation time was also obtained from the cross-linked droplets under different concentrations of both catalysts, HRP (1.25 U/mL, 10 U/mL, 20 U/mL) and H_2O_2 (3 mM, 4 mM, 5 mM).

3.7. Cell cultures for Gel/HA hydrogels

Murine C2C12 myoblasts were expanded in Dulbecco's Modified Eagle Medium (DMEM, + 4.5 g/L + L-glutamine, Gibco) with 1% penicillin/streptomycin (P/S, Gibco) and 20% fetal bovine serum (FBS, Gibco) at 37°C and 5% CO2. Cells were thawed at least two days before carrying out any assay, changing the medium the following day and always seeded under their 10^{th} passage. For each seeding, the medium was removed from flasks (T75-T175) after expansion (always under 70% confluence), then washed with DPBS—before adding trypsin/EDTA (Sigma-Aldrich) to the culture. Flasks were incubated then for 3 minutes at 37°C and trypsin was neutralised with (DMEM+ 1% P/S + 20% FBS). Cells were finally counted using a Neubauer chamber. For cell culture assays, concentrations of $4x10^6$ cells/mL to $8x10^6$ cells/mL were used depending on the culture type (viability – differentiation), being the final volume of the hydrogels of 50 µL.

3.7.1. Hydrogel formation for cell culture experiments

2% w/v Gel-Tyr and HA-Tyr solutions were prepared by dissolving the lyophilized powder in sterile CF-KRB buffer, leaving HA-Tyr solution overnight at 4°C and Gel-Tyr at 37°C for 30 min before use. Once the solutions were completely dissolved, they were filtered through a 0.22 µm syringe filter and distributed among the different compositions in the following ratios of Gel/HA (100/0, 70/30, 50/50, 30/70, 100/0). 12.5 U mL^{-1} HRP solution was then added to the prepared solutions at a volume ratio of 10/80 (HRP solution/ (Gel/HA) solution) and cells were centrifuged (1000 rpm, 5 minutes) and resuspended in media before being added to each HRP + Gel/HA mixture. After every step, solutions were kept in a warm bath to assure constant temperature.

At last, 45 µL of each composition were crosslinked with 5 µL of 20 x 10^{-3} M H_20_2 on a parafilm surface and deposited on each well of the cell culture plate. Finally, medium (DMEM + 1% P/S + 20% FBS) was added to each well and incubated at 37°C. 3 replicates were always used per each composition, taking 5 pictures per replicate, both positive controls cultured with ethanol (cytotoxic) and negative controls on glass were also included.

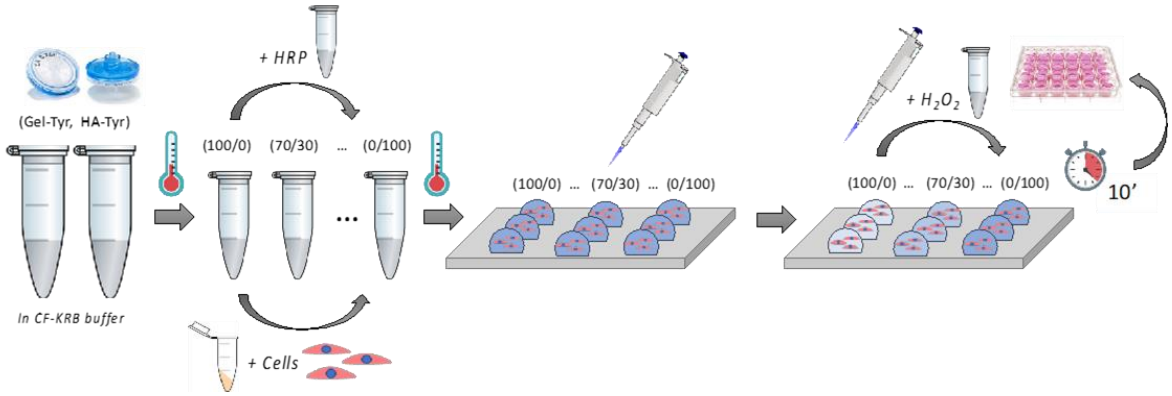

Figure 20. Schematic workflow of manual cell encapsulation and hydrogel formation for cell culture.

3.7.2. 3D printing of Gel/HA hydrogels

Hydrogel precursor solutions used for bioprinting calibration and culture assays were obtained following the same protocol of hydrogel formation and cell encapsulation in control samples.

The bioprinter used for this project was a Biosafety 3DDiscovery™ Evolution system from the company REGENHU (Villaz-St-Pierre, Switzerland) with two different modalities: extrusion-based and droplet-based (micro-valve) printing. UV sterilization and droplet calibration were always performed before any cell printing assay to assure volume accuracy in the cell-laden mixture and the cross-linking solution. Once the desired droplet volumes were established, bioink 2% (w/v) Gel/HA in the company of HRP enzyme and cells (4 – 8 x 10^6 cells/mL) were added into a sterilized commercial syringe (3 mL) with a chamfered 25 G cylindrical tip (Nordson EFD, United States) with the controlled holding temperature of 37°C-39°C.

The required number of samples (25-50 µL, n=3 per composition) were printed on demand onto the substrate (parafilm or non-treated multi-well plate) with a flowing rate of 10 – 20 $\mu L \cdot s^{-1}$ and pressure of 5 - 25 kPa for droplet formation, 5 – 10 $\mu L \cdot s^{-1}$ and 4 – 8 kPa for cross-linking injection and a valve opening time of 25 – 80 ms at 10 – 16 kPa for cross-linking ejection. Non-treated surfaces were selected to assure correct droplet shapes given the high wettability properties of the bioink solutions.

Once samples were cross-linked on parafilm, they were translated to a cell culture multi-well plate and left in the incubator at 37°C until complete gelation (≈ 20 min). Samples

printed directly on the well plate were excluded from this step. Finally, cell media was added to each well and incubated at 37°C and 5% CO_2 using growth media (GM) (DMEM + 1% P/S + 20% FBS) for viability and cell adhesion assays or differentiation media (DM) (DMEM + 1% P/S + 1% ITS-X) for the required period of time (3h-7d).

3.7.3. Cell viability assay (LIVE/DEAD)

To determine cell viability and cytotoxicity of the cross-linking process of the Gel/HA hydrogels, a Live/Dead cell viability/cytotoxicity kit assay (Invitrogen) was used. The Live/Dead assay provides a simultaneous determination of the living and dead cells of a sample through a two-colour fluorescence detection system (Calcein-AM, EthD-1). The polyanionic dye calcein is a cell-permeant dye that becomes fluorescent by entering in contact with live-cell esterase inside viable cells, whereas EthD-1 enters cells with damaged membranes, like the ones found in dead or dying cells, and binds to nucleic acids [50].

C2C12 cells were harvested and seeded at 4 x 10^6 cells/mL, within a 24-well plate, in (DMEM+ 1% P/S + 20% FBS). Cell viability was analysed at 3 h, 1 d and 4 d after seeding in hydrogels with different H_2O_2 concentrations. The medium was removed from the plate wells and hydrogels were washed with DPBS-- twice. Samples were then incubated with Live/Dead solution (1:4 calcein/ethidium) in DPBS-- at 37°C for 20 min, washed again in DPBS-- and observed in an EVOS microscope. 3 replicates were used per each composition, taking 5 pictures per replicate, both positive controls cultured with ethanol (cytotoxic) and negative controls on glass were also included.

Images were processed with the ImageJ 1.58j8 software, where cell viability was calculated as the fraction of live cells among the total number of cells. The total number of cells was used as a cell density parameter for 3h time point, whereas for 4d time points, cell count was used as a non-spread morphology parameter.

3.7.4. Cell adhesion assay (Phalloidin/DAPI)

To analyse the interaction between cells and substrates, cells were immunostained to localize nuclei and actin cytoskeleton. This assay was helpful to study the differences in cell morphology caused by the different gelation methodologies.

C2C12 cells were harvested and seeded at 4 x 10^6 cells/mL again, within a 24-well plate, in (DMEM+ 1% P/S + 20% FBS). Cell morphology was analysed at 7d in different

compositions and with different H_2O_2 concentrations. Hydrogels were washed twice with PBS after media removing, fixed with 4 % formaldehyde for 30 min and washed again twice. Blocking buffer (BB) and washing buffer (WB) were prepared in PBS/1%BSA/0.02% Tween 20, and PBS/0.5% Tween 20 respectively. Cells were then permeabilized with 0.1% Triton X-100 in PBS for 20 min, rinse and block with BB for 1 hour. Samples were subsequently incubated with phalloidin (1:200) (Alexa Fluor-488), which stains the actin filaments, in BB for 2 hours), and washed at least 5 times with WB. For nuclei staining, samples were incubated with NucBlue™ for 20 min and washed at least 2 times in WB and one last time in PBS before image acquisition with an inverted Zeiss Axio Observer Z1 fluorescence microscope. Images were again processed with the ImageJ 1.58j8 software. Each washing step during the entire protocol was carried out for 5 minutes in gentle agitation.

ImageJ 1.58j8 software was used to analyse the immunostained pictures, where cell density was calculated as the total number of cells counted per image and then normalized by surface. Cell growth factor was obtained as the ratio between the final cell number and the original cell number.

3.7.5. Myogenic differentiation assay

C2C12 cells were cultured at a seeding density of 8 x 10^6 cells/mL, within a 24-well plate for 7 days at 37°C. Cells were cultured under differentiation conditions (DMEM + 1% P/S + 1% Insulin-Transferring-Selenium-X (ITS-X, Gibco)) once the cells were properly attached to the surface.

After the culture, cells were fixed, permeabilized and blocked following the same protocol as the adhesion assay. Samples were then stained for sarcomeric myosin with mouse primary antibody (1:250) (MF-20, Developmental Studies Hydridoma Bank), which stains the sarcomeric myotubes, in BB at room temperature for 2 hours; washed several times with WB and then secondary conjugated antibody (1:200) (Cy3 a-mouse) was incubated in BB with phalloidin (1:200) at room temperature for another 2 hours. Samples were then washed at least 5 times and one last time in PBS before image acquisition. Each washing step during the entire protocol was carried out for 5 minutes in gentle agitation.

3.8. Design and calibration of the bioprinting system

Bioprinting in three dimensions (x, y, z) is permitted by a mobile block of printheads and a build platform. During the printing process, 2D dispensing is performed side-to-side (x) by the printhead over the build platform, where the latter is responsible for the system´s back-to-front (y) movement. Once a layer is finished, the printhead´s top-to-bottom or vertical (z) motion allows layer-by-layer displacement, generating the designed 3D object.

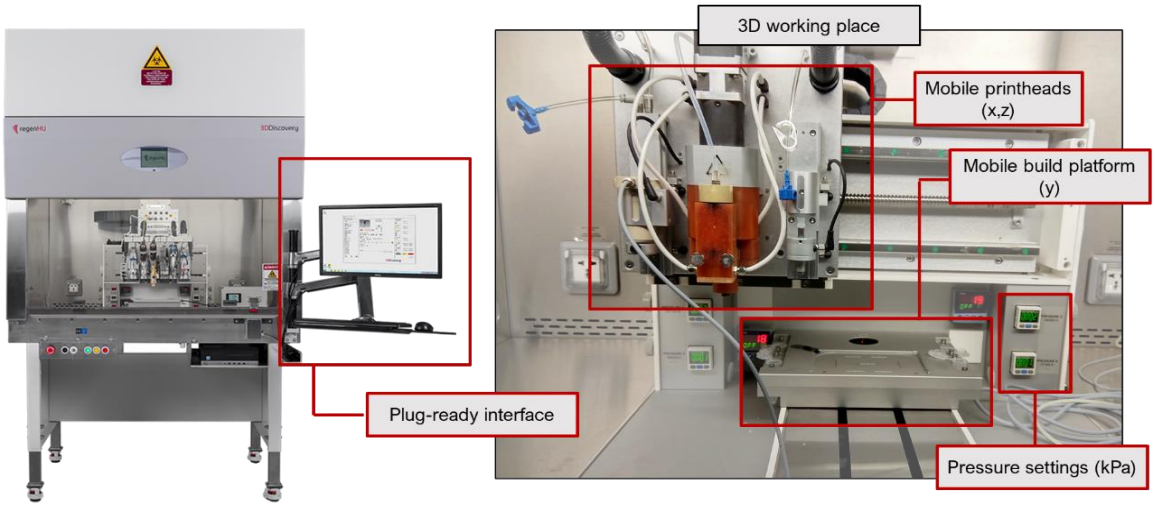

Figure 21. Biosafety 3DDiscovery™ Evolution bioprinting system.

The bioprinter used for this project was a Biosafety 3DDiscovery™ Evolution system from the company REGENHU (Villaz-St-Pierre, Switzerland). Pressure settings can be manually adjusted for each printhead at any moment of the deposition while being visually displayed on both right and left panels inside the cabinet. Platform and cartridge heaters are also available during the printing process in case of working with temperatures higher than room temperature. Besides, the build platform offered the possibility to work not only with traditional printing beds such as coverslips or petri dishes but also with multi-well culture plates, which facilitates sample handling.

Our system counted with 3 different printing modalities: a piston-driven pneumatic extruder, a microvalve system also driven by a pneumatic piston, and a fused deposition modelling system. Due to the early stage of this research and the system´s incompatibility with hydrogel bioinks, FDM usage was discarded from the bioprinting process. The printing protocols for calibration and hydrogel printing were designed with the Software Suite BioCAD™ (REGENHU, Switzerland) included in the system, which is based on commonly known CAD design tools. Hydrogel and cross-linker solutions were prepared in a similar way to the

manual protocol and were later introduced into Optimum 3cc Syringe Barrels or Cartridges (Nordson EFD, United States) for their dispense.

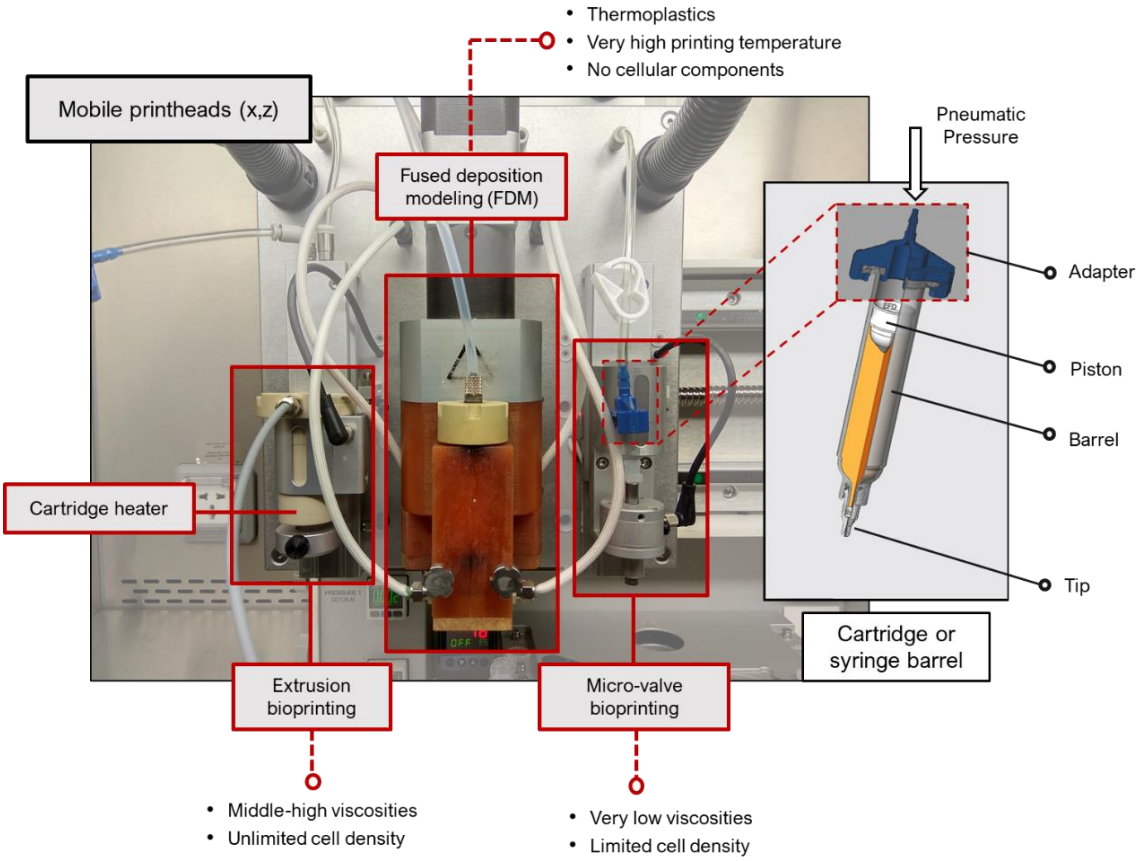

Figure 22. Printhead modalities in the 3D printing system: pneumatic extrusion, fused deposition modelling, and a DOD micro-valve.

3.8.1. Design of the bioprinting protocol

The printing protocol design was based on the limitations of the two left printing modalities and the Gel/HA bioink solutions. This project aimed to design a viable bioprinting protocol for the automated dispensing and generation of enzymatically cross-linked Gel/HA hydrogels in multi-well plates for their further assessment in drug screening and delivery. Initially, Gel/HA precursor solutions enzymatically reticulate in contact with HRP and H_20_2, where the latter results cytotoxic when concentrations are high enough. Likewise, the cross-linking process once started occurs within minutes, rapidly increasing the overall viscosity of the bioink and directly affecting flow rate, the physical integrity of the construct and shear stress sensed by the embedded cells.

Therefore, in a similar way to the manual hydrogel formation, it is important to separate the printing process into two different steps, 1) droplet formation and posterior 2) cross-linking addition.

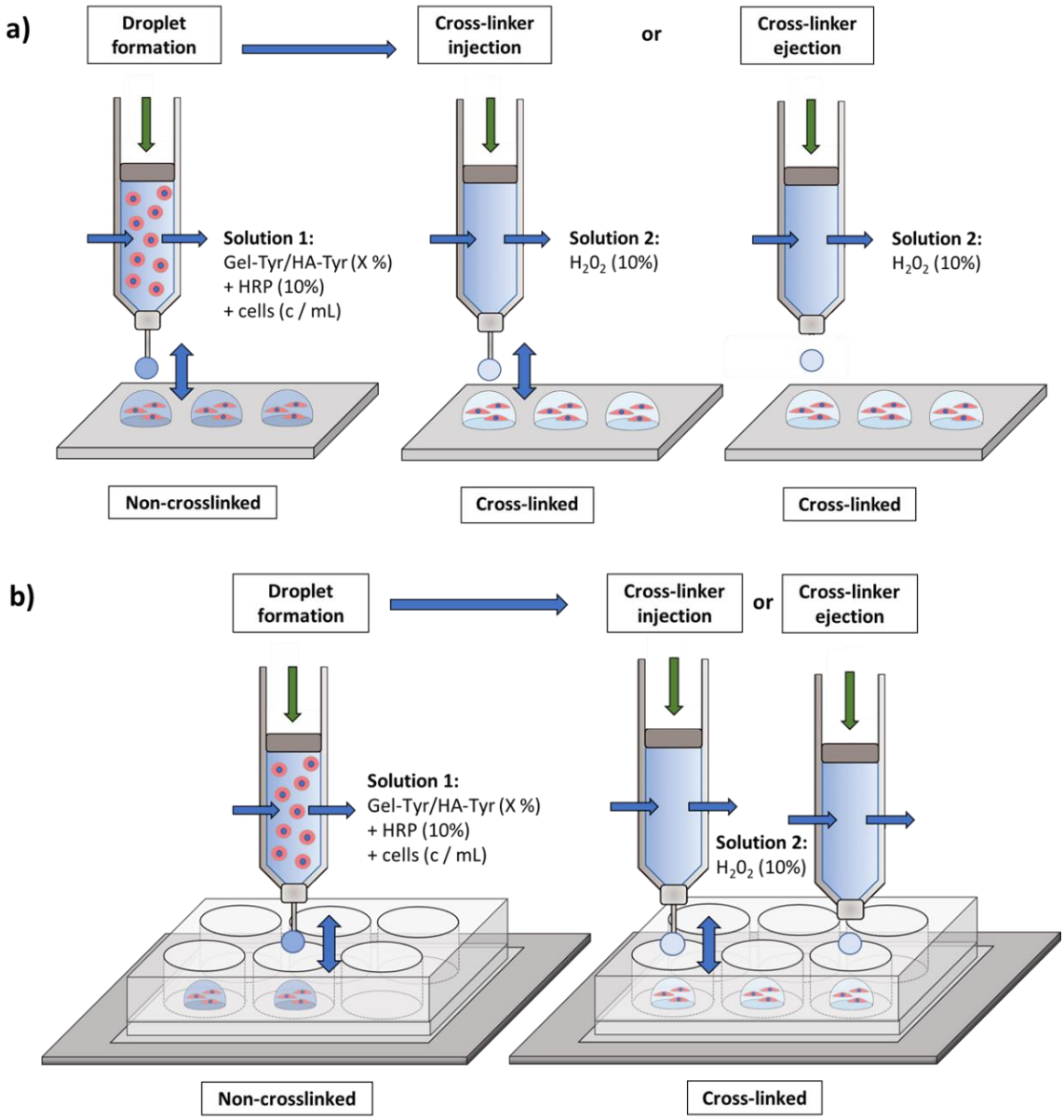

Figure 23. Conceptual design of the bioprinting protocol: (a) Protocol calibration and testing in a hydrophobic substrate and (b) final protocol printing in culture multi-well plates.

On the other hand, 2% Gel/HA solutions are poorly viscous, acquiring water-like consistency at physiological temperature (< 10 mPa s). Very low viscosities benefit from droplet-based technologies such as the micro-valve (1-70 mPa s) (187,188), where sample volumes can easily reach the nanoscale with excellent reproducibility and accuracy; however, cell sedimentation is generally the main concern in long printing times, leading to

clogging issues at relatively high cell densities (> 3 x 10^6 cells/mL) (185). In situations where higher cell concentrations are used, as is the case of this project (4-8 x 10^6 cells/mL), micro-valve bioprinting is not considered the best alternative for droplet formation. Extrusion bioprinting offers no limitation in cell density and bioink viscosity, although it is strongly recommended for materials with middle-high viscous properties given the problems of spreading, time lags and lack of consistency attributable to constructs with low viscosity. For all these reasons, droplet formation was decided to be performed using extrusion whereas cross-linking process could be implemented in both modalities. Apart from this, the protocol´s design was divided into two stages: calibration, where samples would be dispensed in a hydrophobic surface similar to the bottom of the well, introduced into a culture plate and analysed; and final bioprinting, where samples would be dispensed from the beginning in each well.

This protocol presents some main advantages: first, it provides the researcher with some versatility depending on the 3D printer´s available modalities, number of printheads and project´s budget; second, it establishes a useful starting point for the improvement of either materials with similar properties or slightly different ones; and on top of that, it facilitates their possible use in multi-material bioprinting in the long run.

3.8.2. Calibration of the bioprinting protocol

Once the bioprinting protocol was decided, operational parameters in both modalities were considered and adjusted to assure the printing process did not present any harmful effects to the cells survival, was easily reproducible and accurate in solution dispensing.

The printed droplet volumes can be directly or indirectly set by the modification of the available operational parameters of the 3D printing system in question. In this case, the required droplet volumes were mainly obtained by the adjustment of the printing pressure and the time of application, the nozzle gauge and geometry, printing distance to the surface and the cartridge temperature.

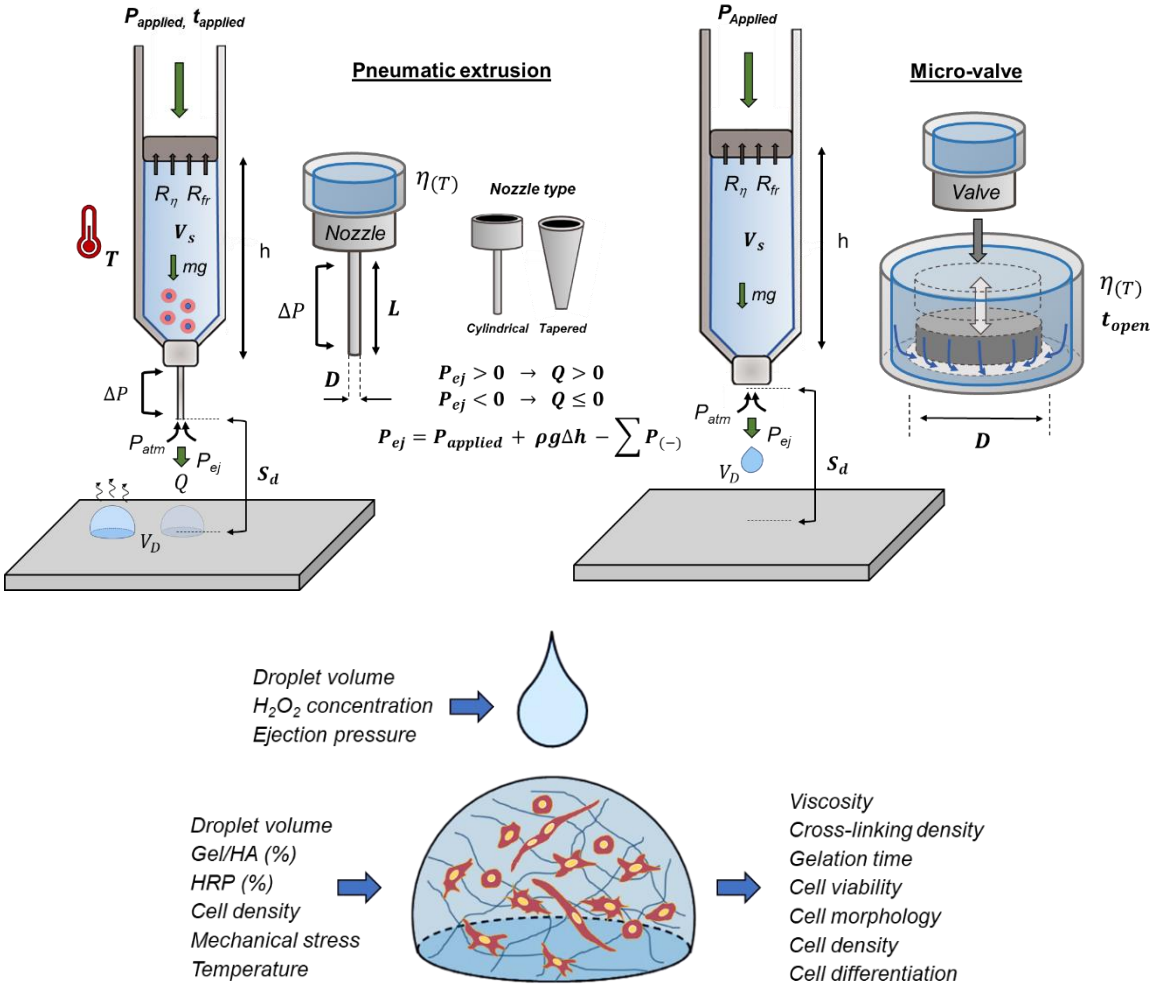

Figure 24. Illustration of the operational parameters of both modalities, pneumatic extrusion and micro-valve bioprinting, and bioink characteristics. Operational parameters of the system include the pneumatic pressure applied ($P_{Applied}$), cartridge temperature (T), the volume of solution (V_s) inside the cartridge, standoff distance (S_d) and nozzle geometry such as inner diameter (D), length (L) or type. Modification of these parameters is responsible for changes in viscosity, flow rate and shear stress. Printing time is described by a different parameter in each modality, where $t_{applied}$ in extrusion is defined as the time in which pneumatic pressure is applied, and t_{open} represents the time in which the valve gate is unblocked by the plunger during pressure application. Modification of bioink composition also affects its physical properties and cell viability.

Nozzle selection and flow rate

Flow rate during printing was analysed in three different types of 25 G (D = 250 µm) nozzle tips: general-purpose, chamfered, and tapered (Nordson EFD, United States). General-purpose tips are made of polished passivated stainless steel for a wide range of fluids and applications, where tips ending in chamfered shaped allow microdot applications of low viscous fluids. On the other hand, tapered tips are normally made of plastic and are recommended for smooth flows in applications for medium-to high-viscosity fluids.

To assess the influence on flow rate produced by the applied pressure ($P_{applied}$) and the cartridge volume (V_s), both parameters were set at different values, $P_{applied}$ (4 kPa, 5 kPa, 6 kPa) and V_{sol} (1 mL, 2 mL, 3 mL). To discard possible viscosity interferences at the nozzle tip, buffer solution was used for the dispensing ($\eta \approx 1$ mPa·s^{-1}) at room temperature (T_{room} = 17°C - 20°C).

Individual droplets ($V_d \leq 10$ µL, $n \geq 4$) were dispensed on a parafilm substrate at different time shots ($t_s \leq 0.7$s) at the same standoff distance (h=0.3 mm) where flow rate (Q) in each case was calculated as the droplet final volume divided by its dispensing time. Droplet volume was approximately obtained from each sample by means of a 20 µL micropipette (Eppendorf).

Flow gradient was calculated as the slope of the regression line for each data set of $P_{applied}$ and V_{sol} as a descriptor of flow rate variability.

Density and viscosity approximation

Density of the different precursor solutions was calculated based on Gel and HA density of dry polymer, ρ_{gel} = 1,44 g·cm^{-3} (235) and ρ_{HA} = 1,229 g·cm^{-3} (236) and buffer solution ($\rho \approx$ 1 g·cm^{-3}). Ideal behaviour was assumed to estimate the density of the mixtures (70/30, 50/50, 30/70), using the mass fraction (*X)* and density of pure Gel and HA hydrogel solutions at x w/v (%) ($\rho_{(x\%)}$), as well as the volume fraction of the mixtures.

$$\rho_{solution} = \frac{1}{(X_1/\rho_1) + (X_2/\rho_2)} \qquad \begin{matrix} X_1, \rho_1 = dry\ polymer \\ X_2, \rho_2 = buffer\ solution \end{matrix} \qquad \text{(Eq. 1)}$$

$$\rho_{blend} = \left(\frac{V_{gel(x\%)}}{V} \cdot \rho_{gel(x\%)}\right) + \left(\frac{V_{HA(x\%)}}{V} \cdot \rho_{HA(x\%)}\right) \qquad \text{(Eq. 2)}$$

Relative viscosity values were roughly approximate at 37°C for further calculation by following Hagen-Poiseuille´s flow equation (102):

$$Q = \frac{\pi \Delta_P R^4}{8\eta L} \quad \text{(Eq. 3)}$$

where Q is the dispensing flow rate (m^3/s), Δp is the pressure drop between the beginning and the end of the nozzle tip (Pa), R is the inner radius of the nozzle tip (m), η is the dynamic viscosity of the bioink (kg/(m·s)), and L is the length of the nozzle tip. The apparent viscosity of the buffer solution (mQ water in its vast majority) was taken as a reference point (η ≈ 1) for direct comparison.

Calculation of Reynolds number, shear stress and pressure drops intervals

Shear stress inside the barrel and nozzle tip was previously calculated to assure no damage to the cell suspension during the printing process. The nature of flow can be verified through the calculation of Reynold´s number (R_e), which determines flow conditions:

$$Re = \frac{\rho Q}{15\pi D\eta} \quad \text{(Eq. 4)}$$

where ρ is the density of the bioink (kg/m^3), Q is the dispensing flow rate (m^3/s), D is the diameter of either the syringe barrel or the nozzle tip (m), and η is the dynamic viscosity of the bioink (kg/(m·s)). In laminar regimes (Re < 2100), the velocity profile is stable and parabolic across the diameter, finding the maximum shear stress at the barrel wall. In these cases, the wall shear stress, τ_{wall} (N/m^2 = Pa), for each flow rate can be easily calculated according to Hagen-Poiseuille´s equation (Eq. 3):

$$\tau_{wall} = \frac{4Q\eta}{\pi R^3} \quad \text{(Eq. 5)}$$

where Q is the dispensing flow rate (m^3/s), η is the dynamic viscosity of the bioink (kg/(m·s)), and R is the inner radius of either the syringe barrel or the nozzle tip (m).

Shear stress effect on cells will be dependent on the cell type, the level of force exerted on cells and the time of application. Theoretical values for pressure drop inside the nozzle tip were also represented using (Eq. 3) to show tip diameter, bioink viscosity and flow rate influence. Printing pressures must be always above the pressure drop value for the generation of a positive flux gradient. Bioinks in this study were considered Newtonian (n=1) for all calculations.

Evaporation rate approximation

The evaporation rate of different droplet sizes of buffer solution was experimentally obtained using a Theta optical tensiometer (Biolin Scientific, Stockholm, Sweden). Images were taken every 100 seconds for 15 mins at room temperature. Droplet height and contact radius were obtained with help of the ImageJ 1.58j8 software for each image, where droplet volume was approximately adjusted and calculated afterwards using the formula of the spherical cap:

$$V_c = \frac{\pi h_d}{6} \cdot (3r_c^2 + h_d^2) \qquad \text{(Eq. 6)}$$

where V_c is the droplet volume (µL), h_d is the droplet height (mm), and r_c is the droplet contact radius. The evaporation rate was then expressed as the volume loss per unit of time for different initial droplet volumes.

Cell sedimentation rate

Cells suspended in poorly viscous solutions ($\rho < \rho_{cell} = 1.1$ g/mL) (237) tend to sediment due to gravity´s action. The sedimentation rate of cells was calculated using the following formula:

$$v_s = \frac{d^2(\rho_c - \rho_v)g}{18\eta} \qquad \text{(Eq. 7)}$$

where v_s is the sedimentation rate (m/s), d is the cell diameter (m), ρ_c *and* ρ_v are the density of the cell and the solution (kg/m3) respectively, g is the gravitational acceleration (m/s^2), and η is the dynamic viscosity of the bioink (kg/(m·s)).

Standoff distance and physical printing design in CAD environment

Standoff distance calibration plays an important role in both steps of the bioprinting protocol, (1) droplet formation and (2) cross-linking injection or ejection, and hence it is necessary to adjust it before printing.

For droplet formation and cross-linking, standoff distance calibration was based on the droplet height and reference values shown in literature for microextrusion and droplet-based modalities. Droplet height for the different Gel-Tyr droplet volumes (1 µL - 50 µL) was obtained via image from the optical tensiometer, where the height of each sample was calculated using ImageJ 1.58j8 software.

Standoff distance intervals obtained in this part of the study were afterwards used for the adjustment of the physical operational parameters involved in the different stages of the bioprinting protocol.

3.9. Statistical analysis

Data were reported as mean-standard deviation. Pre-processing and normalization of data with the D'Agostino-Pearson omnibus test were performed to assure normal distribution. Analysis of statistical differences was conducted using student T-test and One-way ANOVA (Graphpad Prism 6.0) for two-sample comparison or different groups respectively, using a Tukey HSD post hoc test to compare the different groups for normal distributions or a Dunn´s test on the contrary case. Differences were considered significant $*p \leq 0,05$.

4. Results and discussion

4.1 Degree of substitution

The degree of substitution can be explained in this case as the number of phenol moieties found in the polymer's side chains per 100 COOH molecules. This parameter was quantified by means of a spectrophotometer (238), determining the concentration of tyramine graft in Gel and HA chains at 275 nm. The degree of substitution obtained for Gel was $4.16x10^{-4}$ mol Tyr/mg whereas HA obtained a value of $2.57x10^{-4}$ mol Tyr/mg. These values, divided by the COOH mol/mg in each polymer, resulted in an average percentage of substitution of 34.64% and 6.5% respectively, which agreed with previous results (171).

Product	Absorbance (a.u)	[Tyr] grafted (mol/mg)	Substitution degree (%)	Average (%)
Gelatin-Tyr	0.1032	4.13E-04	34.43	
Gelatin-Tyr	0.1033	4.14E-04	34.46	
Gelatin-Tyr	0.1050	4.20E-04	35.03	34.64 ± 0.34

Product	Absorbance (a.u)	[Tyr] grafted (mol/mg)	Substitution degree (%)	Average (%)
HA-Tyr	0.0623	2.49E-04	6.30	
HA-Tyr	0.0663	2.65E-04	6.71	6.5 ± 0.29

Table 3. Degree of substitution in Gel-Tyr and HA-Tyr hydrogels.

4.2 Gelation times

	Gelation time (min)					
Gel/HA hydrogel	HRP / H_2O_2 1.25 u/mL / 2 mM	HRP (u/mL) 10 u/mL	HRP (u/mL) 20 u/mL	H_2O_2 (mM) 3 mM	H_2O_2 (mM) 4 mM	H_2O_2 (mM) 5 mM
Gel-Tyr	6.4 ± 1.1	4.3 ± 0.5	4 ± 0.4	4.2 ± 0.4	3.4 ± 0.6	3.1 ± 0.7
70/30	6.9 ± 0.5	3.2 ± 0.6	3 ± 0.4	4.4 ± 0.4	4.2 ± 0.3	4.0 ± 0.4
50/50	6.5 ± 0.6	2.2 ± 0.5	2.2 ± 0.5	3.5 ± 0.3	3.3 ± 0.4	3.2 ± 0.4
30/70	7.1 ± 0.6	2.0 ± 0.4	1.4 ± 0.2	5.5 ± 0.3	5.2 ± 0.5	3.0 ± 0.5
HA-Tyr	9.4 ± 1.5	1.5 ± 0.3	1.2 ± 0.2	6.6 ± 0.4	5.5 ± 0.5	5.1 ± 0.3

Table 4. Gelation experimental time values of 2% (w/v) Gel/HA hydrogels depending on HRP and H_2O_2 final concentrations. One of the catalysers was always kept constant to assure no interaction effects.

In ***Figure 25,*** it is visible how pure HA and all Gel/HA hydrogels are transparent, whereas pure Gel samples became translucent during the cross-linking process.

Figure 25. Droplets of the different 2% w/v Gel/HA hydrogels (50µL, n=3) were used to determine samples cross-linking time. Pure Gel-Tyr (100/0) hydrogels developed a whitish hue, becoming translucent, while the rest of the compositions remained transparent. Gelation time was estimated as the time when hydrogel samples could be detached as a unit from the parafilm surface.

As it was expected and observed in ***Table 4***, gelation time in the different hydrogels Gel/HA 2% w/v increased with the proportion of hyaluronic acid in the composition, with time values from 5 min (for pure Gel samples) to 10 min (for pure HA samples). Similar time values were obtained in other studies (171), which in addition to the values obtained through the analysis of the degree of substitution, suggests similar cross-linking and mechanical behaviour to the hydrogels synthesized following the same procedure in previous research (171, 118, 119).

HA in CF-KRB solutions is more viscous than Gel at the same weight/volume percentage, meaning precursor solutions viscosity hinders catalysers diffusion and slow down the gelation process (18, 171). Lower degrees of substitution in HA-Tyr, in comparison to Gel-Tyr, may be also involved in longer cross-linking reactions.

As it is reflected in ***Table 4,*** gelation times in all compositions were significantly reduced when the concentration of any of the catalysers HRP/H_2O_2 was increased at constant polymer concentration.

HRP catalyses the cross-linking reaction, oxidizing two tyramine molecules in each cross-linking cycle, with H_2O_2 as oxidant co-substrate (239). Increasing the quantity of H_2O_2 in solution reduced gelation time in all samples according to their proportion of HA, following a similar trend to the original HRP/H_2O_2 ratio. In the presence of excess H_2O_2, HRP can adopt sometimes an inactivated configuration due to excess oxidation (241); despite this, all compositions reduced their gelation times each time H_2O_2 was increased, meaning excess H_2O_2 regarding HRP inactivation was not achieved in any condition. Changes in the cross-linking time were more sudden in blends with higher HA ratios when using HRP. This is caused by an acceleration of the rate of formation of tyramine cross-links (240), which is closely related to the quantity of available HRP in the solution.

Explained from a physical perspective, HRP molecules are evenly distributed inside the precursor solution whereas H_2O_2 molecules are only introduced when the cross-linking reaction is required. When HRP concentration is low, H_2O_2 molecules in diffusion have to cover longer distances inside the solution to reach neighbour HRP molecules to start the cross-linking process. Provided one HRP molecule can only oxidize two tyramine molecules per cycle in presence of H_2O_2, the cross-linking time in a determined location will be mainly dependent on the number of cross-links per unit of time generated by each HRP molecule nearby. Therefore, if the number of H_2O_2 molecules is increased at constant HRP, the rate of formation of cross-links in the area won't be affected. Yet, the chances of H_2O_2 reaching new HRP molecules in other areas of the precursor solution will increase. In the particular case of hydrogels with higher contents of HA, whose molecule chains are considerably more rigid than gelatin ones, increasing the formation of tyramine cross-links will cause a faster obtainment of structural integrity, even at lower diffusion power and cross-linking densities.

Control of gelation time and precursor solutions of low polymer concentration possess several advantages for drug delivery vehicles and injectable scaffold applications. Fast gelation times are required for in situ local drug delivery to prevent the diffusion of hydrogel precursor solution, drugs and growth factors out of the target site or the surrounding hydrogel formation. On the other hand, slower gelation times are desirable in injectable scaffold applications for tissue engineering to correctly fit the defect site.

3D printing systems benefit from precursor solutions of low polymer concentration and fast gelation times due to their facility to encapsulate bioactive molecules or cells in the hydrogel matrix without losing their physical integrity during printing. In our system, it is necessary to use minimum H_2O_2 concentrations since the remaining H_2O_2 can induce cytotoxicity

effects. H_2O_2 changes to H_2O and oxygen after decomposition via the enzymatic reaction, which means it should be possible to obtain high cell viabilities provided that the remaining H_2O_2 in sample is negligible. This can be achieved by optimising HRP/H_2O_2 ratios as well as the number of possible tyramine cross-links without significantly modifying hydrogel´s mechanical properties.

Selection of the calibration surface

To assure a correct calibration, hydrogels wettability and shape were also analysed with the help of the optical tensiometer on different substrates, looking for similar characteristics to the one we would usually obtain in cell culture multi-well plates, which would be the ultimate printing bed of the system. Glass hydrophilic nature produced significant spreading issues on samples, which could lead to excessive evaporation and gelation irregularities. Plastic petri dishes, on the other hand, generate similar contact angles to parafilm, being both hydrophobic surfaces and more convenient for droplet calibration and gelation. Plastic petri dishes and cell culture well plates are conventionally made of non-treated clear polystyrene, and in theory, they should possess similar wettability properties. Given that, parafilm layers make a better candidate since they can be easily adapted to glass coverslips with insignificant alterations in the overall surface height, are fungible and sterilisable with UV light, they do not need much space in the build platform and some of the printing systems are already adapted for their use, making them particularly manageable and effective as printing calibration substrates.

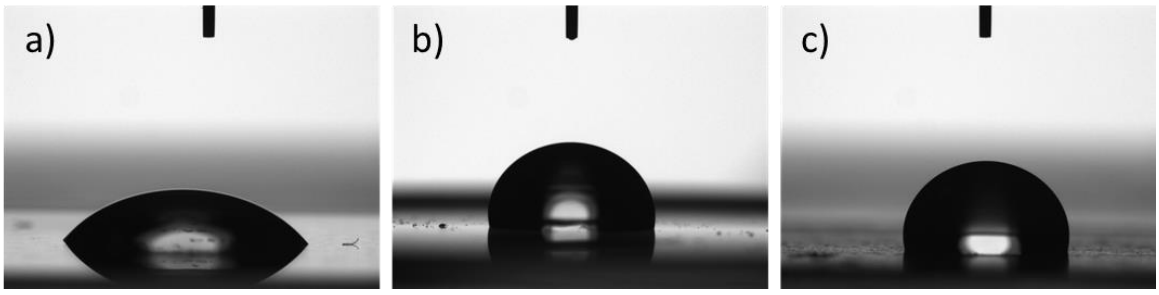

Figure 26. Droplets of precursor solution on different substrates. (a) Glass coverslip, (b) plastic petri dish and (c) parafilm. More stable and rounded droplets were achieved in more hydrophobic surfaces, which help to maintain constructs physical integrity during the printing and cross-linking process.

4.3 Flow rate analysis

Flow rates in laminar flow regimes are dependent on the applied pressure and resistance to flow. Resistance to flow includes viscosity, length of the channel, and channel diameter as well as nozzle geometry. Tapered nozzle tips, compared to cylindrical geometries, are commonly known to produce less mechanical stress on cells as a result of their different entrance and exit nozzle diameters, triggering higher-pressure gradients (and flow rates), at the same viscosity values.

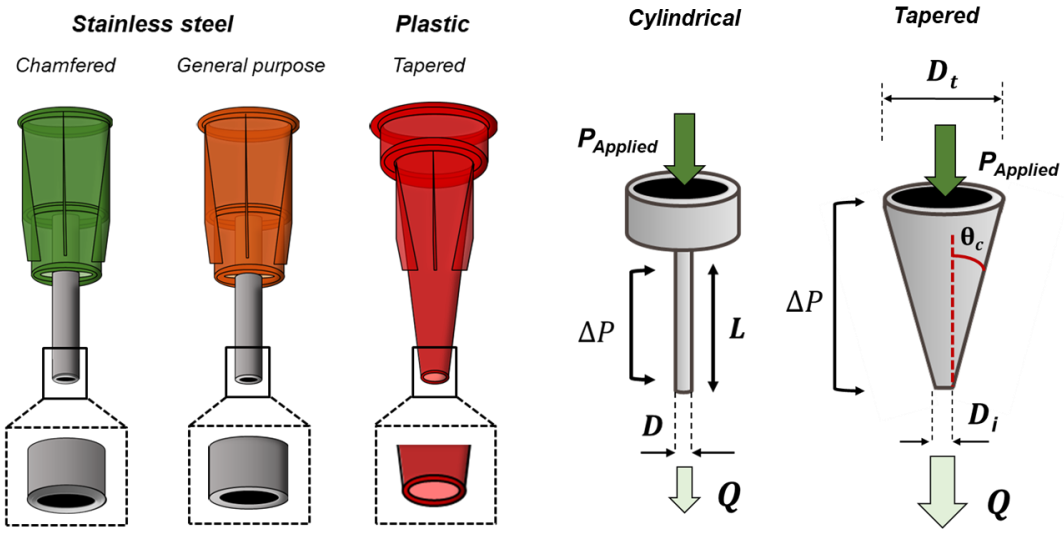

Figure 27. Geometry of the different types of nozzle tip: chamfered, general-purpose and tapered. The only apparent difference between chamfered and general-purpose tips lies in the shape of the tip exit. While general cylindrical tips only possess a polished finish, chamfered tips are designed with a special outer diameter taper, reducing the surface area and preventing wicking for more accurate dispensing control.

For the simple case of a Newtonian bioink (flowing index n=1) flowing through a cylindrical nozzle, the flow rate can be approximate by the Hagen-Poiseuille law (102):

$$Q_{cylindrical} = \frac{\pi \Delta_P D^4}{128 \eta L} \qquad \text{(Eq. 8)}$$

where Q is the dispensing flow rate (m^3/s), Δp is the pressure drop between the beginning and the end of the nozzle tip (Pa), D is the inner diameter of the nozzle tip (m), η is the dynamic viscosity of the bioink (kg/(m·s)), and L is the length of the nozzle tip. For tapered nozzle geometries otherwise, the flow rate may be expressed by (96):

$$Q_{tapered} = \frac{\pi D_i^3 D_t^3}{32}\left[\frac{3n\Delta_P tan\theta_c}{2\eta(D_i^{3n} - D_t^{3n})}\right]^{1/n} \quad \text{(Eq. 9)}$$

where D_i and D_t are the nozzle entrance and exit diameters respectively. The effect of nozzle geometry (cone-half angle θc) is evident on flow rate, and in the case of non-Newtonian fluids with shear-thinning properties (n<1), increments are even more accentuated. Thus, in situations where the extrusion pressure is limited, tapered nozzles result advantageous for achieving a higher volumetric flow rate, particularly when dispensing highly viscous materials. Poorly viscous inks, however, do not require high-pressure levels for their dispensing and may find some significant alterations in flow rate when small pressure changes are applied.

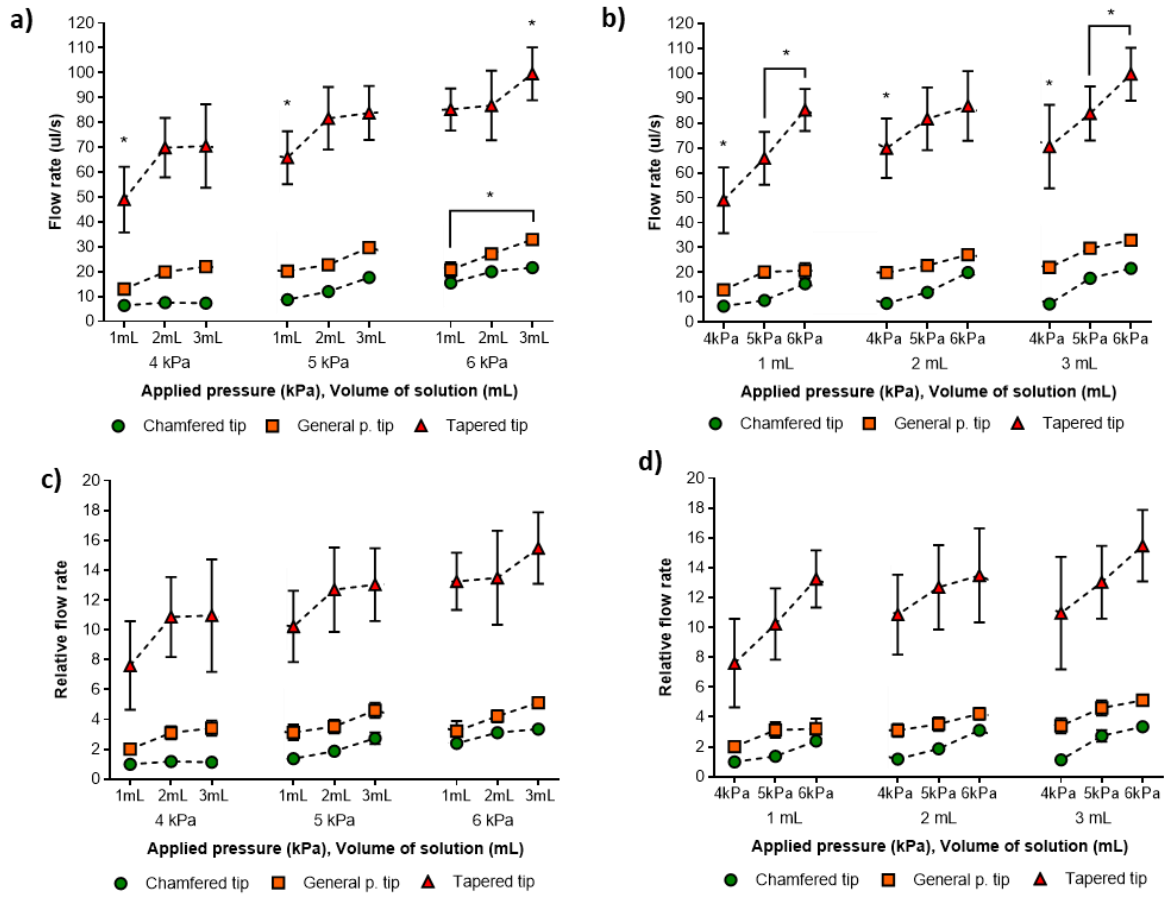

Figure 28. Experimental flow rate values from buffer precursor solution through the different 25 G nozzle tip geometries. (a) Influence of the total volume of solution in the cartridge and (b) pneumatic pressure, and their relative values (c) and (d) respectively to the minimum flow rate found in the entire assay (chamfered, 4 kPa, 1 mL). Dispersion in data is represented as the time lag during the printing process. Significant differences (*) $p \leq 0.05$.

To analyse the influence of pressure, the CF-KRB buffer precursor solution ($\eta \approx 1$ mPa·s^{-1}) was extruded through different nozzle geometries with the same gauge and tip length. Pressure influence was reflected by means of two different factors, the resultant pressure from the application of pneumatic pressure of the printing system ($P_{applied}$), and the hydrostatic pressure resulting from the own bioink weight inside the cartridge reservoir (V_{sol}).

From ***Figure 28*** is possible to infer some main ideas. First, as we had already foreseen from literature, tapered geometry triggered flow rates with at least a 4- to 5-fold increase compared to the rest of the nozzle tips. Although pressure influence is visible in all the nozzles, tapered tips seemed to be more sensitive to pressure changes at low viscosity generating greater differences in flow rate between conditions as well as bigger dispersions inside each condition. Significant differences in pneumatic pressure can be problematic in systems where pressure resolution is not ideal. In our case, pressure´s resolution was 1 kPa, sufficient for fluids with higher viscosity or droplet-based modalities, but rather difficult to operate with water-like consistency inks and when requiring accurate volume dispensing as it is proven in ***Figures 28 and 29***. Dealing with significant differences in the volume of solution also becomes a challenge, increasing calibration´s difficulty as well as its time when larger precursor solutions are required. Moreover, higher pressure gradients are responsible for longer time lags (data dispersion), increasing volume dispensing inaccuracy at faster printing speeds and causing higher chances of non-crosslinked samples.

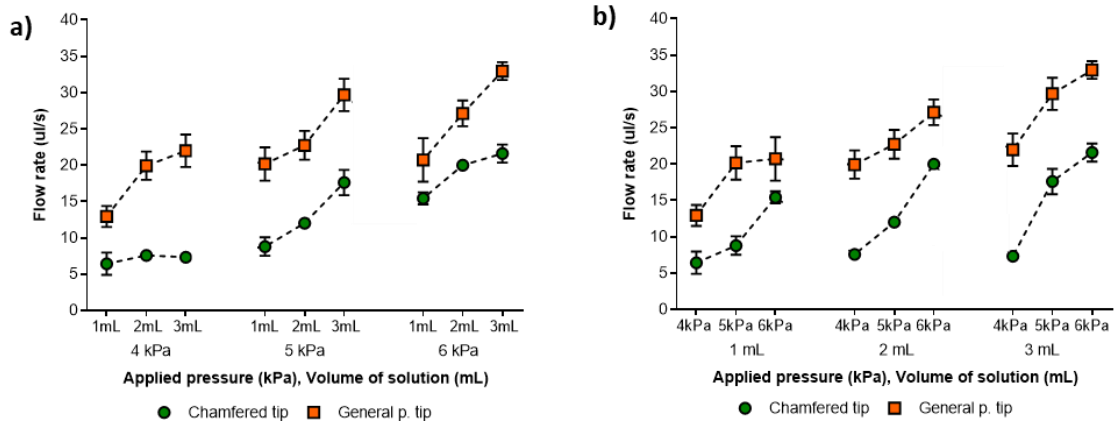

Figure 29. Flow rates values in 25 G chamfered and general-purpose tips, both cylindrical. (a) Influence of solution weight (volume) in cartridge (mL) and (b) pneumatic pressure (kPa).

Flow rate in cylindrical tip geometries (general-purpose and chamfered), also seemed to vary between conditions, but pressure influence was found significantly smaller. Moreover, data dispersion was negligible, generating very low time lags during printing, especially in chamfered tips. Slightly higher viscosities should provide more stable droplet dispensing, however, temperature influence in this project was not assessed given the incredible amount of already processed parameters.

To complete the analysis, a regression line for each data set was calculated as a way of measuring flow variability when either printing pressure or volume of solution was modified. Pressure and printing times in this experiment were intended to reduce volumetric artefacts as much as possible, as well as the ink´s dependency on viscosity as a result of temperature differences at the nozzle exit. Tapered nozzle tips possessed the biggest gradient index in both factors, being maximum when solution volume was changed and therefore no longer used for protocol study or cell culture assays.

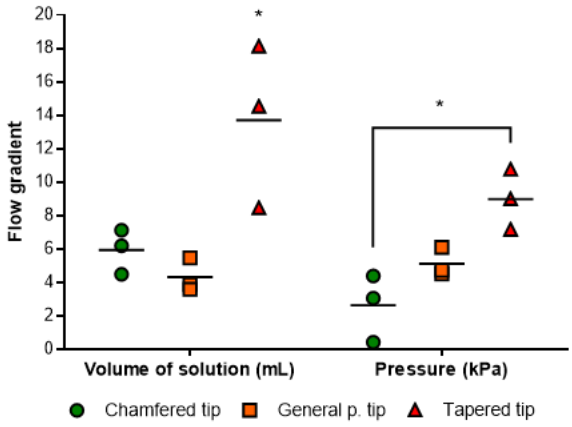

Figure 30. Flow gradient in the different 25 G nozzle tip geometries. Flow gradient experimental values can be expressed as a parameter of flow variability when changing one of two factors. Significant differences denoted as (*) for $p \leq 0.05$.

Chamfered and general-purpose tips possessed similar levels in both flow gradients, however, chamfered tips possessed lower data dispersion, grip issues and flow rate variations, making them adequate for their use in microdot applications for very poor viscous bioinks.

In conclusion, the use of tapered nozzle tips, although being generally more beneficial for cell survival, could be particularly counterproductive for this printing protocol because of the strong pressure influence on flow rate involved during the printing process and its

possible negative effect on cross-linking dispense. When selecting a cylindrical nozzle, choosing an adequate tip diameter will be the more efficient way to control and operate with particular flow rates as well as assuring an unharmful effect on cell survival. Besides, in thermoresponsive inks such as gelatin, controlling the printing temperature not only at the syringe or cartridge barrel but also at the printing tip, will be crucial to ensure a constant flow rate. In that case, tips with shorter lengths and bigger diameters (G < 25) will be more advantageous to diminish pressure and viscosity's influence during printing when resolution is not a key requirement.

4.4 Density and viscosity approximation.

Parameters such as the Reynolds number (Eq. 4) or cell sedimentation rate (Eq. 7) are highly influenced by the solution density and therefore needed to be calculated for posterior analysis. Density values from Table 5 were obtained from Eq. 1 and Eq.2 for the different polymer blends and different polymer concentrations in solution (w/v) (%). The density value established for all the following calculations was from pure Gel solution at 2% (w/v), since it was found to be the maximum value of all the polymer series studied in this project. However, as it is noted, solution density does not change much when either increasing polymer concentration in the same composition or changing the proportion of Gel/HA.

	Solution density ($g \cdot cm^{-3}$)				
Gel/HA solution	Gel/HA concentration (w/v) (%)				
	2	3	4	5	10
100/0	1,0060	1,0090	1,0119	1,0148	1,0286
70/30	1,0053	1,0079	1,0105	1,0130	1,0252
50/50	1,0048	1,0072	1,0096	1,0119	1,0229
30/70	1,0044	1,0065	1,0086	1,0107	1,0206
0/100	1,0037	1,0055	1,0072	1,0090	1,0172

Table 5. Theoretical density values of Gel/HA hydrogel solutions at different polymer concentrations (w/v) (%).

The viscosity of the different hydrogel precursor solutions obtained in ***Table 6*** was a key parameter involved in the calculation of different variables including the Reynolds number, shear stress, pressure drop and cell sedimentation. Given the impossibility of using some equipment for material characterisation during the pandemic, apparent viscosity at low shear

rates could not be directly measured by a rotational or shear rheometer. Instead, viscosity in the different solutions was predicted using Hagen-Poiseuille's flow equation (Eq. 3) and the applied pneumatic pressure (($P_{applied}$) during printing, assuming poor frictional forces due to viscosity. According to this equation, the existing delta of pressure (Δp) found in the barrel from the surface of the plunger to the nozzle exit is directly proportional to the fluid's viscosity and flow resistance. When using small constant flow rates and same nozzle geometries, pneumatic pressure can be then approximate to the pressure drop inside the barrel, and therefore viscosity for every solution blend could be estimated.

$$Q = \frac{\pi \Delta_P R^4}{8\eta L} \longrightarrow \frac{P_2 - P_1}{\eta_{sol}} = K \longrightarrow P_{applied} \gtrapprox P_2 - P_1 = \Delta_P$$

Due to the high molecular weight of HA, solutions with higher proportions were expected to possess higher viscous properties, leading to the use of greater levels of pneumatic pressure during printing at constant flow rate.

Viscosity (mPa · s)	Pressure drop (kPa)	Gel/HA hydrogel	Applied pressure (kPa)	Viscosity interval (mPa · s)
1	4,8	100/0	10-11	1,5-2
1,5	7,2	70/30	12-13	2-2,5
2	9,6	50/50	15-16	2,5-3
2,5	12,0	30/70	17-19	3-3,5
3	14,4	0/100	22-24	4-4,5
3,5	16,8			
4	19,2			
4,5	21,6			
5	24,0			
5,5	26,4			

Table 6. Approximate theoretical values of viscosity of the different 2% (w/v) Gel/HA hydrogel precursor solutions at printing temperature (37 °C). Given the values of pneumatic pressure applied ($P_{applied}$) and flow rate (Q) for droplet dispensing, estimated viscosity intervals could be obtained by the application of the flow Hagen-Poiseuille equation (Eq. 3) in which is possible to calculate the pressure drop (Δp) inside a cylindrical needle. Influencing parameters such as volume of solution, tip geometry, temperature and flow rate were constant during the assay. Rest of parameters normally included in fluild´s resistance to flow (viscosity changes, friction coefficient or wall-piston friction) were considered negligible, due to the small differences found in solution consistency.

4.5 Calculation of Reynolds number, shear stress and pressure drops intervals

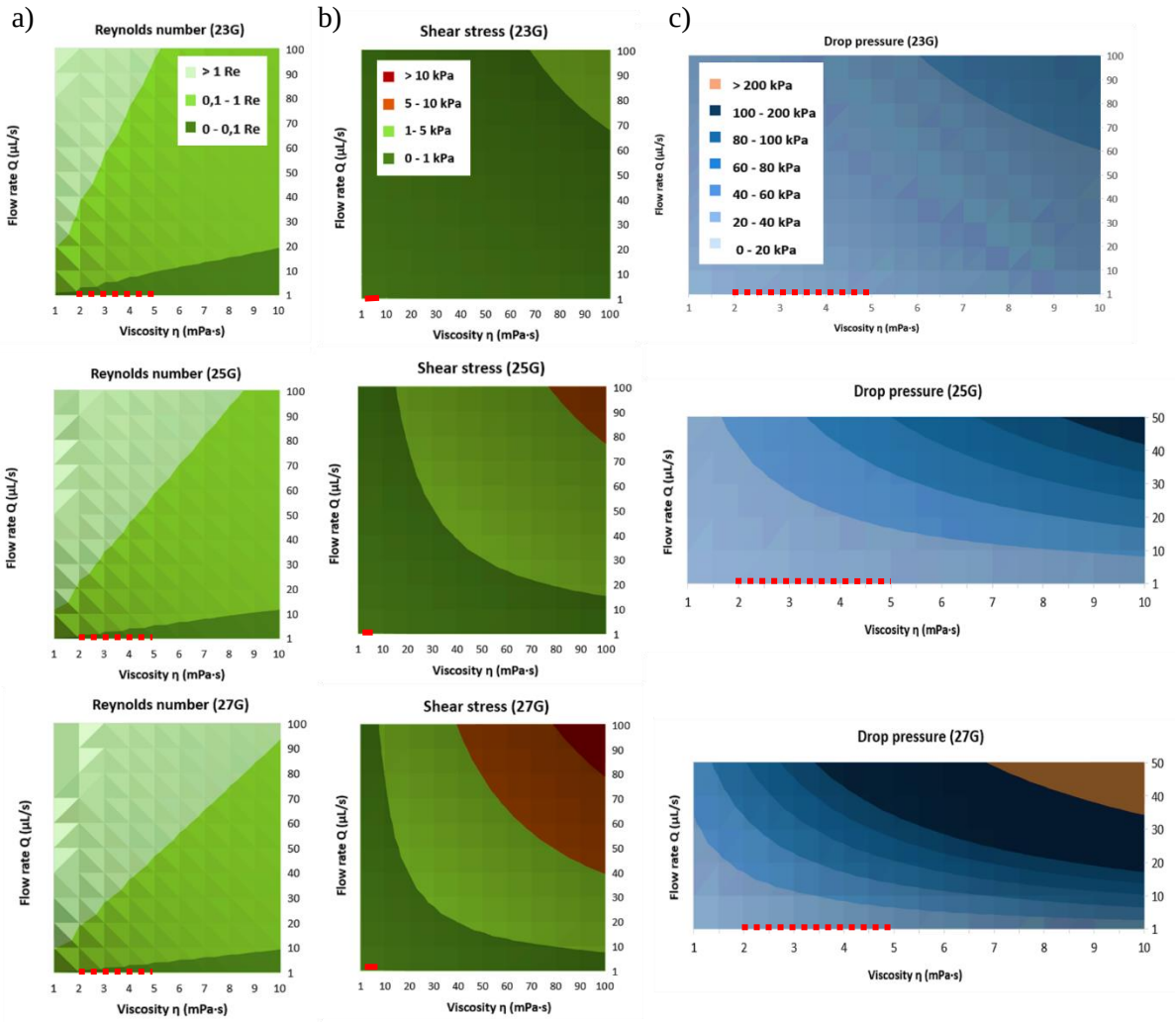

Figure 31. (a) Reynolds numbers, (b) theoretical shear stress and (c) pressure drop values for 23 G (Ø 330 µm), 25 G (Ø 250 µm) and 27 G (Ø 200 µm) cylindrical nozzle tips. Values are dependent on solution viscosity η (mPa·s) and flow rate Q (µL/s). Shear stress values for the different nozzle gauges ($\eta_{Gel/HA\ (37\ °C)}$ = 2 – 5 mPa·s (red), Q = 10 – 20 µL/s) were significantly lower to the pressure threshold (< 5 kPa) visibly harmful for fibroblast cells obtained from literature, meaning no differences in cell viability should be found regarding the effect of mechanical stress. Tip diameter influence is obvious on the printing pressure. According to the Hagen-Poiseuille equation (Eq. 3) and as shown in the graphs, the pressure drop inside the needle will increase by a factor of 16 (i.e. $\Delta p \sim D^{-4}$) decreasing the nozzle diameter by a factor of 2.

Evolution of Reynolds numbers, shear stress and pressure drop for the different nozzle diameters in function of the viscosity and flow rate were calculated following *Eq. 3* to *Eq. 5* as shown in ***Figure 31.***

Motion of fluids is notoriously hard to predict. The Reynolds number (Re), with the property of being dimensionless, plays an important role in foreseeing the patterns in a fluid's behaviour through cylindrical conduits (e.g., nozzle tips) which can be normally categorized as laminar (Re < 2100), turbulent (Re > 4000) or something in between (2100 < Re < 4000).

As it was already mentioned in the introduction, velocity profiles in laminar flows are stable and parabolic across the conduit diameter, finding the maximum shear stress at the barrel and nozzle walls. In this case, maximum shear stress can be easily calculated from the Hagen-Poiseuille´s flow equation (*Eq. 3*) as described in *Eq.5*. Reynolds number for the different nozzle tips was confirmed to be Re < 2100 for viscosities from η = 1 – 10 mPa·s. Materials with higher viscosities (η > 10 mPa·s), either caused by their polymer density or variations in temperature, will acquire lower Reynolds numbers provided the use of adequate flow rates, ensuring laminar behaviour.

Shear stress levels, on the other hand, gradually increased when either increasing viscosity or flow rate, however, the selection of the nozzle diameter became the most determinant factor to ensure appropriate levels of cell stress (< 5 kPa). Although higher gauges presented considerably lower tolerances to the sudden increase in any of both parameters, all hydrogel precursor solutions should be safe to print through 23 G, 25 G, 27 G nozzles at physiological temperature ($\eta_{Gel/HA}$ (37-39 ºC) = 2 – 5 mPa·s). Due to the thermo-responsive properties of Gel and HA, viscosity in the different precursor solutions was expected to dramatically increase when decreasing the printing temperature, augmenting in turn the levels of shear stress (***Figure 32***). When these changes in temperature are inevitable or cause abrupt distortions in the viscosity of fluids, the use of lower gauges or tapered geometries can diminish any harmful effect on cells, protecting them from mechanical forces within the solution. Even though none of the Gel/HA hydrogel samples required high printing resolutions given the simplicity of their shape profiles, it was still considered interesting for the project to determine the limits of safe shear stress at high gauges (Ø 250 – 200 µm) in the event of working with more complex and precise architectures for future applications.

Pressure drop was found the most sensitive parameter to changes in viscosity, being strongly dependent on the nozzle diameter and connected to the bioink's resistance to flow. From ***Figure 31*** it was possible to infer some general ideas.

It is worth stressing how polymer density in some bioinks can substantially enhance the influence of small nozzle diameters on pressure drop. Polymers, such as the case of Gel or HA, can hold severe fluctuations in viscosity when their solution density (w/v (%)) is just increased by a few times. Gel solutions at 5% w/v, for instance, possess similar viscosities at 40ºC to the obtained in this project ($\eta < 10$ mPa·s), but can easily reach viscosities up to 1000 mPa·s when temperature decreases to 20ºC, meaning a 100-fold increase compared to the estimated viscosity ($\eta_{(20ºC)} < 100$ mPa·s) of Gel/HA hydrogels at 2% w/v (249). Higher Gel densities (10%-30% w/v), generally more attractive for 3D bioprinting due to their good fluid behaviour during printing, can simply display viscosities of $400 < \eta < 1300$ mPa·s at physiological temperature (37ºC), demanding much higher printing pressures (250).

Shear stress level

Physiological level	Acceptable	Possible cell damage	Cell damage
7 Pa	*1-5 kPa*	*5-10 kPa*	*> 10 kPa*

Pneumatic pressure requirements

Low	Medium	Demanding	Highly demanding
< 200 kPa	*200-400 kPa*	*400-700 kPa*	*> 700 kPa*

	Nozzle gauge (G)								
	23 G			25 G			27 G		
	η (mPa·s)			η (mPa·s)			η (mPa·s)		
	10	100	1000	10	100	1000	10	100	1000
Shear stress (kPa)	0,01	0,15	1,48	0,07	0,65	6,52	0,13	1,27	12,73
Pressure drop (kPa)	3,32	33,16	331,63	23,99	239,90	2398,99	58,57	585,69	5856,90

Table 7. Effect of bioink's viscosity on shear stress and pressure drop at Q = 10 µL/s at different cylindrical nozzle gauges. Above, shear stress levels and pneumatic pressure requirements (low, medium, high) according to literature. Below, comparison table for theoretical shear stress and pressure drop values regarding bioink's viscosity when passing through cylindrical nozzle tips.

Depending on the quality of resolution desired for each application, some current 3D bioprinters on the market may face physical limitations in terms of pneumatic pressure (P > 400 kPa) (251) when using very fine needles alongside high enough viscous bioinks. To take

an example, the popular CELLINK's Benchtop Bio X™ and X6™ bioprinter devices (252), well-known for the application of very promising hydrogel bioinks, possess an internal oil pump merely capable of reaching 200 kPa of pneumatic pressure, whereas in the company of an additional external air compressor can go up to 700 kPa. From ***Table 7*** we can easily deduce how some of these pressure levels will be insufficient for applications where viscosity reaches $\eta > 100$ mPa·s in any of the mentioned nozzle diameters.

Furthermore, many cartridge heaters do not normally cover the surface of the nozzle tip, generating lower temperatures at the nozzle exit. Bioinks with abrupt changes in viscosity, as a direct consequence of small changes in temperature, tend to suffer from important variations in flow rate during printing, leading to the continuous modification of the pneumatic pressure and ultimately to printing failure. Sudden increases in viscosity can also lead to probable clogging issues where the accumulation of high pressures inside the barrel can be eventually responsible for cell damage and much longer printing times.

In the case of our 2% w/v Gel/HA hydrogel solutions, 25-27 G nozzles so far presented significant variations in pressure when viscosity was incremented or decremented by a few units affecting flow rate and requiring precise optimisation processes before and during printing.

In summary, due to the high values in shear stress and required pneumatic pressure in 27 G cylindrical nozzles, we decided to continue all the following assays with chamfered 25 G nozzles, which are still considered good for high-resolution requirements, low-pressure applications and safe to use for high cell densities.

4.6 Evaporation rate

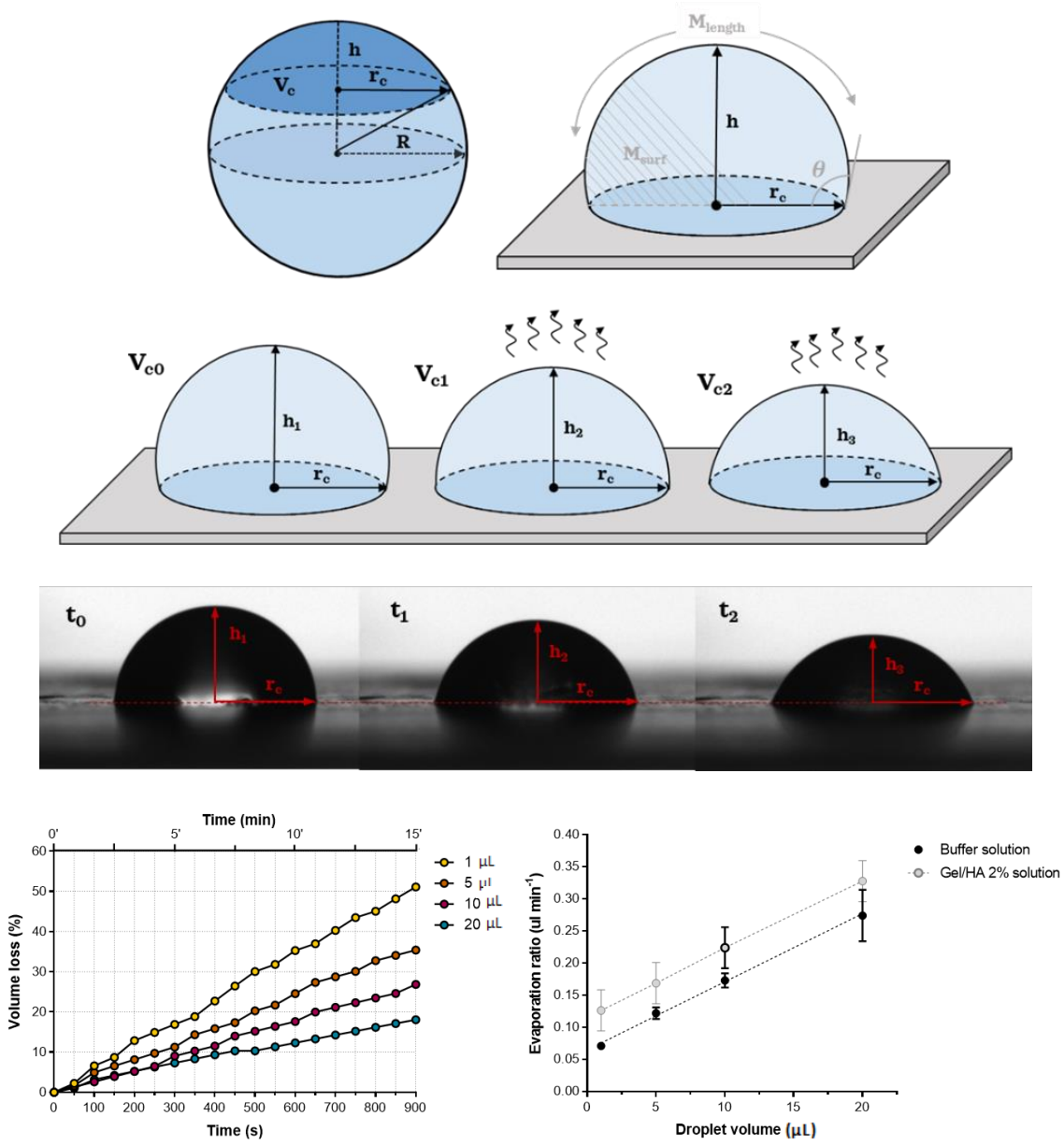

Figure 32. Evaporation rates of the buffer solution and 2% (w/v) Gel/HA precursor solutions at room temperature (20-25 ºC). Evaporation rate was found very similar between the solvent and the hydrogel solution. The evaporation rate was described as the volume loss over time at different droplet volumes. Larger exposed surfaces to the environment as well as higher temperatures accentuate the effect of evaporation.

Due to the elevated water content in hydrogels, these materials inherently tend to evaporate, even more before the cross-linking process as t as possible using deeply cleaned tips fis observed in ***Figure 3***2. Water evaporation constitutes a serious risk for the nozzle tip (material clogging) as well as for the structure integrity (irregular flow rates) and thus it is

recommended to always print as fast as possible using properly cleaned tips for each protocol stage. In cell-laden hydrogels, the necessity of retaining the original shape is also determinant for the scaffolds success. In this stage of our research, droplet shape was not significantly important and samples could be entirely cross-linked before droplet structure was irreversibly lost, even when incubated at 37º C. Besides, due to the low polymer density of our precursor solutions, even in the event of material clogging, bioinks could be effortlessly reheated for a few minutes and managed to print again without compromising cell viability.

4.7 Cell sedimentation rate

Viscosity (mPa·s)	Sedimentation rate ($\mu m \cdot s^{-1}$)	minimum samples / min		
		10 µL (n)	25 µL (n)	50 µL (n)
1,0	20,5	18	7	3
1,5	13,7	12	4	2
2,0	10,2	9	3	1
2,5	8,2	7	2	1
3,0	6,8	5	2	< 1
3,5	5,9	5	1	
4,0	5,1	4	1	
4,5	4,6	3	1	
5,0	4,1	3	1	
5,5	3,7	3	< 1	
6,0	3,4	2		
6,5	3,2	2		
7,0	2,9	2		
7,5	2,7	2		
8,0	2,6	1		
8,5	2,4	1		
9,0	2,3	1		
9,5	2,2	1		
10,0	2,0	1		

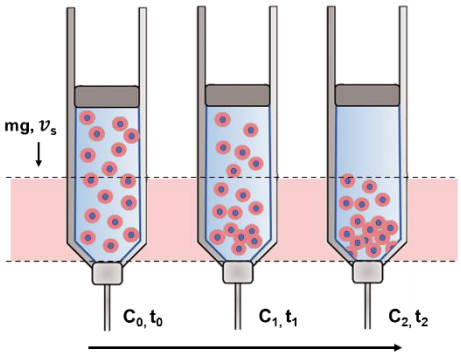

Table 8. Theoretical values of cell sedimentation rate at different solution viscosities based on *Eq. 7*. Minimum number of 10µL, 25µL, 50µL droplets dispensed per minute were calculated based on cell sedimentation speed and the total distance (top-bottom) of 1mL solution in the cartridge barrel. Tolerance was set in maximum increment of 25% of the original cell density at the cartridge bottom (500 µL). Using the viscosity interval for each hydrogel precursor solution, it is possible to establish a reference droplet dispensing rate. Decreasing bioinks volume or hydrogels viscosity will directly increase the total amount of droplets per minute required to avoid possible cell sedimentation.

When the solution density is lower than the density of the cellular components inside it, cells tend to sediment as a result of gravity. Cell sedimentation in this project for both modalities, extrusion-based and droplet-based, was a concerning factor given the poor viscous properties of 2% w/v Gel/HA hydrogel precursor solutions (***Tables 8 and 9***). Elevated cell sedimentation rates are generally related to clogging issues at the nozzle exit causing eventual printing failures. Cell sedimentation rates were calculated for all Gel/HA compositions according to the approximate intervals of polymer density and solution viscosity presented in ***Tables 5 and 6.*** The minimum number of samples per minute needed to avoid significant effects of cell sedimentation in sample were also calculated for different sample volumes, with a maximum tolerance of 25% cell density increment in the lower half part of the bioink solution inside the cartridge. Temperature plays an essential role in reducing cell sedimentation given its power to suddenly increase fluids viscosity without producing any negative effect in cell viability when used for small periods. Based on *Eq. 7*, bioinks with minimum viscosity $\eta > 20$ mPa·s, even at very low polymer density, could be safely used for printing without significant differences in cell concentration (printing times < 1h).

Gel/HA hydrogel	Viscosity interval (mPa · s)	minimum samples / min		
		10 µL (n)	25 µL (n)	50 µL (n)
100/0	2-1,5	12-9	4-3	2-1
70/30	2,5-2	9-7	2-3	1
50/50	3-2,5	7-5	2	1
30/70	3,5-3	5	2-1	1
0/100	4,5-4	4-3	1	1

Table 9. Reference droplet dispensing rate for the different 2% w/v Gel/HA hydrogel precursor solutions depending on the approximate viscosity values obtained in *Table 6.* Minimum number of 10µL, 25µL, 50µL droplets dispensed per minute in 1mL solution in the cartridge barrel. Tolerance was set in maximum increment of 25% of the original cell density at the bottom half part of the bioink solution in the cartridge (500 µL).

4.8 Standoff distance calibration

We tested the generation of cross-linked hydrogel samples (droplet formation and cross-linking processes) employing the two available bioprinting strategies, extrusion-based and droplet-based bioprinting. The standoff distance, the distance that exists between the nozzle tip and the printbed, is commonly known in bioprinting for its relevant influence on the formation of accurate and stable samples.

4.8.1. Droplet formation by extrusion-based printing

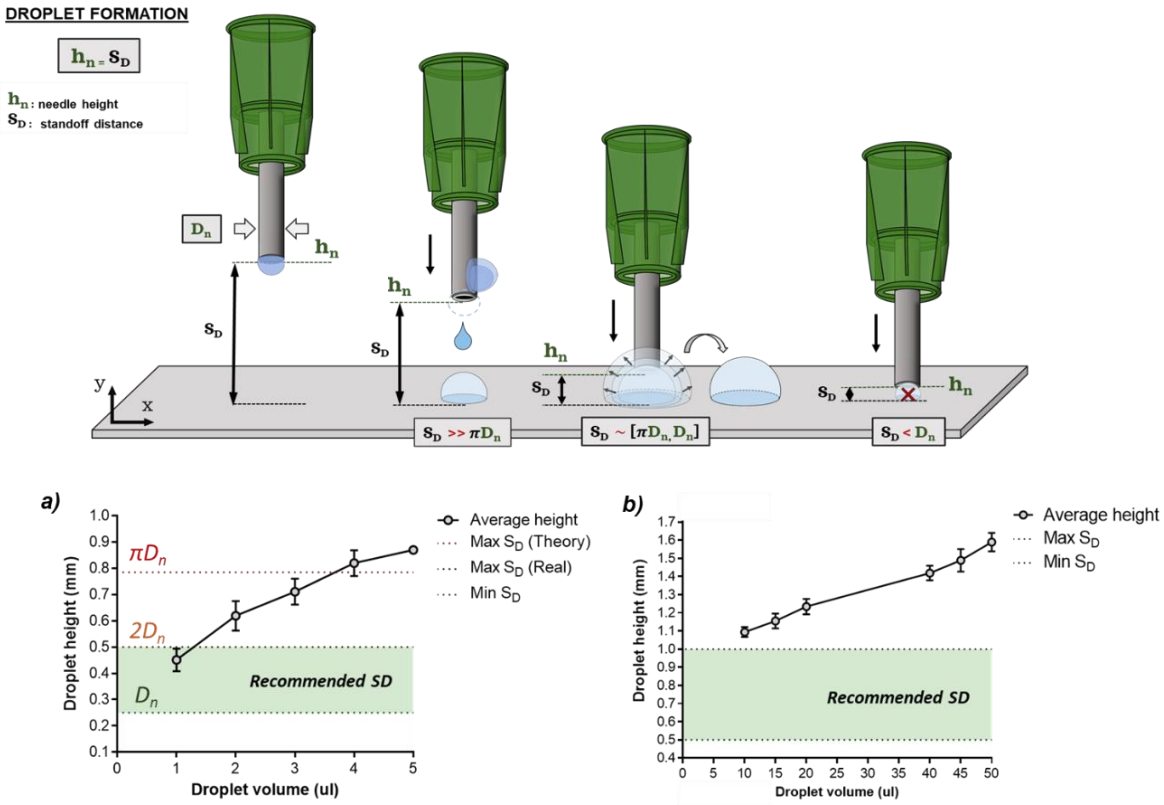

Figure 33. Calibration of the standoff distance for droplet formation through extrusion-based printing modalities using chamfered 25 G nozzles. (a) Droplet heights for 1-5 µL and (b) 10 – 50 µL droplet volumes and their recommended printing distance (green area) compared to the ones established by literature ($2D_n - \pi D_n$). Incorrect distances affect droplet shape as well as the ejection pressure. Longer S_D are controlled by the capillary rise effect and bioink's wettability, producing very unstable droplets. Flow rates in shorter S_D are affected by alterations in the ejection pressure, modifying the original droplet volume.

The height of different droplet volumes was analysed by a Theta optical tensiometer and ImageJ software. Afterwards, groups of droplets (n=15) with different volumes were

extruded at different standoff distances, analysing possible shape variations in each set. Correct working standoff distance intervals were considered the ones with no influence on flow rate, which allowed an accurate dispense of the bioink onto the printbed without shape distortions. Recommended standoff distance intervals for droplet formation (1-50 µL) by extrusion were consequently established between one and two times the nozzle diameter (Dn, 2Dn) (Figure 33), selecting as an optimal distance value the one around half the height of each droplet size group.

4.8.2. Cross-linking injection (extrusion-based printing)

Similarly to the analysis of droplet formation, standoff distance for the injection of the cross-linking solution was studied by the assessment of cross-linked samples at different nozzle heights. Given the high probability of appearance of uneven droplet profiles or the occasional printing of droplets of different volumes during the same process, the correct standoff distance had to be prepared for all the possible droplet outcomes presented in ***Figure 34.***

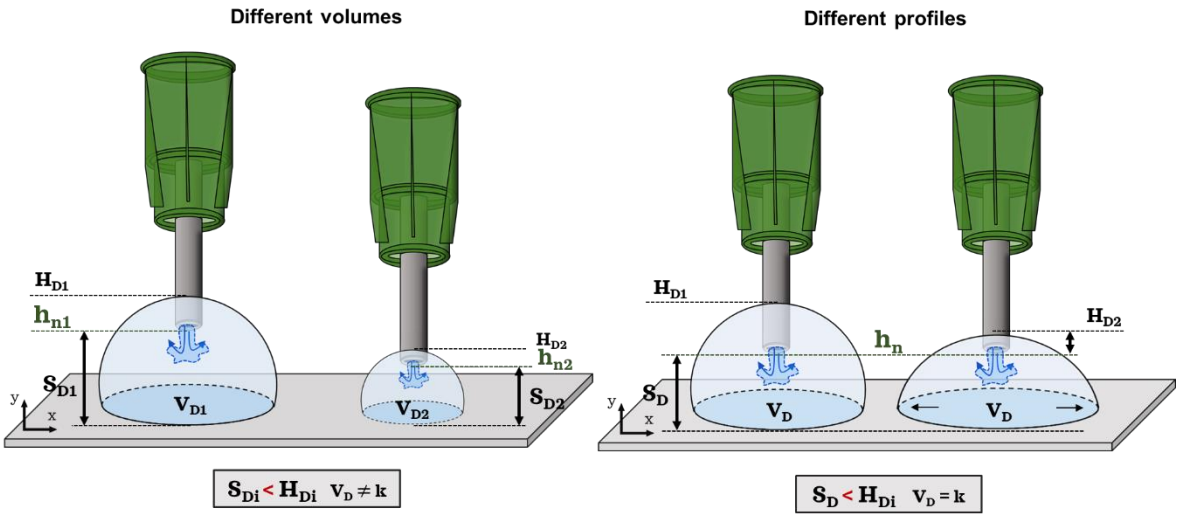

Figure 34. Schematic diagram of standoff distance calibration for cross-linking injection for different droplet volumes (left) and similar droplets with uneven shapes (right). Some 3D bioprinters allow setting a single standoff distance for each layer deposition of a printing process. Samples with different volumes or uneven shapes can possess significant differences in height, which can lead to the cross-linking failure of some of the hydrogel samples. It is therefore important to determine the working intervals for each possible condition in order to assure a proper cross-linking reaction.

Eventually, recommended standoff distance for each droplet group (n=15) was set up in 70% of the minimum height obtained for each set (***Figure 35***), assuring in that way that the nozzle tip always reached the droplet surface regardless of its profile.Similarly, these values provide a correct diffusion mechanism of the cross-linking solution going from the upper part through the rest of the sample by means of the effect of gravity.

The contact of the nozzle tip with Gel/HA hydrogels during the cross-linking involved the possibility of nozzle clogging and the injection failure in the successive samples. This could be solved by simply exchanging the nozzle tips during the process and assuring a correct level of positive pressure onto the sample.

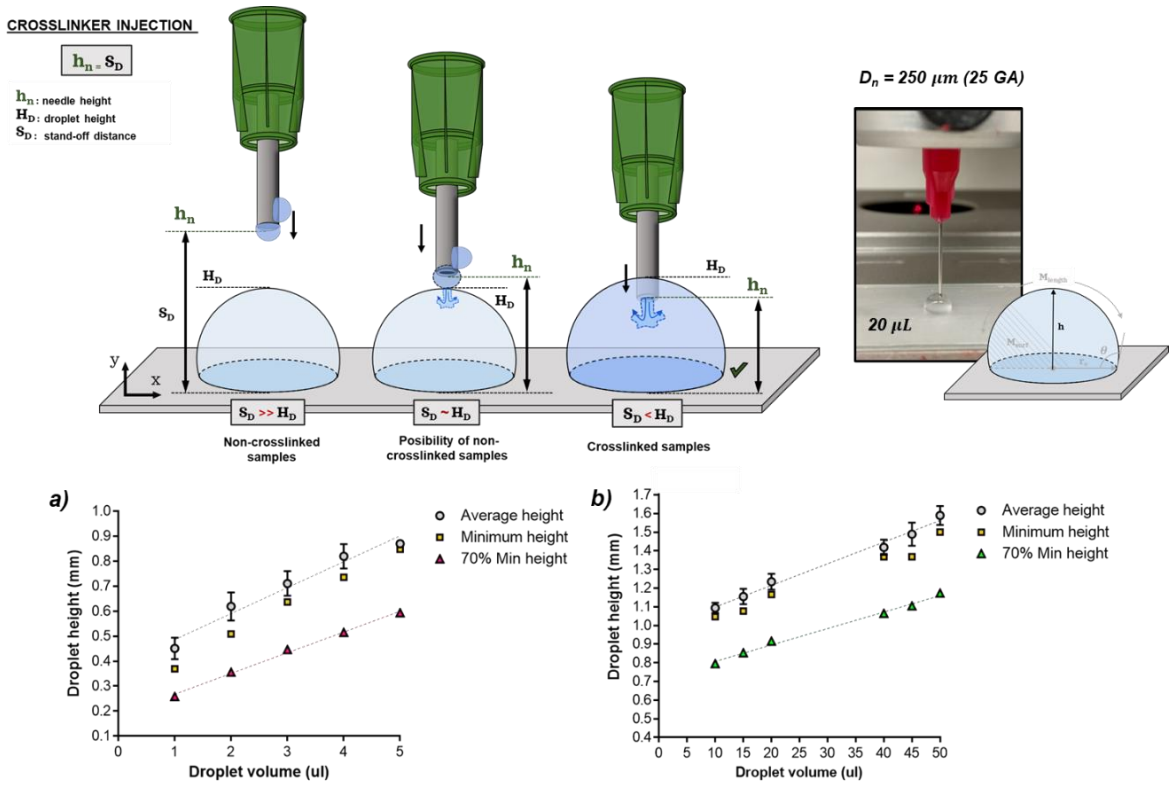

Figure 35. Calibration of the standoff distance for cross-linking injection in extrusion-based printing modalities using chamfered 25 G nozzles. (a) Recommended distance for the cross-link addition in 1-5 µL and (b) 10 – 50 µL droplets based on their 70% of the minimum volume height (triangle). Values around these distances guarantee an appropriate cross-linking administration. Longer distances than the established may not reach the target surface, reducing the chances of a sample being cross-linked, and shorter ones may deposit the cross-linking solution (or part of it) in the lower part of the droplet, also leading to non-uniformities during the reticulation process.

4.8.3. *Droplet and cross-linking ejection (droplet-based printing)*

The generation of droplets, as well as the addition of cross-linking, were also tested in a micro-valve printing system (droplet-based technology). Both protocol stages were totally reliant on the standoff distance.

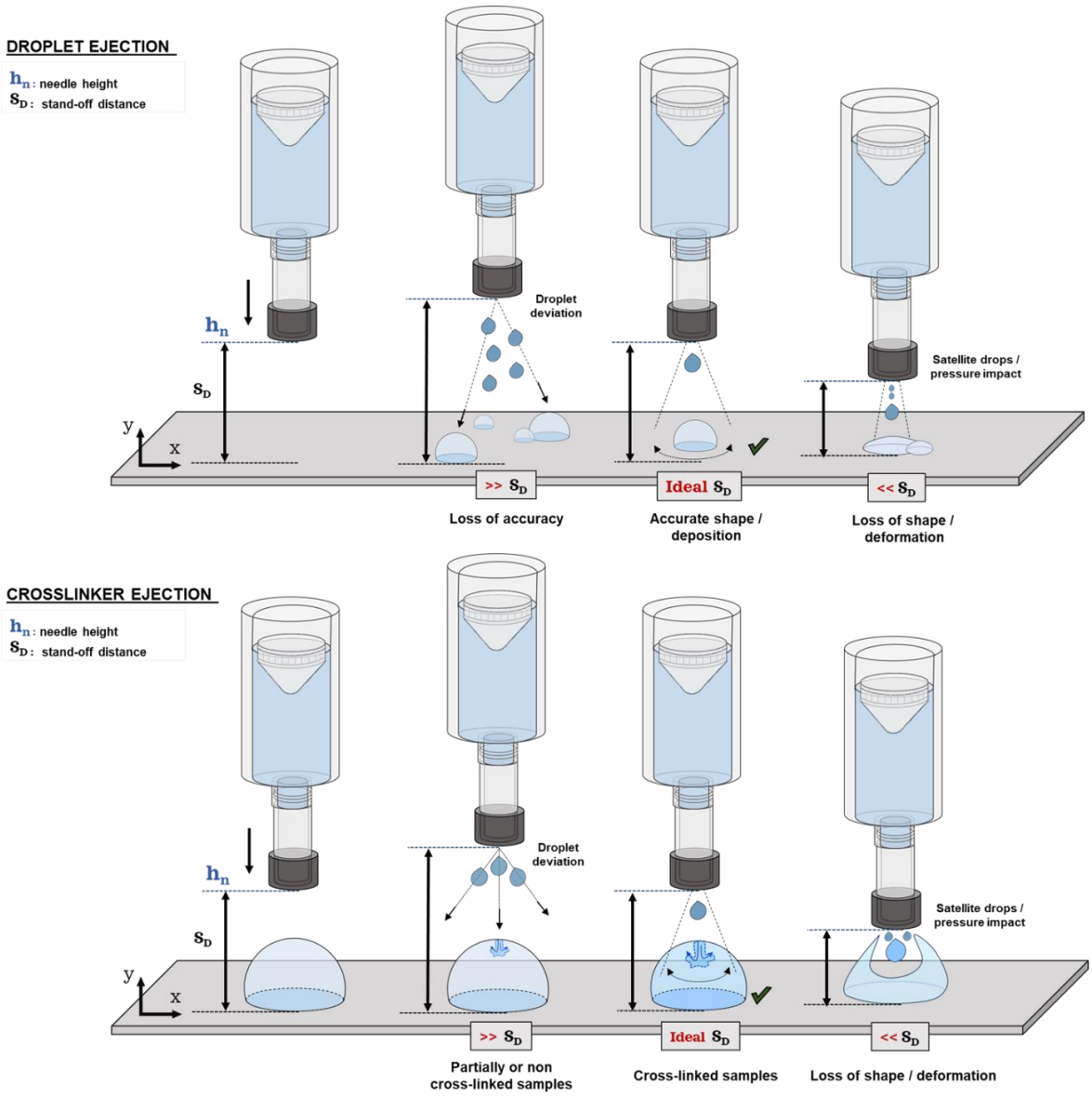

Figure 36. Calibration of the standoff distance for droplet deposition and cross-linking ejection in droplet-based non-contact printing modalities (micro-valve). Droplet volume is regulated by the standoff distance, the valve opening time t_{open} as well as the pneumatic pressure. Shorter standoff distances (<< S_D) and excessive pressures can cause distortions in the droplet shape or even its destruction. Longer distances (>> S_D) and deficient pressures, on the contrary, may end up in droplet deviation and fragmentation, where droplet cross-linking is undermined.

Due to the very low viscosity of the studied bioinks, droplet formation was easily achieved through the calibration of the standoff distance and the number of shots, which defines the number of droplets ejected per each single deposition point (described in point ***4.9***).

Micro-valve systems, due to the absence of a nozzle tip, tend to suffer from cross-contamination in multi-step protocols and thus they normally require a complete cleaning process of the printing valve between steps (different solutions). In the particular case of enzymatic cross-linking, the lack of cleansing can cause several clogging issues at the nozzle, attributable to the reactive rests of polymer fibres alongside enzymes inside the nozzle that enter into contact with the cross-linking solution. Our system, counting with only one micro-valve printhead, implicated longer printing times when performing both protocol steps (droplet formation and cross-linking) with the same technology compared to the extrusion-based system, increasing the chances of cell sedimentation and cell cytotoxicity in samples as well as the loss of the desired shape. Hence, and provided the obvious advantages that present any non-contact technology, micro-valve printing for this project was decided to be used solely for the step of cross-linking, being also the one selected for all the cross-linking stages in cell culture assays.

As it is observed in ***Figure 37***, droplet volume remained practically stable (± 1 µL) with the increase of pneumatic pressure, providing evidence of its weak influence in this system as well as the one resulting from the solution weight. On the other hand, standoff distance, although also modifying the droplet size, was neither particularly influential.

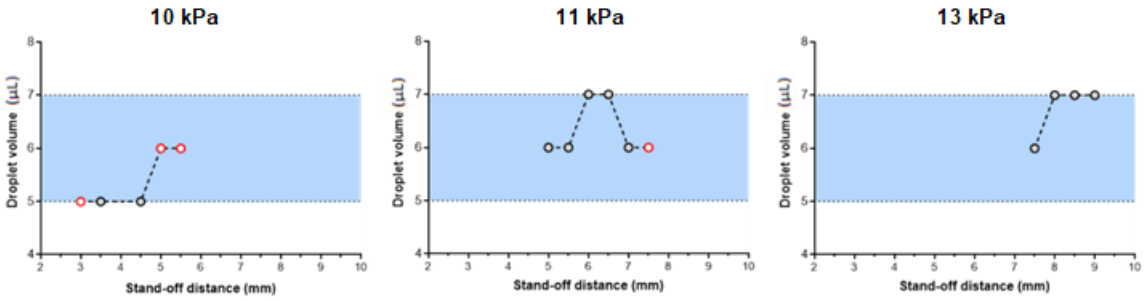

Figure 37. Calibration of standoff distance (3 – 9 mm) in micro-valve printing for different pneumatic pressure, t_{open} = 80 ms (Ø 300 µm) and shots = 1. Pressure resolution (± 1 kPa). Some configurations generated unstable droplets (red) due to the inadequate level of pressure or distance to the printbed. Droplet volumes, unlike in extrusion systems, are less dependent on pneumatic pressure, which increases volume dispense accuracy.

4.9 Bioprinting protocol design

Once all the important physical parameters involved in the bioprinting process were analysed and adjusted, it was time for the design and calibration of the spatial coordinates of the complete protocol, in other words, it was the time to establish beforehand the exact location of every single droplet or cross-linker deposition on the printbed, which is normally described as a set of coordinates (x,y,z axis) in a 3D cartesian system.

Our protocol was designed based on similarities to the already existing manual protocol of hydrogel gelation. In such protocol, Gel-Tyr/HA-Tyr solutions including cellular components and HRP, are firstly formed on the substrate or multi-well plate by precise deposition with the help of a micropipette. Afterwards, the cross-linking solution including H_20_2 is added on top of each droplet or introduced inside, mixing gently then both solutions if desired for a more homogeneous reaction. As we already mentioned during the introduction, micropipettes directly provide the dispensing of accurate volumes previously set by the user, which seldom occurs when working with printheads. All parameters involved in the simple deposition of a single hydrogel sample by hand (volume, pressure, time employed, distance to the surface, pipette tip, sample location) are chosen and easily adjusted at will by the user at the moment of pipetting. In 3D automated systems, a digital model similar to the popular sketches from CAD software is processed by software tools that slice and translate it into a set of coordinates and functions describing the deposition pattern(s) followed by the printhead(s), the order in which they are printed, and the location of each deposition point. The data are then loaded into the 3D bioprinter, where some parameters such as pneumatic pressure, cartridge temperature or the initial standoff distance can be modified before, during, and after the printing process thanks to the user-friendly operational interface generally included in the printing device.

Standoff distance in the Biosafety 3DDiscovery™ Evolution bioprinter is conceived slightly differently from its physical concept (***Figure 38***). While in physical systems, standoff distance and nozzle height refer to the same concept (distance from the substrate to the nozzle tip), some working systems operate with the original length of the nozzle tip as a nominal value after an automated process of calibration, representing the distance zero point from the nozzle tip to the substrate ($S_D = 0$).

Apart from the general standoff distance, the system also counts with other useful parameters in the Z-axis, which are described below and used for the design of the different protocol stages.

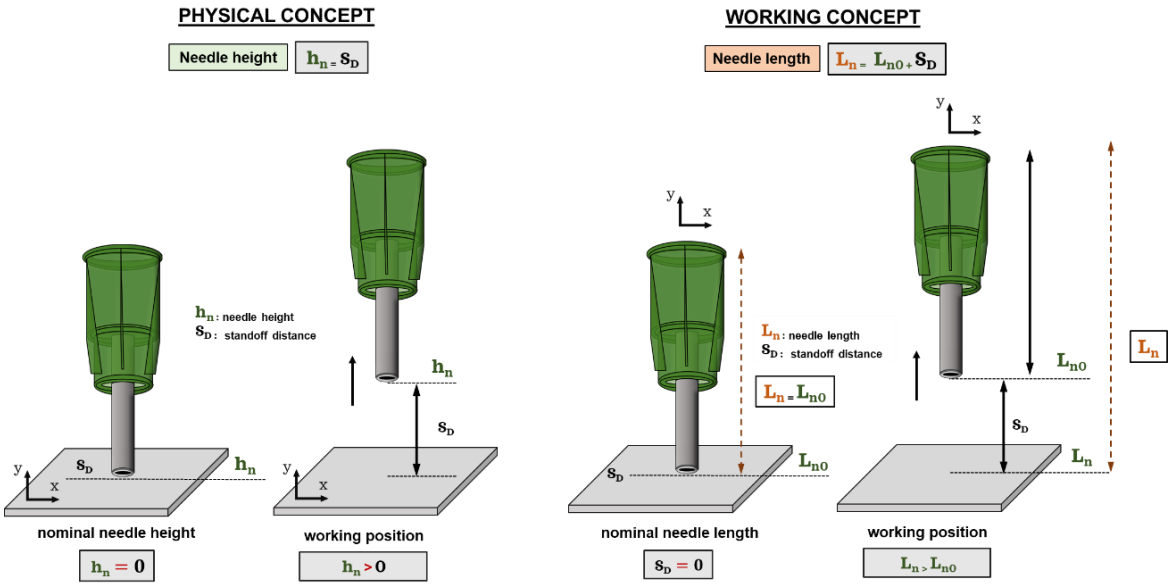

Figure 38. Representation of the standoff distance in different systems according to the centre of the cartesian coordinates (Z axis). Whereas in physical or mathematical models, standoff distance is described as the distance between the tip and the printing substrate or the needle height from the printbed ($S_D = h_n$), some 3D printing systems work with nozzle nominal lengths ($L_{n0} \neq 0$) placing the origin of the coordinate system at the base of the nozzle tip, not on the printbed substrate. Longer standoff distances are achieved by the increment of the total needle length ($L_n > L_{n0}$).

Important parameters in the Z-axis inside protocol design (3DDiscovery™)

Lift nozzle (H_L): Distance in mm from the current printing layer in the Z-axis. The printhead will lift the tip or nozzle to this point every time printhead needs to travel around the workspace without dispensing.

Safe position (H_S): Distance in mm from the build platform in the Z-axis. The printhead will lift the tip or nozzle to this point when the system executes a tool change or/and after printing completion.

Shots: Depending on the system, it can refer to the number of seconds pressure that will be applied when printing (extrusion bioprinting) or the number of droplets to dispense at a unique point of the platform (micro-valve).

Needle length (H_n or L_n) or standoff distance (S_D): Distance in mm from the base of the tip or nozzle to the build platform in the Z-axis. It is necessary to be set prior to any deposition process. When calibration occurs, needle length will reach its nominal value, being always different from zero. In the case of requiring a minimum standoff distance or

needle height, needle length can be manually adjusted, where the new needle length will be the sum of its nominal value and the added distance between tip and substrate.

The bioprinting protocol was designed in three separated phases: droplet size calibration, protocol testing with incorporated cells and the ultimate bioprinting protocol for cell culture assays (***Figure 39***). Droplet calibration and protocol testing were performed on parafilm substrates, a surface similar to the bottom of the wells in non-treated culture plates. Standoff distance (H_{n1} // L_{n1}) for the formation of droplets was decided based on ***Figure 35*** using the extrusion printhead. Once droplet calibration in the first part was successful, protocol testing included the adjustment of a second standoff distance ($H_{n2} > H_{n1}$ // $L_{n2} > L_{n1}$) for cross-linking dispensing using the micro-valve system and the collected data in ***Figure 35.*** (1) Droplet and (2) cross-linking location for each sample possessed the same (x,y) coordinates, only differing in their standoff distance (z) and printing order. Lift nozzle (H_L) and safe position (Hs) were set at least at 30 and 50 mm respectively for both phases. After a couple of assays with effective hydrogel gelation, cellular components were included in the bioink. Once cross-linked hydrogel samples could be detached from the substrate as a single structure, they were transferred to a culture multi-well plate, cultured for a few days, and analysed.

Ultimate bioprinting protocol additionally included the geometry and depth of each cell culture plate well as the new printbed substrate for the different samples. Without a correct adjustment of each well centre position (x,y), droplet formation or cross-linking ejection was unstable and unpredictable. All parameters in the Z-axis in this final part of the design had to consider the additional thickness of the bottom of the multi-well plate (D) as well as the total height of the plate (C), regardless of the plate model. Therefore, standoff distances H_{n1} and H_{n2} increased to H_{n1} + D and H_{n2} + D, and safety height parameters H_L and Hs to H_L + C and Hs + C respectively.

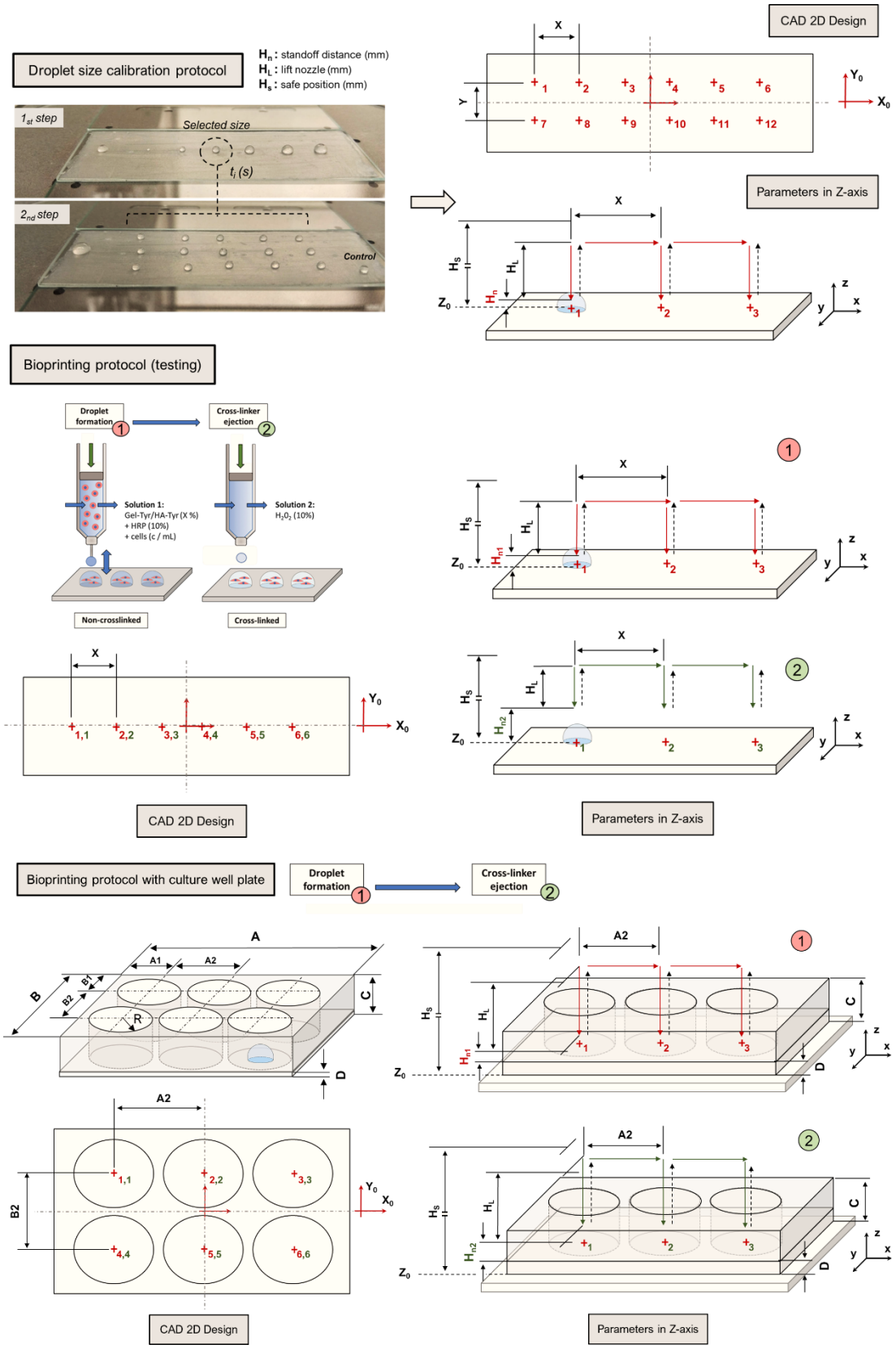

Figure 39. Stages of the bioprinting protocol design: droplet calibration with no cellular components, cell printing for its testing and optimisation, and final bioprinting protocol in cell culture well plates. Parameters of interest in the Z-axis are H_n, H_L and H_S, all nozzle tip positions during the bioink dispensing.

4.10 Cell culture studies

4.10.1 Cell viability and cytotoxicity

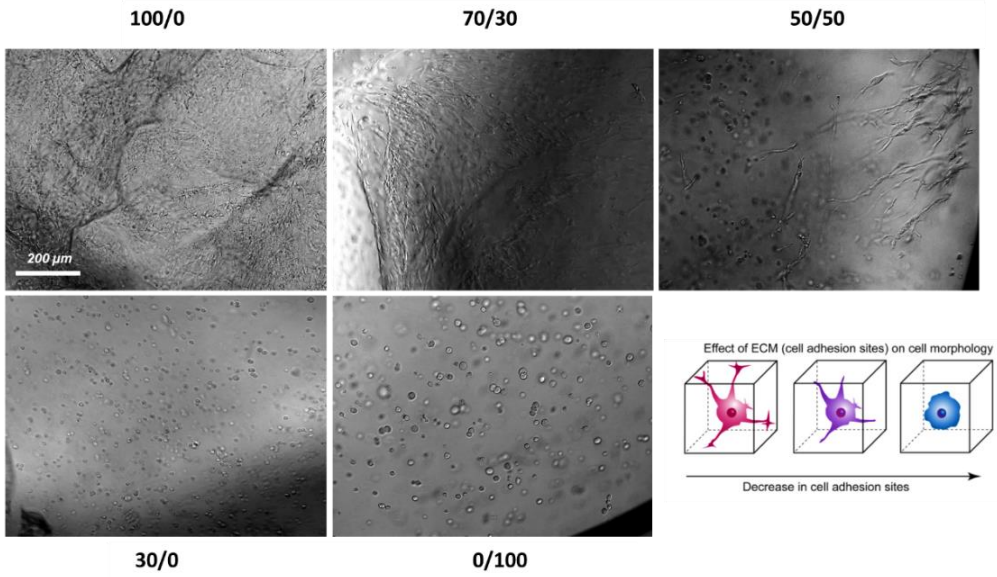

Figure 40. Brightfield images of the different Gel/HA compositions at 4 days of culture. Scale bar is 200 µm. Notice the difference in cell morphology from totally spread in pure Gel-Tyr to globular shape in pure HA-Tyr depending on the available number of adhesion domains found in the substrate. Spread cell morphologies and highly dense cell populations may be difficult to count with the Live/Dead staining in longer periods, due to the entire permeation of Calcein-AM in cells cytoplasm. Only rounded shaped cells could be easily detected in posterior assays.

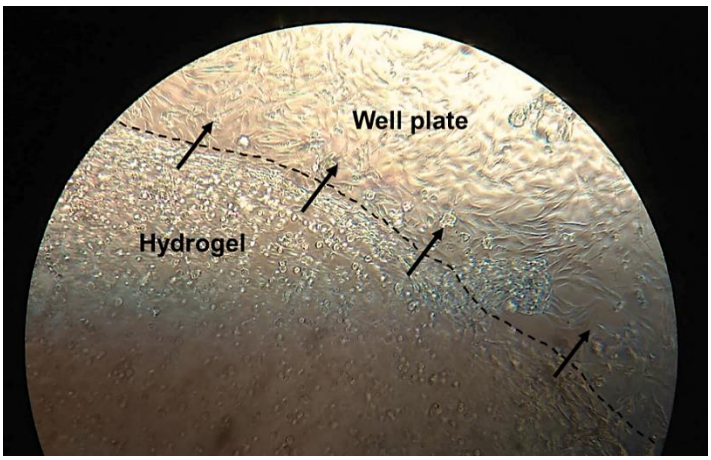

Figure 41. Optical microscope image (10x) of cells C2C12 in a Gel/HA hydrogel at 4 days of culture. Cell population outside the hydrogel is a product of the sedimentation, migration and detachment from the material. Cells behaviour denoted a good proliferation and survival to the cross-linking process, which could be also observed in posterior cell printing cultures.

Cell viability and density were measured by the analysis of Live/Dead assays as well as some visual parameters such as cell morphology and behaviour. Due to the diverse number of available binding domains between Gel and HA, initial cell cultures performed both by hand and 3D printing presented different cell morphologies between compositions after 4 days of culture (***Figure 40***) as previous studies had already shown (32). A tendency to sediment and detach from the hydrogel was also observed in all conditions (***Figure 41***) where hydrogels with higher proportions of Gel denoted higher numbers of cell detachment. Cell detachment and later adhesion to the bottom of the well plate was seen as a positive indicator since it suggested good cell viability and weak cytotoxicity during the cross-linking process. Samples cultured under contamination during incubation or cytotoxic processes of encapsulation presented no cell detachment or proliferation in any condition. These samples were always discarded and thrown away.

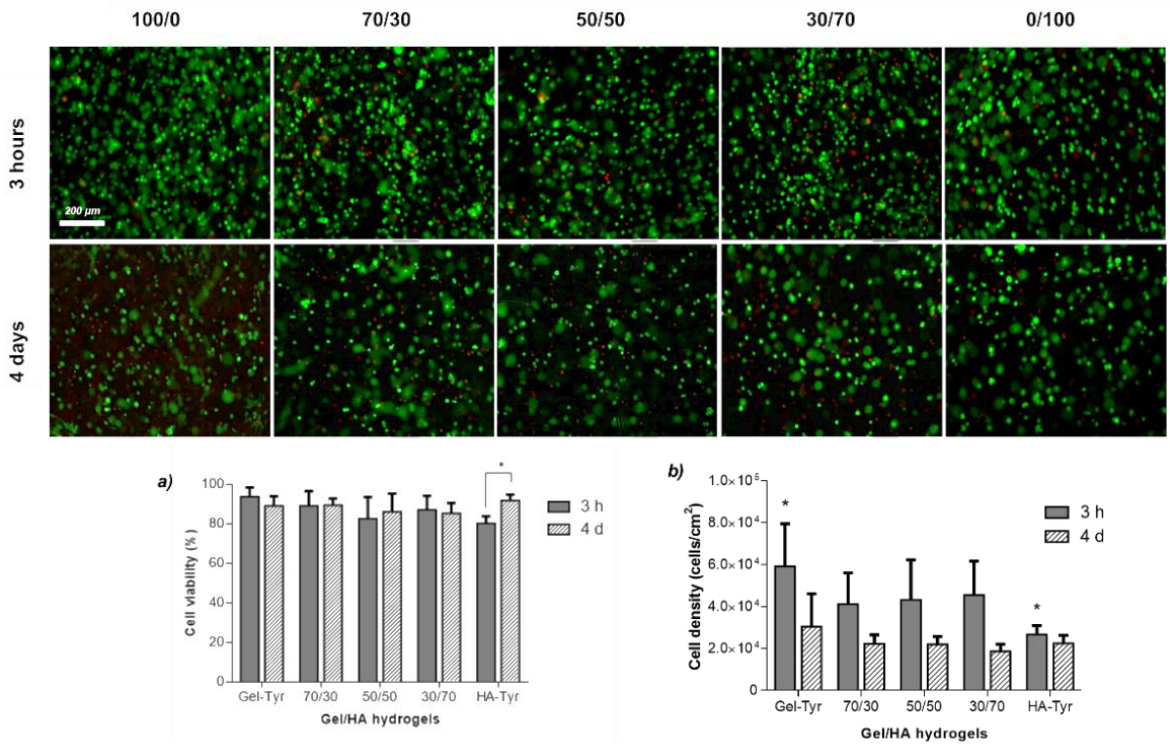

Figure 42. Viability assay of C2C12 cells in control 2% (w/v) Gel/HA hydrogels (50µL, n=3) after 3h and 4d of culture. As indicated by the two-colour fluorescence dyes, living cells (calcein-AM, green) and dead cells (EthD-1, red). Scale bar is 200 µm. a) Cell viability percentages, defined as the ratio between live cell count and total cell count, b) approximate cell density values in the different hydrogels. Symbol (*), denotes significant differences with $p<0.05$. All hydrogel compositions presented similar viability values. However, cell densities decreased with higher HA contents probably due to differences in the number of available binding domains between Gel and HA.

Control and printed samples in multiple assays (***Figures 42 and 43***) presented highly similar cell viabilities, denoting no apparent shear stress or chemical cytotoxicity during the printing process. Hydrogel compositions, as expected, presented an overall decreasing trend with regard to their cellular densities depending again on the available binding domains of Gel and HA, finding always the minimum cell density in pure HA hydrogels. Cell density in general, although expected to be higher after a few days of culture, appeared to be significantly lower in some of the assays. However, as it was previously commented, packed and spread cells were difficult to recognise by Live/Dead assays through a fluorescence microscope, attributable to the penetration of Calcein-AM into the entire cell cytoplasm. The use of nuclei staining was limited for this type of assays since nuclei dyes may result cytotoxic when used in big enough quantities. Besides, due to the probable event of cell detachment (cell loss) after seeding, densities were likely higher than the observed. Cell loss during printing alongside cell sedimentation could also explain the overall lower cell density in printed samples compared to controls in both time points, as cells may have attached to the cartridge-needle walls during the extrusion process and then to the bottom of the well plate, another supporting idea of the nonexistent cell damage during deposition.

Hydrogel peroxide (H_20_2) acts as a co-substrate for HRP-catalysed cross-linking reactions. H_20_2 is one of the major members of reactive oxygen species (ROS) and plays an essential role as a beneficial signalling agent (253-257) or a cytotoxic hazard in physiological and pathological processes (258-266). This molecule has been extensively studied for its participation in some metabolic pathways of cancer cells (267), given its natural secretion during chronic inflammatory responses. Oxidative stress generated by externally added H_20_2 induces stress-induced premature senescence (SIPS) in a variety of cell types (268-270), being one of the most important causative factors for the induction of cell apoptosis.High concentrations of this molecule have proven to be highly cytotoxic, depending on the cell type's sensitivity to oxidate stress, cell concentration, the ability of these to eliminate H_20_2, the used volume of medium as well as the exposure time (258,259).

Differences in the cell concentration likely contribute to the large variation found in the cytotoxic concentrations of H_20_2 reported in numerous papers. Such differences, nonetheless, are very difficult to determine, as relevant information on cell density and culture medium volume most often are not published. For instance, studies in gingival fibroblasts demonstrated how SIPS could be induced by a concentration of H_20_2-treatment as low as (> 20 μM) when compared to other types of fibroblasts (271). However, H_20_2 under subtoxic concentrations has also been demonstrated to induce a higher proliferative activity in human

dorsal fibroblasts, rabbit lens epithelial cells, baby hamster kidney fibroblasts and embryonic Chinese hamster ovary fibroblasts (256, 259, 272, 273). Apart from this, H_20_2 is known to cause degradation/depolymerization of various polymers at relatively high concentrations and long exposure times, including Gelatin (310), HA (311,312), or even other Gelatin grafted with phenol moieties (Gel-Ph) hydrogels (313).

Different supplementation of culture medium with antioxidants and precursors (274,275), as well as different contents of peroxide-consuming additives in the culture medium like pyruvate (276,277) or serum albumin (278) found in fetal bovine serum (FBS), have also been oarthritic chondrocytes in synovial fluid under oxidative stress, redshown to increase the ability of some cell types to eliminate H_20_2 during culture (258). Likewise, some studies have pointed out the ability of HA to protect human osteoarthritic chondrocytes in the synovial fluid under oxidative stress, reducing the levels of hydrogen peroxide and superoxide (O_2) in patients with knee osteoarthritis via multiple intracellular regulations, including anti-oxidation, anti-apoptosis, promotion of protein synthesis, and cell survival (279).

There are several documented research studies assessing the effects of H_20_2 on cell proliferation and survival of C2C12 cells (280-285), some of them presenting cell death at H_20_2 concentrations as low as 100 µM at cell densities of 5 x 10^4 cells/cm^2 (280) or inducing atrophy and loss in myoblasts myotubes at 1mM for 24h culture (282). Despite this, our system decomposes H_20_2 molecules into H_20 as part of the HRP-catalysed cross-linking reaction, and hence the possible cytotoxic effects of hydrogen peroxide in enzymatically cross-linked Gel/HA systems may greatly differ from other cell culture models, even when using the same cellular line. Additionally, due to the high concentration of C2C12 cells used in each hydrogel (4 - 8x10^6 cells/mL) alongside the elevated volumes of medium, sometimes including 20% FBS, effects of H_20_2 on cells could be even milder than expected. In order to study the possible cytotoxic effects of inaccurate cross-linking dispense (higher H_20_2 concentration) as well as its study for potential applications in drug testing, cytotoxicity assays were performed in printed cross-linked hydrogel samples in presence of higher H_20_2 concentrations (3mM, 4mM and 5 mM), 30 to 50 times the minimum toxic concentration determined in previous studies (280).

From ***Figures 43 and 44*** it is possible to infer that the increase of H_20_2 concentration up to 5 mM in the cross-linking solution did not produce significant variations in cell viability due to any cytotoxic hazard. Some compositions even presented higher cell densities than their

regular printed samples, probably because of an increase in the cross-linking density that produces hydrogels to be less swollen, in other words, to be more compacted. We hypothesise that when the cross-linking solution is diffused through the hydrogel precursor solution, HRP and phenol moieties immediately react with the H_20_2 molecules nearby, decomposing them into H_20 and preventing them from interacting with cells. The remaining H_20_2 is then eliminated by the very same cells in culture after a short time. Pure HA hydrogels, as the composition with the lowerest degree of tyramine substitution, could be the one more affected by H_20_2 increment, however, presented similar cell viability and density values to the regularly printed samples.

Calcium-free Krebs Ringer buffer (CF-KRB) is a solution of several salts dissolved in water which proportions vary from species to species, to create an isotonic solution relative to the body fluids of an animal. A salt solution's basic function is to maintain the pH and osmotic pressure balance in the medium resembling the blood serum in its salt constituents, as well as provide the cells with water and essential inorganic ions for correct cell functioning. Krebs Ringer's solution is frequently used in *in vitro* experiments on organs or tissues such as *in vitro* muscle testing (286-288). CF-KRB also possesses good flow perfusion, facilitating the flow of H_20_2 molecules throughout the hydrogel precursor solution. Despite this, CF-KRB participation in the cross-linking of Gel/HA hydrogels in other projects demonstrated to be fairly high cytotoxic when using particular cell types, as is the case of primary human hepatocytes (286). Hepatocytes viability in synthesised Gel/HA hydrogels with CF-KRB, presented a dramatic decrease after 1 day of culture (20% cell viability), becoming almost inexistent (0,5%) after 7 days. In our project, although several successful results were obtained when using the CF-KRB solution in C2C12 cells, truth is that there were also numerous discarded assays with similar results. Cells in contact with CF-KRB solution for long enough times ($t > 15$-20 min) resulted in general in very low initial cell viabilities, generating hydrogels with no cell proliferation or cell detachment from samples during the following days. We strongly recommend the use of alternative buffer solutions for prospective assays, given the large quantity of discarded samples we faced during this project combined with the time employed for the preparation of each 3D printed deposition and their following successive culture.

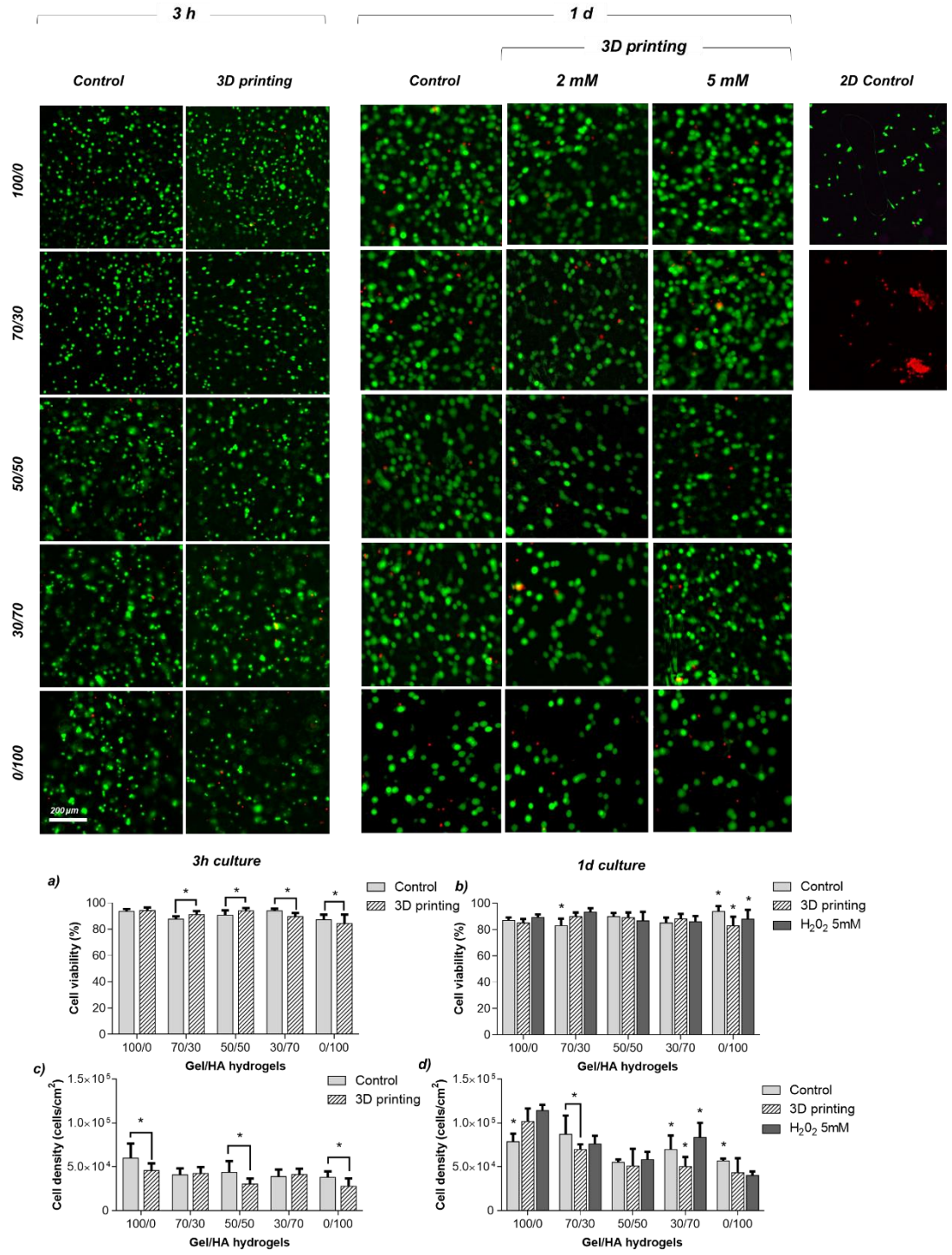

Figure 43. Viability assays of cells C2C12 in 2% (w/v) Gel/HA hydrogels at different time points (3 h, 1d) and conditions (control, 3D printing, 3D printing + 5mM). Samples were formed and cross-linked by hand or by printing automated process to assess the influence of mechanical stress and possible contamination during deposition. Scale bar is 200 µm. Cell viability at (a) 3h and (b) 24h culture. Cell density at (c) 3h and (d) 24h culture. Samples at higher H_20_2 molarity (5mM) were included in the 3D printing protocol to evaluate the effects of possible excess H_20_2. Symbol (*), denotes significant differences with $p<0.05$.

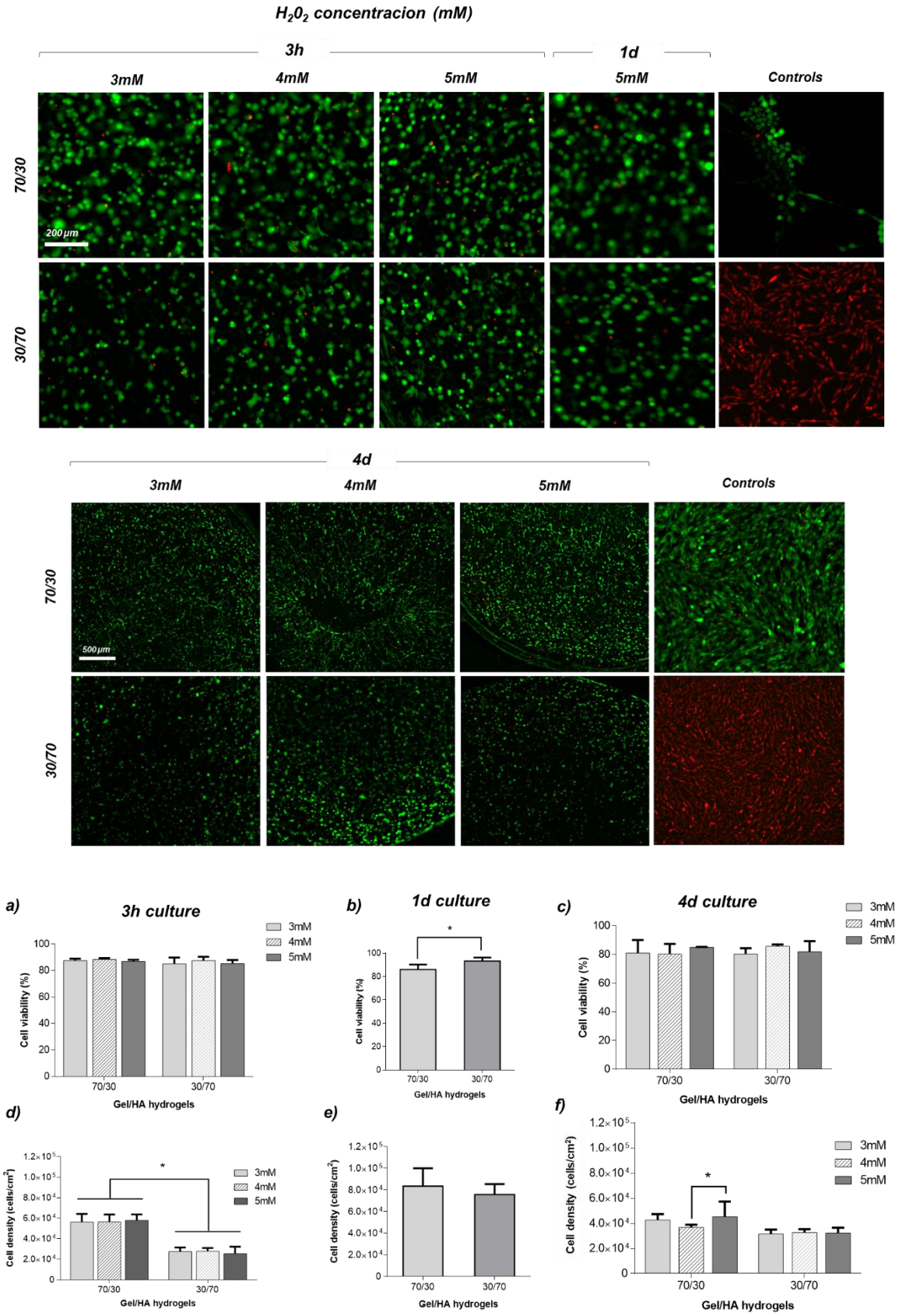

Figure 44. Cytotoxicity assay of cells C2C12 in printed Gel/HA 70/30 and 30/30 hydrogels at (a) 3h, (b) 1d (5mM) and (c) 4d of culture and their respective cell densities (d-f). Samples were printed with higher H_2O_2 concentrations in all samples from 3mM to 5mM to continue the evaluation of H_2O_2 cytotoxicity.

4.10.2 Cell adhesion and morphology

Once cell viability in Gel/HA hydrogels was demonstrated to be successful up to 4 days of culture by our designed 3D printing protocol, cell morphology and adhesion were studied after 7 days of culture to ensure correct cell proliferation and adhesion over longer periods (***Figures 45 and 46***).

Assays were performed in different hydrogel compositions and culture conditions, including differentiation medium at higher cell concentration. The cell line of C2C12 cells possesses very short periods of differentiation, being perfect for their study and analysis. Cell adhesion and morphology were also evaluated in hydrogels cross-linked at different H_20_2 molarities, in order to continue with the assessment of the possible cytotoxic effects presented in cells.

Higher cross-linking densities are usually responsible for modifications in the hydrogel pore size and pore interconnectivity, swelling ratio, hydrogel stiffness and hydrogel degradation rate among others. Increasing either or both of the two catalysers (HRP/ H_20_2) decrease the time required to gain structural integrity during the process of cross-linking given the rise of the rate of cross-link formation, preventing samples from losing their designed shape as well as from cell sedimentation issues. Decreasing the gelation time also provides a faster-pace deposition in printed scaffolds with several layers, reducing the time for each layer to achieve certain mechanical integrity and facilitating the generation of more complex and on a bigger scale constructs. Hydrogels in this project were only cultured at different H_20_2 molar ratios, since HRP is found non-cytotoxic regardless of its concentration, and therefore its employment is considered safe for any prospective Gel/HA hydrogel obtention.

Both 70/30 and 30/70 Gel/HA compositions showed an increment in the number of spread cells and general cell density, given the rise of the number of cross-links. Despite the impossibility of analysing the mechanical properties of any cross-linked samples for the same reason, we could not provide rheological data of the precursor solutions, we predicted an increase of the overall hydrogel stiffness as a result of the increment of cross-link density, which can be detected by cells and modify their behaviour.

Antibody against myosin could not be recognised in the different culture assays (***Figure 46***), however, a change in cell morphology could be appreciated regarding the fusion of some cell cytoskeleton and stretched morphologies in some of the pictures when compared to the rest of the conditions. Possible reasons for the failure of the antibody against myosin were thought to be related to the use of inadequate concentrations of the MF-20b or Cy3 antibodies

(for $8x10^6$ cells/mL) during the staining process or the own failure of any of the two antibodies. The failure of the differentiation-induced medium is unlikely to be the cause since cell morphological differences (more elongated shapes without lateral nanopodia and thicker cytoskeleton structures (more absorbance)) seen in samples should not have happened in the absence of ITS-X. Samples cultured in differentiation medium seemed to retain their original higher cell numbers, which supports the idea of no probable cell cytotoxicity or damage during printing. The number of spread cells, in comparison to the rest of 30/70 samples, was also observed to significantly increase with no apparent reason.

Even though the staining of some conditions could not be completely achieved, all the tested hydrogels, regardless of their composition or culture condition, were successfully generated by our designed 3D printing protocol, which denoted the lack of any harmful shear stress or cytotoxicity during the process. We could therefore establish an advantageous alternative for the processing and cell encapsulation of enzymatically cross-linked Gel-Tyr/HA-Tyr hydrogels, becoming less time consuming and dependent on the researcher's ability to manually cross-link samples.

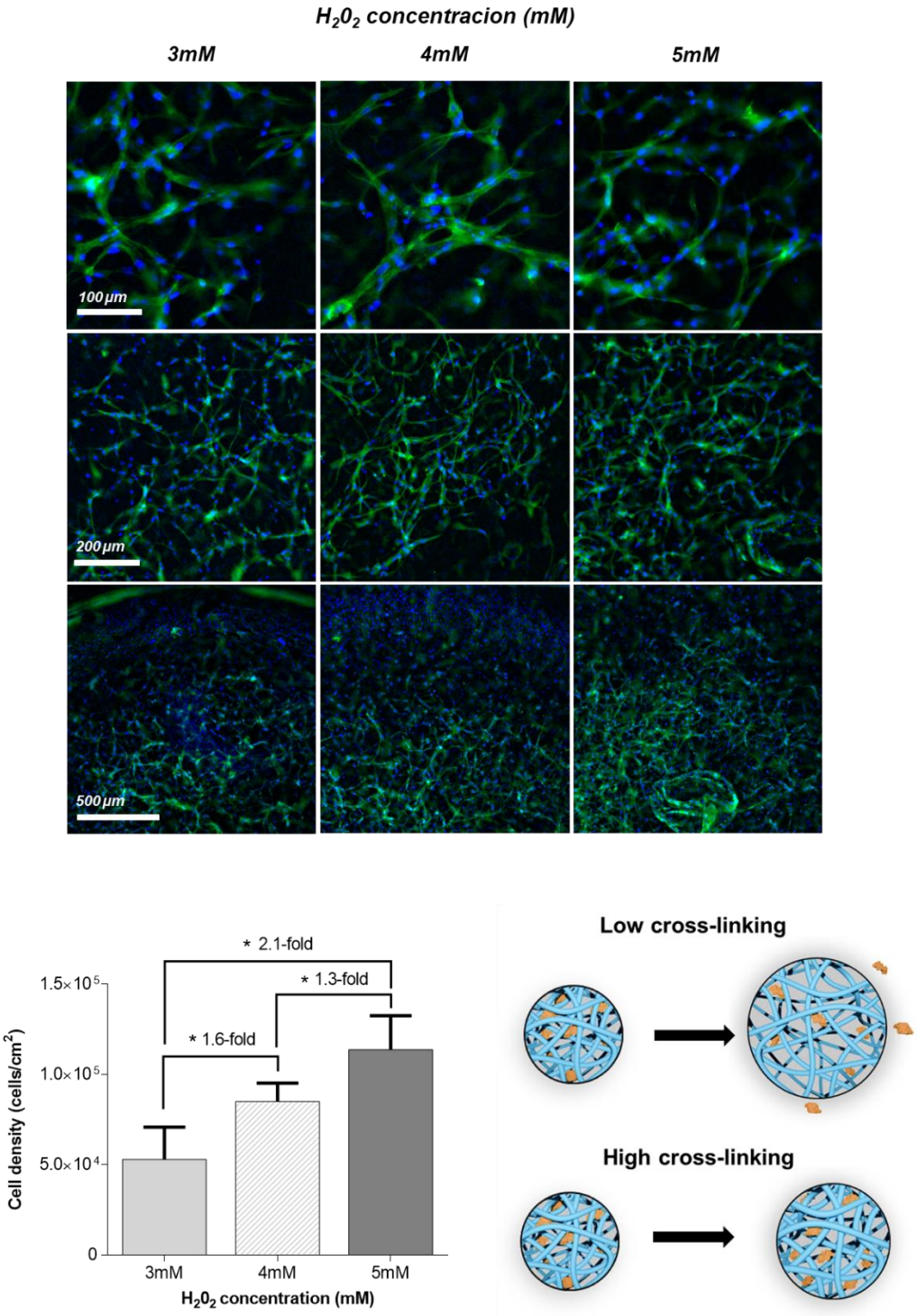

Figure 45. Adhesion of cells C2C12 in Gel/HA 70/30 hydrogels at 7 days of culture (above) by means of 3D printing. H_2O_2 concentration in samples was increased from 2 mM to 3mM, 4mM and 5mM. Actin and DAPI were used to stain cell cytoskeleton (green) and cell nuclei (blue) respectively. The increase of cell density between compositions may be mostly due to a general increase in the cross-linking density (bottom right). Pictures also denoted a possible increase of cell spreading in higher cross-linked hydrogels.

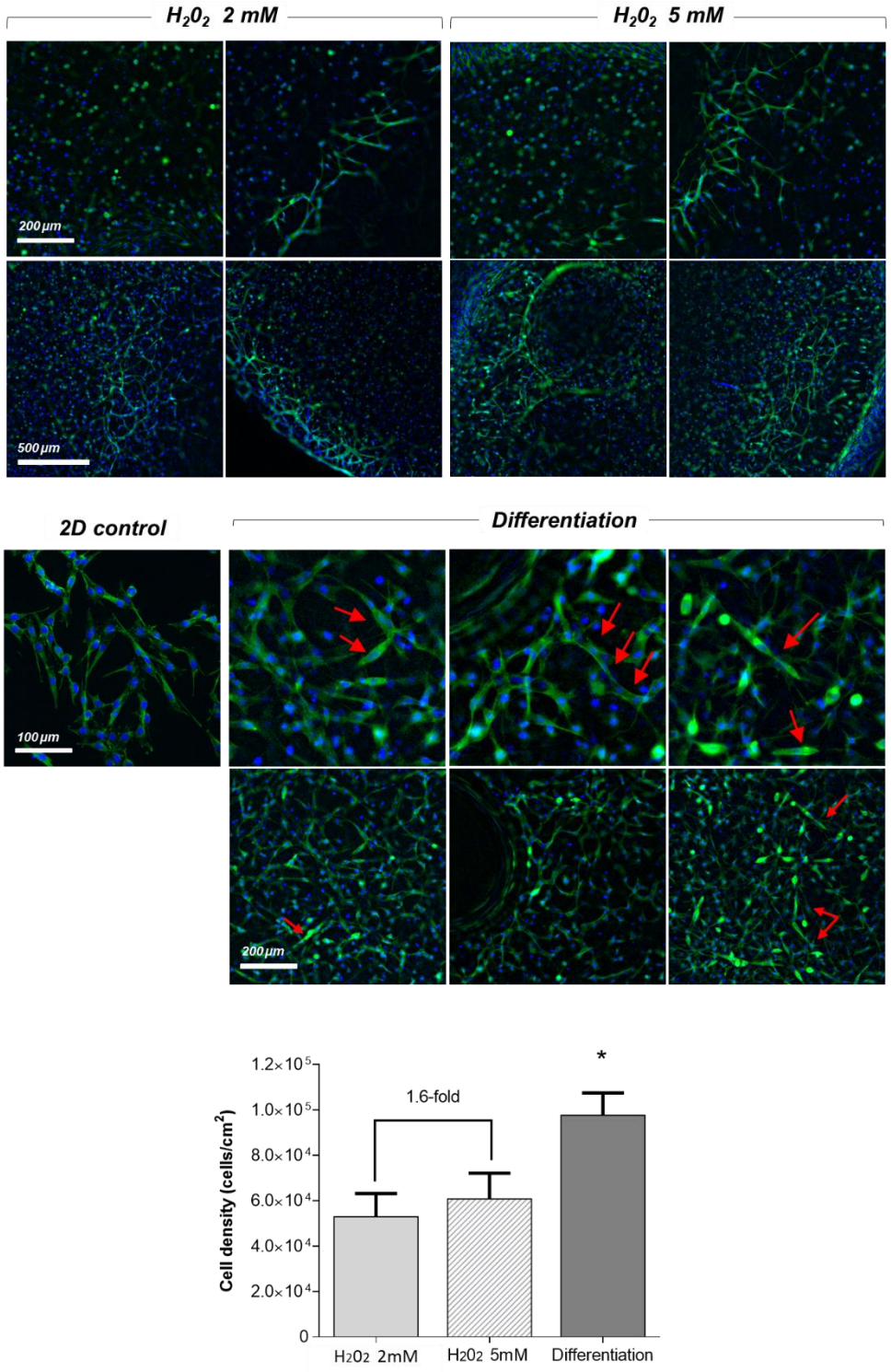

Figure 46. Adhesion and differentiation of cells C2C12 to Gel/HA 30/70 hydrogels at 7 days of culture by means of 3D printing (control, H_2O_2 5mM, differentiation). Antibody against myosin was not recognised, although differences in morphology could be observed in the actin cytoskeleton when compared to the other conditions (red arrows). Again, an increase in H_2O_2 in comparison to control samples denoted an increase in the cell density, most probably caused by the increase in the polymer cross-linking density of the hydrogel.

5. Conclusion

Improving the ability to predict the efficacy and toxicity of drug candidates earlier in the drug discovery process speed up the introduction of new drugs into clinics. In drug discovery, the conventional procedure of screening drug compounds starts with 2D culture tests, followed by animal model tests and finally clinical trials. 2D and animal models are usually nonpredictive and often unrelated to in vivo human responses, given their different nature and organization of native tissues. 3D in *in vitro* systems, albeit still encountering some serious limitations, have remarkably advanced the drug screening process since 3D tissue models can closely mimic native tissues and, in some cases, the physiological response to drugs. 3D bioprinting, among the different in vitro systems, is a highly promising technology that possesses numerous advantages such as high precision control over size, high-throughput capability, tailored and accurate microarchitecture, coculture and vascularisation ability with minimum cross-migration of cells, and low risk of cross-contamination (164,290). Besides, 3D bioprinted tissue models for pharmaceutical use are not subject to the rigorous safety and ethical issues required for implantation into humans, easily providing valuable relevant preclinical data.

The present study offered a complete evaluation of the different operational parameters involved in the design of a viable and reproducible 3D bioprinting protocol of enzymatically cross-linked Gel-Tyr/HA-Tyr hydrogels as potential skeletal and chondrogenic 3D models for future applications in vitro drug testing and toxicology analysis of drug candidates.

Influencing parameters such as bioinks viscosity, gelation time, nozzle geometry and diameter, flow rate, pneumatic pressure, polymer solution weight, shear rate, temperature, cell sedimentation rate, as well as standoff distance were evaluated and adjusted based on their use in two different printing modalities, extrusion-based for the formation of hydrogel droplets and droplet-based micro-valve bioprinting for the ejection of cross-linking. After a laborious assessment, we eventually demonstrated the excellent viability of our designed bioprinting protocol by means of several cell culture studies, which quantified the possible cell cytotoxicity and mechanical stress damage not only in different hydrogel compositions but also in various culture conditions. This evaluation was performed via the analysis of cell viability, density, morphology and behaviour at different time points, resulting in a very positive outcome and potential application development.

Both systems were found to possess advantages and disadvantages regarding bioinks limitations and printing dynamics. Extrusion bioprinting offered no range limitation either in terms of bioink's viscosity or vehicle´s cell density, providing an extensive range of possibilities in multi-material printing. Yet, as it was revealed, very poorly viscous materials (as the bioinks meant for this project) were lacking independence from external stimuli such as the printing pressure or the own bioink's weight at the cartridge reservoir, generating significant unstable flow rates either during the same printing process or when tried to replicate. Moreover, extrusion-based systems possess limited printing resolution, limiting sometimes the direct fabrication of some microstructures. It is reasonable to think that, for non-continuous printing applications like ours (droplets), extrusion bioprinting might not be the most beneficial strategy on the table, however, with previous extensive calibration hydrogel droplets with very low-resolution requirements were eventually and successfully replicated, without any related findings of cell sedimentation or cell damage. Nozzle geometry also played an important role in keeping constant flow rates, where tapered nozzles tips, albeit offering higher-pressure gradients at lower shear stress levels, exhibited the greatest sensitivity to pressure changes, difficulting the dispensing of similar droplets at high sample volumes. This could be sorted out by the selection of cylindrical nozzle tips, well-known geometries for general purpose applications and more precise depositions counting with a vast variety of diameters and tip lengths. Given the very low viscosity bioinks presented in this study, we decided to opt for chamfered cylindrical tips, a particular type of cylindrical geometry with smaller tip contact surfaces specially designed for microdot applications requiring very stable flow rates and without gripping issues.

On the other hand, droplet-based micro-valve guaranteed a more accurate dispensing due to the poor influence of applied pressure and the absence of nozzle tip. Another benefit relies on its non-contact working mode. Nozzles in this system do not need to be in direct contact with samples or the substrate surface in order to dispense material, becoming exempt from clogging issues at the tip exit and thus providing the easiest and most effective dispensing mechanism of these two modalities. However, droplet-based modalities are rather constrained by one important parameter: time. Poor viscosity and pico-scale flow rates tend to originate longer printing times, which enhance the effect of sedimentation at lower cell densities ($\rho > 3x10^6$ cells/mL). In addition, lacking a nozzle tip, albeit preventing material build-up at the tip itself, does not prevent material clogging inside the micro-valve, forcing the worker to perform regular deep cleaning practices between cross-linking steps. In systems with single micro-valve printheads like our case, this inconvenience can induce

large increments of the time required for printing in multi-step protocols, eventually becoming detrimental for cells as well as for samples mechanical integrity. In the current circumstances, droplet formation and cross-linking of all analysed hydrogels yet feasible by both methodologies were decided to be performed by extrusion bioprinting and micro-valve ejection respectively.

Parameters affecting cell viability were evaluated regardless of the technology, focusing on the maximum shear stress and pressure drops achieved in laminar flow regimes (Re < 2100). Wall shear stress was found to be relatively low in comparison to the established threshold level in other studies (τ_{max} < 5 kPa) with values from 30 Pa (η < 10 mPa·s, Q < 20 μL/s, 23G nozzle) to 250 Pa (η < 10 mPa·s, Q < 20 μL/s, 27G nozzle) during very small printing periods. Even in the event of a sudden increase of bioinks viscosity (η < 100 mPa·s) due to temperature variations, shear stress in extrusion-based printing should not be expected to reach dangerous stress levels, assuring correct cell dispensing and viability in less favourable situations. Pressure drop, on the other hand, presented a different possible scenario when reaching the application of certain levels of pneumatic pressure (P > 200 kPa) at high nozzle gauges, very usual in extrusion systems, as the maximum pressure applied by some current benchtop 3D printers on the market may be insufficient. Similar problems appear for minimum pressure resolutions, which in some cases have been seen to reach the 6 kPa, much higher than the pressure difference required to significantly alter printing flow rates in our system (± 1 kPa). The micro-valve system was capable of producing small accurate cross-linking ejections at low pneumatic pressure (P < 15 kPa), being more effective for high-resolution applications in low viscous bioinks.

Cell viability and adhesion did not either present significant differences in cell survival when using extrusion bioprinting even when H_20_2, cytotoxic on cells at relatively low concentrations, was increased. We can confirm then that the cross-linker deposition, by either one or the other method, would be accurate enough and totally safe for the cells until further investigation.

CF-KRB solution used for the hydrogel precursor solutions was found acceptable for hydrogel cross-linking of Gel-Tyr/HA-Tyr samples, however, we strongly suggest the investigation of buffer solution alternatives for future research as its use during long hydrogel formation processes presented a significant rise in cell death of cells C2C12 and other used cells types in previous studies.

Gelation times were decreased by means of increasing any of the used catalysers HRP/H_2O_2 during the cross-linking process, where higher H_2O_2 concentrations did not apparently change samples cell viability but incremented the average cell density of all compositions when compared to the initial H_2O_2 ratio. From our point of view, higher cross-linking densities seemingly generated less swollen hydrogels with lower cell to cell distances, artificially raising the cell population numbers. However, it is also a real possibility that higher cross-link ratios increase the general stiffness of hydrogels, generating more attractive environments for cell proliferation. This appealing mechanism, schematically described in ***Figure 46***, could be employed in further printing applications to help maintain the structural integrity of the cell-laden hydrogels of this consistency as well as to decrease the average printing time of more complex hydrogel structures. About the above, it is important to highlight that an increase of the cross-linking density may be responsible for not only one but a few hydrogels physical properties such as hydrogel pore size and pore interconnectivity, swelling ratio, hydrogel stiffness and degradation rate, properties that are mainly responsible for cellular behaviour and whose alterations could also undermine some already achieved optimal behaviours. We hence suggest an extensive analysis of some of these properties prior to any further application.

In summary, we successfully designed and implemented a 3D bioprinting protocol for enzymatically cross-linked Gel-Tyr/HA-Tyr hydrogels without any side effects, which was, all in all, the main goal of this Master in Research project.

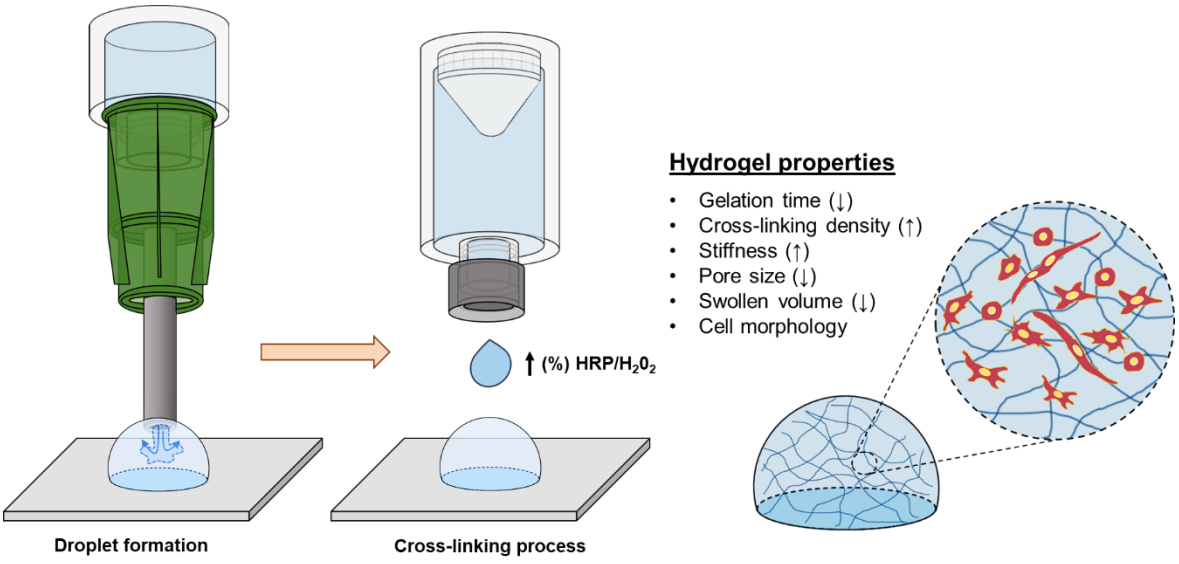

Figure 47. Influence of the cross-linking HRP/H_2O_2 concentration on different hydrogel properties. Depending on the cell type, cell morphology would be positively or negatively affected by the overall increment of hydrogel stiffness.

6. Future work: "What's next?"

Bioink support strategies for complex hydrogel scaffolding

As we have repeatedly commented in our study, soft hydrogels such as 2% w/v Gel-Tyr/HA-Tyr generate less stable and significantly weaker 3D constructs that tend to collapse during the fabrication process and/or upon exposure to physiological conditions. Furthermore, the low mechanical strength and high wettability of hydrogel bioinks often result in poor shape fidelity and spreading of the deposited filaments or pico-scale droplets, making high-resolution fabrication of complex tissue structures impractical.

In order to overcome this limitation, numerous strategies have been developed for stabilising the deposited bioink in a non-destructive manner at different stages of the printing process, which can be divided into two main categories: bioink cross-linking and bioink support. The effectiveness of the bioink cross-linking strategy when used as the only means of stabilisation depends on, as it has already seen in our project, (1) a fast cross-linking reaction during or shortly after deposition in order to avoid spreading and collapsing of the printed material, and (2) the printing's scheme ability to self-support bioinks deposition without collapsing until cross-linking of the bioink is attained. Most biologically relevant structures, however, contain complex spatial geometries that generally include elements with overhang angles, making fabrication impossible without providing adequate support to overhangs even at rather fast cross-linking processes.

Printing strategies have been developed, in which the fabricated structures are supported by external elements, that hold and preserve their shape until final structural and mechanical integrity are accomplished through the cross-linking process (291,292). These elements, represented in ***Figure 48***, can be printed at the same time as bioinks as part of the fabrication procedure. At the end of this process and once the bioink structure is stabilised, the support materials can be extracted or preserved as an integral part of the printed structure.

The most simple supporting strategy is based on the fabrication of external structures incorporated in the digital design of the object that stabilises and hold the different deposited bioinks, providing them with an external and/or internal platform to lean on. These structures are generally composed of acellular natural or synthetic biocompatible substances with excellent mechanical properties and good printability. In the case of hydrogels, this can be translated in bioprinting using cell-laden hydrogel with another more viscous sacrificial hydrogel or hybrid bioprinting of biodegradable synthetic polymer shell with cell-laden

hydrogel bioinks. Some good examples of synthetic supporting materials are Pluronic F127 (PF127) and polycaprolactone (PCL), whereas alginate and agarose polymers are naturally derived materials.

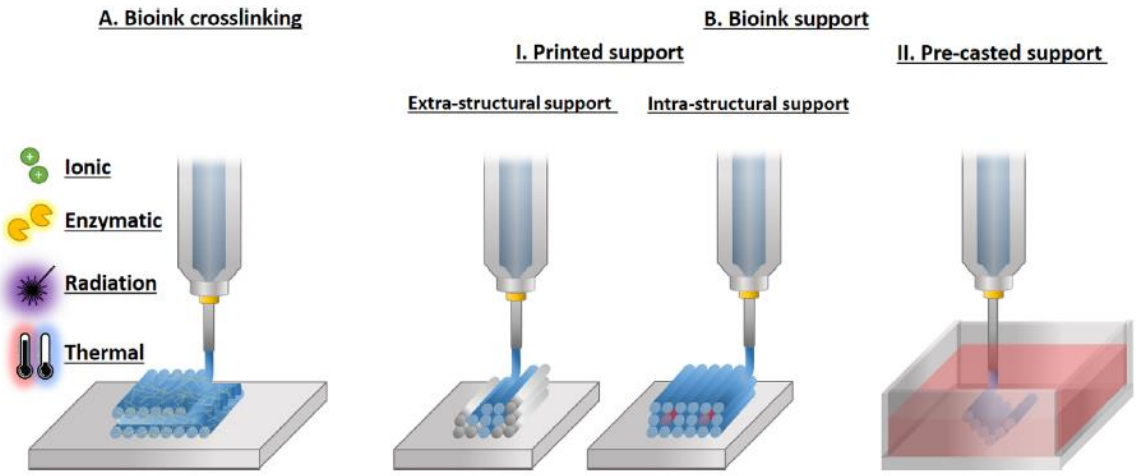

Figure 48. Schematic representation of printout stabilisation methods. (a) Bioink cross-linking- The bioink is reinforced during or after the printing process using ionic, physical, light irradiation or enzymatic cross-linking mechanisms. (b) Bioink support – The incorporation of temporal or permanent elements that mechanically support the extruded or ejected bioink to form the final printed structure. (I) The support ink is or can be co-printed with the bioink, stabilising it externally or internally. Afterwards, the support can either be left (support bioinks) as an integrated part of the structure or sacrificed (fugitive or sacrificial bioinks) to leave voids within. Support material can be patterned around ("extra-structural") and/or within ("intra-structural"). (II) Pre-casted support – The bioink is deposited into a bath pre-filled with support medium of similar density that entraps and retains the position of the deposited strands, allowing free-formation of the printing structure in all dimensions. Later, after the bioink's shape is reinforced, this support can be washed and removed.

Pluronic F127 is a biocompatible co-polymer widely used as a sacrificial material and a bioink's component alike. Above a critical micelle concentration and temperature (T > 30º C), the PF127 undergoes thermally reversible gelation (293), being highly printable and easy to extract by gradual dissolution in aqueous media or by rapid liquefaction at low temperature (4ºC) (294,295). Pure PF127 has been used as a sacrificial support material that maintains the printed structure not only from the outside but also from the inside, sometimes employed for the creation of hollow channels for scaffold vascularization inside the

fabricated hydrogel. Polycaprolactone (PCL) on the other hand, is a common example of a non-sacrificial stabiliser. PCL is a biocompatible, biodegradable, flexible synthetic polymer with a low melting point of 60ºC. Molten material can be extruded into filaments by fused deposition modelling (FDM) and rapidly cooled down by low-temperature atmospheres, generating a rigid, water insoluble supporting framework (296,297). Depending on PCL fibre spacing, orientation, and/or thickness, it is also possible to tune the mechanical stiffness of the graph, optimising its properties to match that of the desired tissue and thus the microenvironment for the seeded cells (192). Furthermore, it is also possible to implement both classes of supporting materials, in order to provide additional support and to generate perfusable, complex, vasculature-like structures.

Unlike natural polymers, some synthetic polymers have the risk of low biocompatibility as well as toxic degradation by-products (298). Using natural polymer-based hydrogels both as cell-laden and supportive sacrificial bioinks works as a tool to mimic the ideal ECM microenvironment for the cells. Alginate and agarose are highly used polysaccharide-based natural polymers as material support, derived from brown algae and seaweed respectively. Alginate has similar properties to the natural ECM, controllable viscosity, highly printable due to its inherent shear-thinning properties, being mostly cross-linked with $CaCl_2$ (especially at room temperature) (299). Agarose has a rapid and gradual gelation kinetics ranging from 20ºC to 70ºC, suitable for mould-based fabrication in 3D bioprinting.

A few important challenges remain when using these support materials though. Sacrificial bioinks should allow oxygen and nutrient diffusion through the printed structure as well as possess a controlled degradation rate, which is not the case with very dense structures such as agarose strips or cross-linked alginate. Besides, cross-linked alginate that requires the use of sodium citrate or ethylenediaminetetraacetate (EDTA) treatments for its dissolution, hinders calcium-dependent cell attachment. Other support materials need to be heated to high temperatures as agarose or cooled down as PF127 to become printable, getting away from cell physiological temperature. Moreover, while the PF127 is highly printable, it has a low cytocompatibility when used at high concentrations. Similar situations are encountered with alginate and agarose when used alone, which may induce apoptosis due to the poor cell-binding domains necessary for cell adhesion and proliferation and hence they are usually used with other functional polymers to create a blend bioink.

Commonly, collagen, gelatin, hyaluronic acid, dextran and fibrin, are employed to develop natural polymer-based bioinks (300) in the company of poor adhesive but highly printable materials (alginate, agarose, etc.), enhancing scaffolds integrity during and after being printed and washing out afterwards the non-crosslinked components (301).

Recently, the development of new sacrificial bioinks has opened new possibilities for hydrogel bioprinting. Some of these bioinks like 3.5% Agarose: 10.5% Alginate (302), 9% Methylcellulose: 5% Gelatin (303,304), or 9% Methylcellulose: 3% Alginate (305) can take place at room temperature and self-erode in the cell culture medium at 37º C without leaving no residues behind. The hydroxyl groups present in alginate and agarose lead to the formation of hydrogen bonds between these two polymers, whilst the calcium ions present in the cell culture medium lead to very loose cross-links between alginate chains. The use of any cross-linking agents has important advantages like ease of implementation, reproducible results at every batch, and a higher speed of printing (302).

The addition of inverse thermal gelling polymers (gel T > 37ºC) such as methylcellulose (MC), a water soluble derivative of cellulose forming viscous solutions in water, can be applied as an agent to temporary increase the low viscosity of other polymer solutions when used at low density, like alginate or gelatin. Since MC does not contribute to the gelation, it is therefore released from the scaffold after the possible cross-linking of the rest of the polymer components, returning the cross-linked hydrogel to its original characteristics as a low concentrated structure (305).

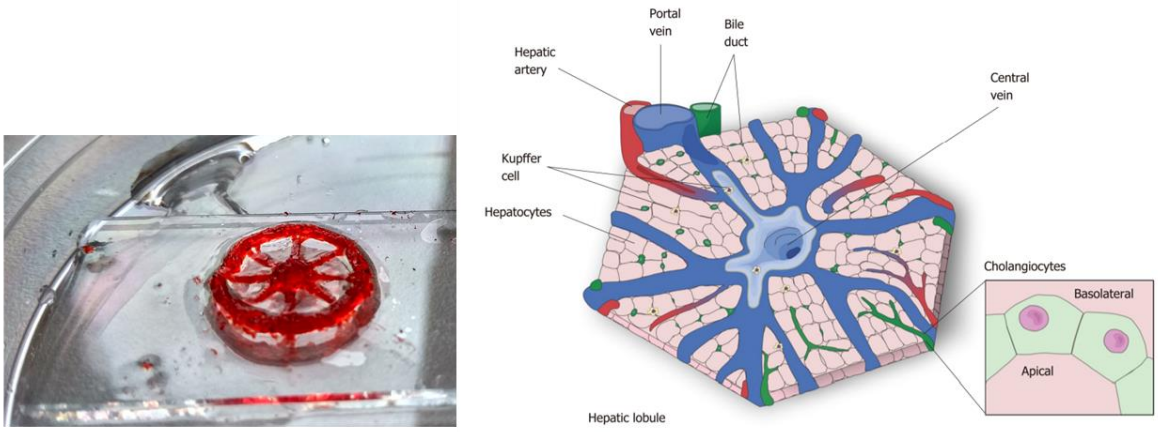

Figure 49. Conceptual liver organoid design by 3D bioprinting. Left, printout sacrificial support material (8% Alginate: 3% Gel) (phenol red added for better visualisation) for vascularization of the portal and central veins. 2% w/v 30/70 Gel-Tyr/HA-Tyr hydrogel (free space). Right, hepatic lobule, microscopic structure of the liver (schematic extracted from (306)).

Given the good biocompatibility and printability of Gel-Tyr/HA-Tyr hydrogels, the implementation of support/sacrificial materials in the printing process could be advantageous for the development of potential models for skeletal muscle, chondrogenic or hepatic tissue (33-35,289). As we can observe in ***Figure 49,*** physically cross-linked Alginate-Gel bioinks can be used as fugitive materials for support and vascularisation until enzymatic cross-linking of Gel/HA hydrogels is complete. Afterwards, due to the solubility of alginate and gelatin at culture medium temperature (37ºC), all non-crosslinked materials would be washed out, only remaining the hydrogel scaffold. Same could be devised for internal support using gelatin, HA or methylcellulose as temporary tickening agents during printing to improve bioinks poor viscosity

Hybrid bioprinting and multiphasic hydrogels (***Figure 50*** and ***51***) can also benefit from bioink support materials in Gel/HA hydrogels. One common orthopaedic issue to be addressed by bioprinting strategies is an osteochondral (OC) defect affecting simultaneously bone- and cartilage-associated zonal compartments in human joints. Cartilage ECM is mainly formed by fibres of collagen type II of different orientations as well as characterized by layers of different biochemical composition and cell density. This cartilage layer is connected to a calcified cartilage layer and the underlying subchondral bone region. Most of the tissue engineering and regenerative medicine techniques applied to the repair and regeneration of cartilage have not addressed the simultaneous repair and regeneration of the subchondral bone, something suggested by recent research studies to be the most common cause of failure of OC autograft and allograft transplantation (309).

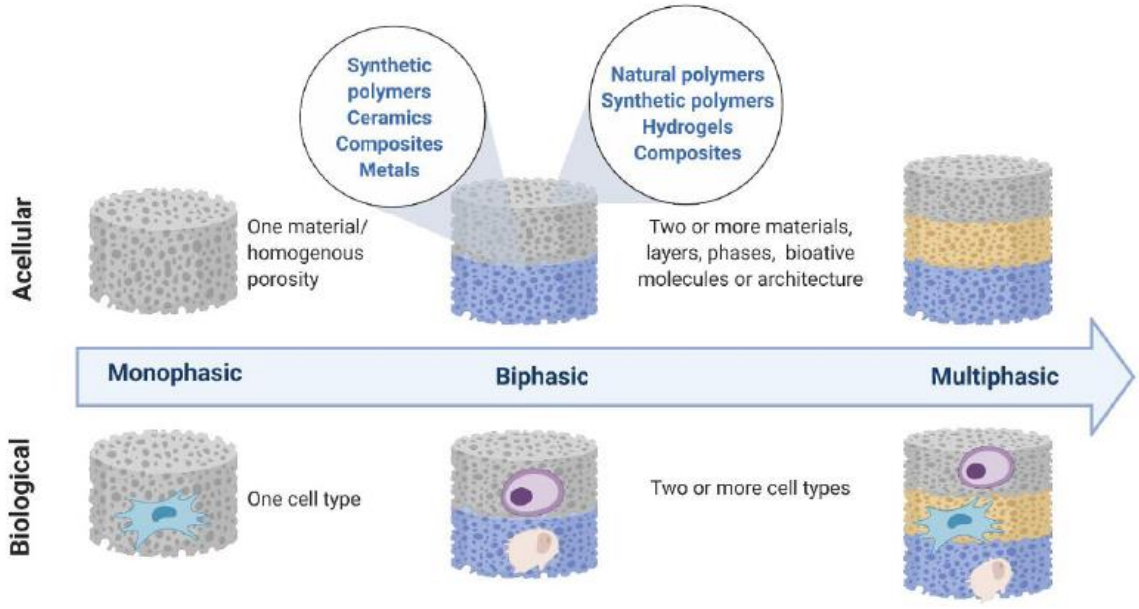

Figure 50. Development of osteochondral scaffolds from monophasic to multi-phasic to mimic the natural OC environment and provide biological and biomechanical cues to the cells specifically for the regeneration of bone or cartilage (307)

The development of biphasic hydrogel scaffolds combined with hybrid bioprinting could be used for the generation of multi-layered full-thickness osteochondral tissue substitutes, with individual geometry based on clinical imaging data, and extrusion-based 3D printing of a cell-laden bioink with primary chondrocytes and a mineralised biomaterial phase. Such scaffold could be used for early treatment of cartilage and osteochondral defects at an early stage of osteoarthritis and could either negate or delay the need for joint replacements.

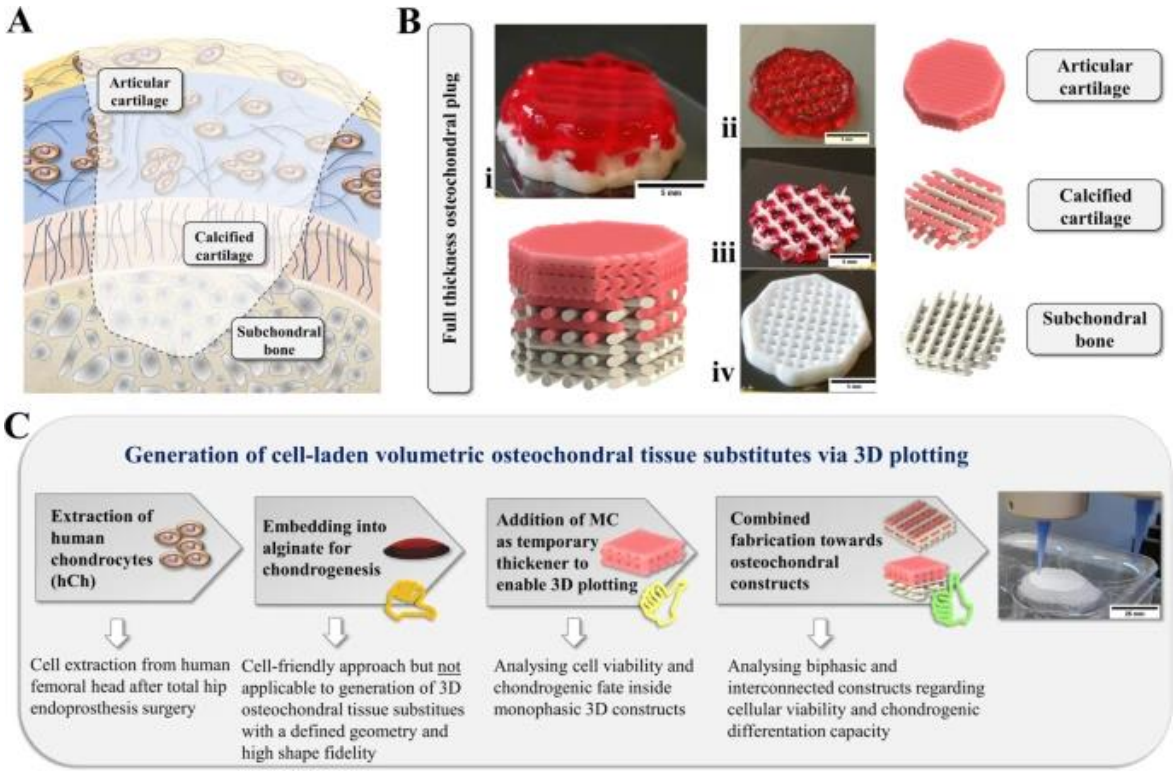

Figure 51. Tissue substitutes for multi-layered osteochondral (OC) defects via extrusion or 3D plotting. (a) Multi-layered OC tissue defects require different repair strategies depending on the layer's architecture, composition, and cell type. (b) A combination of cell-laden hydrogel (AlgMC) and partly mineralised CPC (calcium phosphate cement)-supported zones resembling articular cartilage (ii), underlying layers of calcified cartilage (iii) and subchondral bone (iv). (c) Investigation process regarding mono/biphasic scaffold combinations and analysis paths. Scale bar = 25 mm. (308)

7. References

1. Frantz, C., Stewart, K.M., & Weaver, V.M. (2010). The extracellular matrix at a glance. *J. Cell Sci., 123(24),* 4195−200.
2. Wang, T.W., Sun J.S., Wu, H.C., Tsuang, Y.H., Wang, W.H., & Lin, F.H. (2006). The effect of gelatin-chondroitin sulfate-hyaluronic acid skin substitute on wound healing in SCID mice. *Biomaterials, 27(33),* 5689−97.
3. Bhat, S., & Kumar, A. (2012). Cell proliferation on three-dimensional chitosan−agarose−gelatin cryogel scaffolds for tissue engineering applications. *J. Biosci. Bioeng., 114(6),* 663−70.
4. Cohen, N. P., Foster, R. J., & Mow, V. C. (1998). Composition and Dynamics of Articular Cartilage: Structure, Function, and Maintaining Healthy State. *J. Orthop. Sports Phys. Ther., 28(4),* 203−215.
5. Hoffman, A. S. (2012). Hydrogels for biomedical applications. *Adv. Drug Deliv. Rev., 64,* 18-23.
6. Toh, W.S., & Loh, X.J. (2014). Advances in hydrogel delivery systems for tissue regeneration. *Mater. Sci. Eng. C. Mater. Biol. Appl., 45,* 690-7.
7. Annabi, N., Tamayol, A., Uquillas, J.A., Akbari, M., Bertassoni, L.E., Cha, C., Camci-Unal, G., Dokmeci, M.R., Peppas, N.A., & Khademhosseini, A. (2014). 25th anniversary article: Rational design and applications of hydrogels in regenerative medicine. *Adv. Mater., 26(1),* 85-123.
8. Chopra, A., Lin, V., McCollough, A., Atzet, S., Prestwich, G.D., Wechsler, A.S., Murray, M.E., Oakey, S.A., Yasha Kresh, J., & Janmey, P.A. (2012). Reprogramming cardiomyocyte mechanosensing by crosstalk between integrins and hyaluronic acid receptors. *J. Biomech., 45(5),* 824-31.
9. Levett, P.A., Melchels, F.P., Schrobback, K., Hutmacher, D.W., Malda, J., & Klein, T.J. (2014). A biomimetic extracellular matrix for cartilage tissue engineering centered on photocurable gelatin, hyaluronic acid and chondroitin sulfate. *Acta Biomater., 10(1),* 214-23.
10. Turner, W. S., Schmelzer, E., McClelland, R., Wauthier, E., Chen, W., & Reid, L. M. (2007). Human hepatoblasts phenotype maintained by hyaluronan hydrogels. *J. Biomed. Mater. Res. Part B Applied Biomater., 82B(1),* 156-168.
11. Lai J.Y., (2010). Biocompatibility of chemically cross-linked gelatin hydrogels for ophthalmic use. *J. Mater. Sci. Mater. Med., 21(6),* 1899-911.

12. Lai, J.Y., Ma, D.H., Cheng, H.Y., Sun, C.C., Huang, S.J., Li Y.T., & Hsiue, G.H. (2010). Ocular biocompatibility of carbodiimide cross-linked hyaluronic acid hydrogels for cell sheet delivery carriers. *J. Biomater. Sci. Polym. Ed. 21(3),* 359-76.
13. Jun, I., Kim, S.J., Choi, E., Park, K.M., Rhim, T., Park, J., & Shin, H. (2012). Preparation of Biomimetic Hydrogels with Controlled Cell Adhesive Properties and Topographical Features for the Study of Muscle Cell Adhesion and Proliferation. *Macromol. Biosci.,12(11),* 1502−1513.
14. Lee, F., Chung, J.E., & Kurisawa, M. (2009). An injectable hyaluronic acid-tyramine hydrogel system for protein delivery. *J. Control. Release, 134 (3),* 186−93.
15. Jin, R., Teixeira, L.S., Dijkstra, P.J., Karperien, M., van Blitterswijk, C. A., Zhong, Z.Y., & Feijen, J. (2009). Injectable chitosan-based hydrogels for cartilage tissue engineering. *Biomaterials, 30(13),* 2544−51.
16. Frith, J.E., Cameron, A.R., Menzies, D.J., Ghosh, P., Whitehead, D.L., Gronthos, S., Zannettino, A.C.W., & Cooper-White, J.J. (2013). An injectable hydrogel incorporating mesenchymal precursor cells and pentosan polysulphate for invertebral disc regeneration. *Biomaterials 2013, 34 (37),* 9430−440.
17. Teixeira, L.S., Feijen, J., van Blitterswijk, C.A., Dijkstra, P.J., & Karperien, M. (2012). Enzyme-catalyzed crosslinkable hydrogels: Emerging strategies for tissue engineering. *Biomaterials, 33(5),* 1281−90.
18. Sanmartín-Masiá E., Poveda-Reyes S. & Gallego Ferrer G. (2017). Extracellular matrix–inspired gelatin/hyaluronic acid injectable hydrogels. *Int. J. Polym. Mater. Po., 66(6),* 280-88.
19. Li, Y., Rodrigues, J., & Tomás, H. (2012). Injectable and biodegradable hydrogels: gelation, biodegradation and biomedical applications. *Chem. Soc. Rev., 41(6),* 2193-221.
20. Van Tomme, S. R., Storm, G., & Hennink, W.E. (2008). In situ gelling hydrogels for pharmaceutical and biomedical applications. *Int. J. Pharm., 355(1-2),* 1-18.
21. Bae, K.H., Wang, L.-S., & Kurisawa, M.J. (2013). Injectable biodegradable hydrogels: progress and challenges. *Mater. Chem. B, 1,* 5363-364
22. Radhakrishnan J., Subramanian A., Krishnan U.M., & Sethuraman, S. (2017). Injectable and 3D Bioprinted Polysaccharide Hydrogels: From Cartilage to Osteochondral Tissue Engineering, *Biomacromolecules, 18(1),* 1-26.
23. Balakrishnan, B., & Banerjee, R. (2011). Biopolymer-Based Hydrogels for Cartilage Tissue Engineering. *Chem. Rev., 111 (8),* 4453−74.

24. Ko, D.Y., Shinde, U.P., Yeon, B., & Jeong, B. (2013). Recent progress of in situ formed gels for biomedical applications. *Prog. Polym. Sci., 38 (3−4),* 672−701.
25. Radhakrishnan, J., Krishnan, U. M., & Sethuraman, S. (2014). Hydrogel based injectable scaffolds for cardiac tissue regeneration. *Biotechnol. Adv., 32(2),* 449−61.
26. Censi, R., Fieten, P.J., Di Martino, P., Hennink, W.E., & Vermonden, T. (2012). Hydrogels for protein delivery in tissue engineering. *J. Control Release, 161(2),* 680-92.
27. Su, W.Y., Chen, Y.C., & Lin, F.H. (2010). Injectable oxidized hyaluronic acid/adipic dihydrazide hydrogel for nucleus pulposus regeneration. *Acta Biomater., 6 (8),* 3044−55.
28. Taubenberger, A.V., Woodruff, M.A., Bai, H., Muller, D.J., & Hutmacher, D. W. (2010). The effect of unlocking RGD-motifs in collagen I on pre-osteoblast adhesion and differentiation. *Biomaterials, 31(10),* 2827-35.
29. Shin, H., Olsen, B.D., & Khademhosseini, A. (2012). The mechanical properties and cytotoxicity of cell-laden double-network hydrogels based on photocrosslinkable gelatine and gellan gum biomacromolecules. *Biomaterials, 33(11),* 3143-52.
30. Shu, X.Z., Liu, Y., Palumbo, F., & Prestwich, G.D. (2004). Disulfidecrosslinked hyaluronan-gelatin hydrogel films: a covalent mimic of the extracellular matrix for in vitro cell growth. *Biomaterials 2003, 24(21),* 3825−34.
31. Moulisová V., Poveda-Reyes S., Sanmartín-Masiá E., Quintanilla-Sierra L., Salmerón-Sánchez, M., & Gallego Ferrer, G. (2017). Hybrid Protein–Glycosaminoglycan Hydrogels Promote Chondrogenic Stem Cell Differentiation. *ACS Omega, 2(11),* 7609-20.
32. Poveda-Reyes S., Moulisova V., Sanmartín-Masiá E., Quintanilla-Sierra L., Salmerón-Sánchez M., & Ferrer G. G. (2016). Gelatin-Hyaluronic Acid Hydrogels with Tuned Stiffness to Counterbalance Cellular Forces and Promote Cell Differentiation. *Macromol Biosci., 16(9),* 1311-24.
33. Shu, X. Z., Liu, Y., Palumbo, F., & Prestwich, G. D. (2004). Disulfidecrosslinked hyaluronan-gelatin hydrogel films: a covalent mimic of the extracellular matrix for in vitro cell growth. *Biomaterials 2003, 24(21),* 3825−34.
34. Fan, Z., Zhang, Y., Fang, S., Xu, C., & Li, X. (2015). Bienzymatically crosslinked gelatin/hyaluronic acid interpenetrating network hydrogels: preparation and characterization. *RSC Adv., 5,* 1929−36.
35. Chen, Y.C., Su, W.Y., Yang, S.H., Gefen, A., & Lin, F.H. (2013). In situ forming hydrogels composed of oxidized high molecular weight hyaluronic acid and gelatin for nucleus pulposus regeneration. *Acta Biomater., 9(2),* 5181−93.

36. Zhang, Y. S., Yue, K., Aleman, J., Mollazadeh-Moghaddam, K., Bakht, S. M., Yang, J., Jia, W., Dell'Erba, V., Assawes, P., Shin, S. R., Dokmeci, M. R., Oklu, R., & Khademhosseini, A. (2017). 3D Bioprinting for Tissue and Organ Fabrication. *Annals of Biomedical Engineering, 45(1), 148–163.*
37. Arai, K., Tsukamoto, Y., Yoshida, H., Sanae, H., Mir, T. A., Sakai, S., Yoshida, T., Okabe, M., Nikaido,T., Taya, M., & Nakamura M. (2016). The development of cell-adhesive hydrogel for 3D printing. *International Journal of Bioprinting, 2(2),* 153–162.
38. Donderwinkel, I., van Hest J, C. M., & Cameron, N. R. (2017). Bioinks for 3D bioprinting: recent advances and future prospects. *Polym. Chem., 8(31),* 4451-71
39. Schneeberger, K., Spee, B., Costa, P., Sachs, N., Clevers, H., & Malda, J. (2017). Converging biofabrication and organoid technologies: the next frontier in hepatic and intestinal tissue engineering. *Biofabrication, 9(1),* 3001.
40. Ozbolat, I.T., & Hospodiuk, M. (2016). Current advances and future perspectives in extrusion-based bioprinting. *Biomaterials, 76,* 321-43.
41. Gopinathan, J., & Noh, I. (2018). Recent trends in bioinks for 3D printing. *Biomaterials research, 22(11), 11-.*
42. Li J., Chen M., Fan X., & Zhou H. (2016). Recent advances in bioprinting techniques: approaches, applications and future prospects. *J Transl Med., 14 (271).*
43. Naghavi, M., Abajobir, A. A., Abbafati, C., Abbas, K. M., Abd-Allah, F., Abera, S. F., … Cohen, A.J. (2017). Global, regional, and national age-sex specific mortality for 264 causes of death, 1980–2016: a systematic analysis for the Global Burden of Disease Study 2016. *The Lancet, 390(10100), 1151–1210.*
44. Wolfe, R. A., Merion, R. M., Roys, E. C., & Port, F.K. (2009). Trends in organ donation and transplantation in the United States, 1998-2007. *Am J Transplant. 2009 Apr; 9(4 Pt 2):869-78.*
45. Johnson, R., Collett, D., Birch, R., Fuggle, S., & Rudge, C., (2008). Kidney donation and transplantation in the UK from 1998 to 2007. *Clin. Transpl. 75-88.*
46. Li, Q., Ma, L., & Gao, C. Y. (2015). Biomaterials for in situ tissue regeneration: development and perspectives. *J. Mater. Chem. B. 3, 8921-8938.*
47. Delloye, C., Cornu, O., Druez, V., & Barbier, O. (2007). Bone allografts: what they can offer and what they cannot. *J. Bone Joint Surg. Br. May; 89(5):574-9*
48. Docquier, P. L., Paul, L., Mousny, M., Cornu, O., & Delloye, C. (2007). The use of allografts in paediatric orthopaedic surgery. *Acta Orthop. Belg. Oct; 73(5):551-7.*

49. Engh, G. A, & Ammeen, D. J. (2007). Use of structural allograft in revision total knee arthroplasty in knees with severe tibial bone loss. *J Bone Joint Surg. Am. Dec; 89(12):2640-7*

50. Nevins, M., Hanratty, J., & Lynch, S. E. (2007). Clinical results using recombinant human platelet-derived growth factor and mineralized freeze-dried bone allograft in periodontal defects. *Int. J. Periodontics Restorative Dent. Oct; 27(5):421-7.*

51. Gok, A., Erkutlu, I., Alptekin, M., & Kanlikama, M. (2004). Three-layer reconstruction with fascia lata and vascularized pericranium for anterior skull base defects. *Acta Neurochir (Wien). Jan; 146(1):53-6, discussion 56-7.*

52. Errani, C., Schuster, S., Biagini, R., Casadei, R., De Paolis, M., Bertoni, F., Boriani, S., & Mercuri, M. (2007). Reconstruction with fascia lata allograft of the posterior vertebra elements after resection for aneurysmal bone cyst in a child. *Eur Spine J. Sep; 16(9): 1531–1535.*

53. Dufrane, D., Mourad, M., van Steenberghe, M., Goebbels, R. M., & Gianello, P. (2008). Regeneration of abdominal wall musculofascial defects by a human acellular collagen matrix. *Biomaterials. May; 29(14):2237-48.*

54. Jang, Y.J., Wang, J. H., Sinha, V., Song, H. M., & Lee, B. J. (2007) Tutoplast-processed fascia lata for dorsal augmentation in rhinoplasty. *Otolaryngol Head Neck Surg. Jul; 137(1):88-92.*

55. World Health Organization. (2018). WHO-ONT Global Observatory on Donation and Transplantation (GODT). http://www.transplant-observatory.org

56. Vacanti, J. P., Vacanti, C. A. (2013). The History and Scope of Tissue Engineering. Principles of Tissue Engineering (Fourth Edition). *Academic Press. 3-8, 2014.*

57. Li, Q., Ma, L., & Gao, C. Y. (2015). Biomaterials for in situ tissue regeneration: development and perspectives. *J. Mater. Chem. B. 3, 8921-8938.*

58. Badylak, S. F., & Nerem, R. M. (2010). Progress in tissue engineering and regenerative medicine. *Proc Natl Acad Sci U S A. Feb 23; 107(8):3285-6*

59. Langer, R. (2000). Biomaterials in drug delivery and tissue engineering: one laboratory's experience. *Acc Chem Res. Feb; 33(2):94-101*

60. Penn, I., & Starzl, T. E. (1972). Malignant tumors arising de novo in immunosuppressed organ transplant recipients. *Transplantation 14:407–417.*

61. Penn, I., Halgrimson, C.G., & Starzl, T. E (1971). De novo malignant tumors in organ transplant recipients. *Transplant Proc 3:773–778.*

62. National Kidney Foundation. L. E. Tushla, LCSW. (n.d.). *When a Transplant Fails.* https://www.kidney.org/transplantation/transaction/TC/summer09/TCsm09_TransplaTranspl

63. Pinkowski, J. L., Rodrigo, J. J., Sharkey, N. A., & Vasseur, P. B. (1996). Immune response to nonspecific and altered tissue antigens in soft tissue allografts. *Clin Orthop Relat Res. May; (326):80-5.*

64. Pinkowski, J.L., Reiman, P.R., & Chen S.L. (1989). Human lymphocyte reaction to freeze-dried allograft and xenograft ligamentous tissue. *Am J Sports Med. Sep-Oct;17(5):595-600*

65. Fawzi-Grancher, S., Goebbels, R. M., Bigare, E., Cornu, O., Gianello, P., Delloye, C., & Dufrane, D. (2009). Human tissue allograft processing: impact on in vitro and in vivo biocompatibility. *Journal of Materials Science: Materials in Medicine, 20(8), 1709–1720.*

66. Heise, R. L., Adam Blakeney, B., & Pouliot, R. A. (2014). Polymers in Tissue Engineering. *Advanced Polymers in Medicine, 177–217.*

67. Biomaterials Market Size, Share & Trends Analysis Report By Product (Natural, Metallic, Polymer), By Application (Cardiovascular, Orthopedics, Plastic Surgery) (2020). *By Region, And Segment Forecasts, 2020 – 2027.* https://www.grandviewresearch.com/industry-analysis/biomaterials-industry

68. Donderwinkel, I., van Hest, J. C. M., & Cameron, N. R. (2017). Bioinks for 3D bioprinting: recent advances and future prospects. *Polymer Chemistry, 8(31), 4451–4471*

69. Ige, O. O., Umoru, L. E., & Aribo, S. (2012) Natural products: A minefield of biomaterials. *ISRN Mater. Sci. 2012(), 1-20.*

70. Lu, J.Z., Wu, L. J., Sun, G. F., Luo, K. Y., Zhang, Y. K., Cai, J., Cui, C. Y., & Luo, X. M. (2017). Microstructural response and grain refinement mechanism of commercially pure titanium subjected to multiple laser shock peening impacts. *Acta Mater. 127, 252–266.*

71. Hong, D., Chou, D. T., Velikokhatnyi, O. I., Roy, A., Lee, B., Swink, I., Issaev, I., Kuhn, H.A., & Kumta, P.N. (2016). Binder-jetting 3D printing and alloy development of new biodegradable Fe-Mn-Ca/Mg alloys. *Acta Biomater. 45, 375–386.*

72. Trivedi, P., Nune, K.C., Misra, R. D. K., Goel, S., Jayganthan, R., & Srinivasan, A. (2016). Grain refinement to submicronregime in multiaxial forged Mg-2Zn-2Gd alloy and relationship to mechanical properties. *Mater. Sci. Eng. A. 668, C, 59–65.*

73. Henkel, J., Woodruff, M.A., Epari, D.R., Steck, R., Glatt, V., Dickinson, I.C., Choong, P.F.M., Schuetz, M.A., & Hutmacher, D.W. (2013). Bone regeneration based on tissue engineering conceptions—A 21st century perspective. *Bone Res. Sep 25;1(3):216-48.*

74. Bhat, S., & Kumar, A. (2013). Biomaterials and bioengineering tomorrow's healthcare. *Biomatter Jul-Sep; 3(3):e24717.*

75. Nerem, R. M. (1992). Tissue engineering in the USA. *Medical and Biological Engineering and Computing*, 30(4), CE8–CE12.

76. Langer, R., & Tirrell, D. A. (2004). Designing materials for biology and medicine. *Nature, 428(6982) 487–492, 2004.*

77. Dhandayuthapani, B., Yoshida, Y., Maekawa, T., & Kumar, D. S. (2011). Polymeric Scaffolds in Tissue Engineering Application: A Review. *International Journal of Polymer Science, 1–19.*

78. Fuchs, J. R., Nasseri, B. A., & Vacanti, J. P. (2001). Tissue engineering: a 21st century solution to surgical reconstruction. *Annals of Thoracic Surgery, 72(2), 577–591.*

79. Piskin, E. (1994). Biodegradable polymers as biomaterials. *Journal of Biomaterials Science Polymer Edition (6)775–795.*

80. Ji, Y., Ghosh, K., Shu, X. Z., Li, B., Sokolov, J. C., Prestwich, G. D., Clark, R. A.F., & Rafailovich, M. H., (2006). Electrospun three-dimensional hyaluronic acid nanofibrous scaffolds. *Biomaterials, 27(20), 3782–3792.*

81. Eaglstein, W. H., & Falanga, V. (1998). Tissue engineering and the development of Apligraf a human skin equivalent. *Advances in Wound Care, 11(4 Suppl), 1–8.*

82. Boyan, B. D. , Lohmann, C. H., Romero, J., & Schwartz, Z. (1999). Bone and cartilage tissue engineering. *Clinics in Plastic Surgery, 26(4) 629–645.*

83. Mayer, J. E., Shin'oka, T., & Shum-Tim, D. (1997). Tissue engineering of cardiovascular structures. *Current Opinion in Cardiology, 12(6) 528–532*

84. Mohammad J., Shenaq, J., Rabinovsky, E., & Shenaq, S. (2000). Modulation of peripheral nerve regeneration: a tissueengineering approach. The role of amnion tube nerve conduit across a 1-centimeter nerve gap. *Plastic and Reconstructive Surgery, 105(2), 660–666,*

85. Diedwardo, C. A., Petrosko, P., Acarturk, T. O., Dimilia, P. A., Laframboise, W. A., & Johnson, P. C. (1999). Muscle tissue engineering. *Clinics in Plastic Surgery*, vol. *26(4) 647–656.*

86. Nair, L. S., & Laurencin, C. T. (2007). Biodegradable polymers as biomaterials. *Progress in Polymer Science, 32(8-9), 762–798,*

87. Tang, X., Thankappan, S. K., Lee, P., Fard, S. E., Harmon, M. D., Tran, K., & Yu, X. (2014). Polymeric Biomaterials in Tissue Engineering and Regenerative Medicine. *Natural and Synthetic Biomedical Polymers, 351–371.*

88. Ter Horst, B., Moiemen, N. S., & Grover, L. M. (2019). *Natural polymers. Biomaterials for Skin Repair and Regeneration, 151–192.*

89. Ter Horst, B., Moiemen, N. S., & Grover, L. M. (2019). *Natural polymers. Biomaterials for Skin Repair and Regeneration, 151–192*

90. Girdhar, M., Mohan, A., & Sharma, A. (2016). Blending Strategies of Natural Polymers: A Review. *Trends in Biomaterials & Artificial Organs, 30(1), 61-76.*

91. Desai, M.S., Lee, S.W. (2014). Protein-based functional nanomaterial design for bioengineering applications. *Wiley Interdiscip. Rev. Nanomed. Nanobiotechnol. 7(1), 69–97.*

92. Lin, C.Y., Liu, J.C. (2016). Modular protein domains: an engineering approach toward functional biomaterials. *Curr. Opin. Biotechnol. 40, 56–63.*

93. Freeman, R., Boekhoven, J., Dickerson, M.B., Naik, R.R., & Stupp, S.I. (2015). Biopolymers and supramolecular polymers as biomaterials for biomedical applications. *MRS Bull. 40, 1089–1101.*

94. Vozzi, G., Previti, A., & De Rossi, D. (2002). Microsyringe-Based Deposition of Two-Dimensional and Three- Dimensional Polymer Scaffolds with a Well-Defined Geometry for Application to Tissue Engineering. *Tissue Engineering, 8(6) 1089-1098*

95. Udofia, E. N., & Zhou, W. (2018). Microextrusion based 3D printing - A review, Solid Freeform Fabrication Proceedings of the 29th Annual International Solid Freeform Fabrication Symposium - An Additive Manufacturing. *Conference, SFF 2018, pp. 2033-2060.*

96. Zhao, Y., Li, Y., Mao, S., Sun, W., & Yao, R. (2015). The influence of printing parameters on cell survival rate and printability in microextrusion-based 3D cell printing technology. *Biofabrication, 7(4), 045002.*

97. Aravamudhan, A., Ramos, D. M., Nada, A. A., & Kumbar, S. G. (2014). Natural Polymers. *Natural and Synthetic Biomedical Polymers, 67–89.*

98. Varki, A., Cummings, R., Esko, J., Freeze, H., Stanley, P., Bertozzi, C., Hart, G., & Etzler, M. (1999). *Essentials of glycobiology. Cold Spring Har (NY): Cold Spring Harbor Laboratory Press.*

99. Verreck, G., Chun, I., Rosenblatt, J., Peeters, J., Van Dijck, A., Mensch, J., Noppe, M., & Brewster, M. E. (2003). Incorporation of drugs in an amorphous state into electrospun nanofibers composed of a water-insoluble, nonbiodegradable polymer. *Journal of Controlled Release, Oct 30; 92(3):349-60.*

100. Kim, J. E., Kim, S. H., & Jung, Y. (2016). Current status of three-dimensional printing inks for soft tissue regeneration. *Tissue Engineering and Regenerative Medicine, 13(6), 636–646*

101. Burdick, J.A., & Prestwich, G.D. (2011). Hyaluronic acid hydrogels for biomedical applications. *Adv Mater. Mar 25; 23(12):H41-56.*

102. Khetan, S., & Burdick, J. A. (2011). Patterning hydrogels in three dimensions towards controlling cellular interactions. *Soft Matter 7, 830–838.*

103. Guvendiren, M., & Burdick, J.A. (2010). The control of stem cell morphology and differentiation by hydrogel surface wrinkles. *Biomaterials. Sep;31(25):6511-8.*

104. Marklein, R.A., & Burdick, J.A. (2010). Controlling stem cell fate with material design. *Adv Mater. Jan 12;22(2):175-89.*

105. Dellatore, S.M., Garcia, A.S., & Miller, W.M. (2008). Mimicking stem cell niches to increase stem cell expansion. *Curr Opin Biotechnol. Oct;19(5):534-40.*

106. Hubbell, J.A. (1995). Biomaterials in tissue engineering. *Biotechnology (NY). Jun;13(6):565-76.*

107. J. D. Kretlow, L. Klouda and A. G. Mikos, Adv. Drug Delivery Rev., 2007, 59, 263–273.

108. Kretlow, J.D., Klouda, L., & Mikos, A.G. (2007) Injectable matrices and scaffolds for drug delivery in tissue engineering. *Adv Drug Deliv Rev. May 30;59(4-5):263-73.*

109. Yeo, Y., Geng, W., Ito, T., Kohane, D.S., Burdick, J.A., & Radisic, M. (2007) Photocrosslinkable hydrogel for myocyte cell culture and injection. *J Biomed Mater Res B Appl Biomater. May;81(2):312-22.*

110. Khademhosseini, A., Eng, G., Yeh, J., Fukuda, J., Blumling, J., 3rd, Langer, R., & Burdick, J.A. (2006). Micromolding of photocrosslinkable hyaluronic acid for cell encapsulation and entrapment. *J Biomed Mater Res A. Dec 1;79(3):522-32*

111. Burdick, J.A., & Anseth, K.S. (2002). Photoencapsulation of osteoblasts in injectable RGD-modified PEG hydrogels for bone tissue engineering. *Biomaterials. Nov;23(22):4315-23.*

112. Peppas, N. A. (1997) Hydrogels and drug delivery. *Curr. Opin. Colloid Interface Sci., 2, 531–537.*

113. Gupta, P., Vermani, K., & Garg, S. (2002). Hydrogels: from controlled release to pH-responsive drug delivery. *Drug Discov Today. May 15;7(10):569-79.*

114. Bajpai, A.K., Shukla, S.K., Bhanu, S. and Kankane, S. (2008) Responsive Polymers in Controlled Drug Delivery. *Progress in Polymer Science, 33, 1088-1118.*

115. Ron, E.S., Bromberg, L.E. (1998). Temperature-responsive gels and thermogelling polymer matrices for protein and peptide delivery. *Adv Drug Deliv Rev. May 4;31(3):197-221.*

116. Zhao, B., & Moore, J. S. (2001). Fast pH - and Ionic Strength-Responsive Hydrogels in Microchannels. *Langmuir, 17(16), 4758–4763.*

117. Beebe, D.J., Moore, J.S, Bauer, J.M., Yu, Q., Liu, R.H., Devadoss, C., & Jo, B.H. (2000) Functional hydrogel structures for autonomous flow control inside microfluidic channels. *Nature. Apr 6;404(6778):588-90.*

118. Tan, H., & Marra, K. G. (2010). Injectable, Biodegradable Hydrogels for Tissue Engineering. *Applications. Materials, 3(3), 1746–1767.*

119. Nicodemus, G.D., Bryant, S.J. (2008). Cell encapsulation in biodegradable hydrogels for tissue engineering applications. *Tissue Eng Part B Rev. 2008 Jun;14(2):149-65.*

120. Munaz, A., Vadivelu, R. K., John, J. S., Barton, M., Kamble H., & Nguyen, N.-T. (2016). Three-dimensional printing of biological matters. *J. Sci. Adv. Mater. Devices, 2016, 1(1), 1–17.*

121. Elzoghby, A.O. (2013). Gelatin-based nanoparticles as drug and gene delivery systems: reviewing three decades of research. *J Control Release. Dec 28;172(3):1075-91*

122. Xing, Q., Yates, K., Vogt, C., Qian, Z., Frost, M.C., & Zhao, F. (2014). Increasing mechanical strength of gelatin hydrogels by divalent metal ion removal. *Sci Rep* 2014;4:4706.

123. Schuurman, W., Levett, P.A., Pot, M.W., van Weeren, P.R., Dhert, W.J., Hutmacher, D.W., Melchels, F.P., Klein, T.J., & Malda, J. (2013) Gelatin-methacrylamide hydrogels as potential biomaterials for fabrication of tissue-engineered cartilage constructs. *Macromol Biosci. May;13(5):551-61.*

124. Di Lullo, G.A., Sweeney, S.M., Körkkö, J., Ala-Kokko, L., & San Antonio, J.D. (2002). Mapping the ligand-binding sites and disease-associated mutations on the most abundant protein in the human, type I collagen, *J. Biol. Chem. 277 (6) 4223–4231.*

125. Xia, W., Liu, W., Cui, L., Liu, Y., Zhong, W., Liu, D., & Cao, Y. (2014). Tissue engineering of cartilage with the use of chitosan-gelatin complex scaffolds, *J. Biomed. Mater. Res. B Appl. Biomater. 71 (2) 373–380.*

126. Caliari, S.R., Ramirez, M.A., & Harley, B.A.C. (2011). The development of collagen-GAG scaffold-membrane composites for tendon tissue engineering, *Biomaterials 32 (34) 8990–8998.*

127. Li, M., Mondrinos, M.J., Chen, X., Gandhi, M.R., Ko, F.K., & Lelkes, P.I. (2006). Co-electrospun poly (lactide-co-glycolide), gelatin, and elastin blends for tissue engineering scaffolds, *J. Biomed. Mater. Res. A 79 (4) 963–973.*

128. Li, X., Jin, L., Balian, G., Laurencin, C.T. Greg, & Anderson, D. (2006) Demineralized bone matrix gelatin as scaffold for osteochondral tissue engineering, *Biomaterials 27 (11) 2426–2433.*

129. Chong, E.J., Phan, T.T., Lim, I.J., Zhang, Y.Z., Bay, B.H., Ramakrishna, S., & Lim, C.T. (2007). Evaluation of electrospun PCL/gelatin nanofibrous scaffold for wound healing and layered dermal reconstitution. *Acta Biomater. 2nd TMS Symp. Biol. Mater. Sci. 3 (3) 321–330.*

130. Zhang, Z., Ortiz, O., Goyal, R., & Kohn, J. (2014). Biodegradable Polymers. *Principles of Tissue Engineering, 441–473.*

131. Boccafoschi, F., Ramella, M., Fusaro, L., Catoira, M. C., & Casella, F. (2019). Biological Grafts: Surgical Use and Vascular Tissue Engineering Options for Peripheral Vascular Implants. *Reference Module in Biomedical Sciences, 310-321.*

132. Lee, H., Lum, N., Seow, L. Y., Lim, P. Q., & Tan, L. P. (2016). Synthesis and characterization of types A and B gelatin methacryloyl for bioink applications. *Materials, 9(10), 797.*

133. da Silva, M.A., Bode, F., Grillo, I., & Dreiss, C. A. (2015). Exploring the Kinetics of Gelation and Final Architecture of Enzymatically Cross-Linked Chitosan/Gelatin Gels. *Biomacromolecules, 16(4), 1401–1409.*

134. Shin, H., Olsen, B. D., & Khademhosseini, A. (2012). The mechanical properties and cytotoxicity of cell-laden double-network hydrogels based on photocrosslinkable gelatin and gellan gum biomacromolecules. *Biomaterials*, *33*(11), 3143–3152.

135. Chen, W.Y., & Abatangelo G. (1999). Functions of hyaluronan in wound repair. *Wound Repair Regen. Mar-Apr;7(2):79-89.*

136. Willerth, S.M., Sakiyama-Elbert, S.E., (2007). Approaches to neural tissue engineering using scaffolds for drug delivery. *Matrices Scaffolds Drug Deliv. Tissue Eng. 59 (4-5) 325–338.*

137. Solchaga, L.A., Dennis, J.E., Goldberg, V.M., & Caplan, A.I. *(1999).* Hyaluronic acid-based polymers as cell carriers for tissue-engineered repair of bone and cartilage, *J. Orthop. Res. 17 (2) 205–213.*

138. Ifkovits, J.L., & Burdick, J.A. (2007). Review: photopolymerizable and degradable biomaterials for tissue engineering applications, *Tissue Eng. 13(10) 2369–2385.*

139. Kogan, G., Šoltés, L., Stern, R., & Gemeiner, P. (2007). Hyaluronic acid: a natural biopolymer with a broad range of biomedical and industrial applications. *Biotechnol. Lett. 29 (1) 17–25.*

140. Monslow, J., Govindaraju, P., & Puré, E. (2015). Hyaluronan - a functional and structural sweet spot in the tissue microenvironment. *Front Immunol. May 15;6:231.*

141. Salwowska, N.M., Bebenek, K.A., żądło, D.A., & Wcisło-Dziadecka, D.L. (2016) Physiochemical properties and application of hyaluronic acid: a systematic review. *J Cosmet Dermatol. ;15:520–526.*

142. Koray, M., Ofluoglu, D., Onal, E.A., Ozgul, M., Ersev, H., & Yaltirik, M. (2014). Efficacy of hyaluronic acid spray on swelling, pain, and trismus after surgical extraction of impacted mandibular third molars. *Int J Oral Maxillofac Surg.;43:1399–1403.*

143. Chen, W.Y., & Abatangelo, G. (1999). Function of Hyaluronan in wound repair. *Wound repair Regan.;7:79–89.*

144. The, B.M., Shen, Y., Friedland, P.L., Atlas, M.D., & Marano, RJ.. (2012). A review on use of hyaluronic acid in tympanic membrane wound healing. *Expert Opin Biol Ther.;12:23–36.*

145. Shuborna, N. S., Chaiyasamut, T., Sakdajeyont, W., Vorakulpipat, C., Rojvanakarn, M., & Wongsirichat, N. (2019). Generation of novel hyaluronic acid biomaterials for study of pain in third molar intervention: a review. *Journal of Dental Anesthesia and Pain Medicine, 19(1), 11.*

146. Collins, M. N., & Birkinshaw, C. (2007). Comparison of the effectiveness of four different cross-linking agents with hyaluronic acid hydrogel films for tissue-culture applications. *Journal of Applied Polymer Science, Vol. 104, 3183*

147. Cowman, M.K, Schmidt, T.A, Raghavan, P., & Stecco, A. (2015*)* Viscoelastic Properties of Hyaluronan in Physiological Conditions. *F1000Res. Aug 25;4:622.*

148. Chen, Y.-C., Su, W.-Y., Yang, S.-H., Gefen, A., & Lin, F.-H. (2013) In situ forming hydrogels composed of oxidized high molecular weight hyaluronic acid and gelatin for nucleus pulposus regeneration. *Acta Biomater., 9, 5181−5193.*

149. Camci-Unal, G., Cuttica, D., Annabi, N., Demarchi, D., & Khademhosseini, A. (2013) Synthesis and characterization of hybrid hyaluronic acid-gelatin hydrogels. *Biomacromolecules, 14, 1085−1092.*

150. Vanderhooft, J. L., Alcoutlabi, M., Magda, J. J., & Prestwich, G. D. (2009) Rheological properties of cross-linked hyaluronan-gelatin hydrogels for tissue engineering. *Macromol. Biosci., 9, 20−28.*

151. Levett, P.A., Melchels, F.P., Schrobback, K., Hutmacher, D.W., Malda, J., & Klein, TJ. (2014) A biomimetic extracellular matrix for cartilage tissue engineering centered on photocurable gelatin, hyaluronic acid and chondroitin sulfate. *Acta Biomater., 10, 214−223.*

152. Baker, B. M., & Chen, C. S. (2012). Deconstructing the third dimension – how 3D culture microenvironments alter cellular cues. *Journal of Cell Science, 125(13), 3015–3024.*

153. Bonnier, F., Keating, M. E., Wróbel, T. P., Majzner, K., Baranska, M., Garcia-Munoz, A., & Byrne, H. J. (2015). Cell viability assessment using the Alamar blue assay: A comparison of 2D and 3D cell culture models. *Toxicology in Vitro, 29(1), 124–131.*

154. Gauvin, R., Chen, Y.C., Lee, J.W., Soman, P., Zorlutuna, P., Nichol, J.W., Bae, H., Chen, S., & Khademhosseini, A. (2012). Microfabrication of complex porous tissue engineering scaffolds using 3D projection stereolithography. *Biomaterials 33: 3824–3834.*

155. Jung, C. S., Kim, B. K., Lee, J., Min, B. H., & Park, S. H. (2017). Development of Printable Natural Cartilage Matrix Bioink for 3D Printing of Irregular Tissue Shape. *Tissue engineering and regenerative medicine*, *15*(2), 155–162.

156. Fedorovich, N. E., Alblas, J., de Wijn, J. R., Hennink, W. E., Verbout, A. J., & Dhert, W. J. (2007). Hydrogels as extracellular matrices for skeletal tissue engineering: state-of-the-art and novel application in organ printing. *Tissue engineering*, *13*(8), 1905–1925.

157. Malda, J., Visser, J., Melchels, F. P., Jüngst, T., Hennink, W. E., Dhert, W. J., Groll, J., & Hutmacher, D. W. (2013). 25th anniversary article: Engineering hydrogels for biofabrication. *Advanced materials (Deerfield Beach, Fla.)*, *25*(36), 5011–5028.

158. Burg, T., & Burg, K. (2014). Feasibility of 3D scaffolds for organs. *Rapid Prototyping of Biomaterials*, *221–235.*

159. Lee, H. & Cho, D. W. (2016). One-step fabrication of an organ-on-a-chip with spatial heterogeneity using a 3D bioprinting technology. *Lab on a Chip 16, 2618–2625.*

160. Klebe R. J. (1988). Cytoscribing: a method for micropositioning cells and the construction of two- and three-dimensional synthetic tissues. *Experimental cell research*, *179*(2), 362–373.V. Mironov, N. Reis and B. Derby, Tissue Eng., 2006, 12, 631–634.

161. Gungor-Ozkerim, P. S., Inci, I., Zhang, Y. S., Khademhosseini, A., & Dokmeci, M. R. (2018). Bioinks for 3D bioprinting: an overview. *Biomaterials Science, 6(5), 915–946.*

162. Gudapati, H., Dey, M., & Ozbolat, I. (2016). A comprehensive review on droplet-based bioprinting: Past, present and future. *Biomaterials*, *102*, 20–42.

163. Mironov, V., Kasyanov, V., & Markwald, R. R. (2011). Organ printing: from bioprinter to organ biofabrication line. *Current opinion in biotechnology*, *22*(5), 667–673.

164. Peng, W., Unutmaz, D., & Ozbolat, I. T. (2016). Bioprinting towards Physiologically Relevant Tissue Models for Pharmaceutics. *Trends in biotechnology*, *34*(9), 722–732.

165. Ozbolat, I. T., & Hospodiuk, M. (2016). Current advances and future perspectives in extrusion-based bioprinting. *Biomaterials*, *76*, 321–343.

166. Dababneh, B., & Ozbolat, I. T. (2014). Bioprinting Technology: A Current State-of-the-Art Review. *J. Manuf. Sci. E-T ASME, 136, 061016.*

167. Moroni, L., Boland, T., Burdick, J. A., De Maria, C., Derby, B., Forgacs, G., Groll, J., Li, Q., Malda, J., Mironov, V. A., Mota, C., Nakamura, M., Shu, W., Takeuchi, S., Woodfield, T., Xu, T., Yoo, J. J., & Vozzi, G. (2018). Biofabrication: A Guide to Technology and Terminology. *Trends in biotechnology*, *36*(4), 384–402.

168. Owens, C. M., Marga, F., Forgacs, G., & Heesch, C. M. (2013). Biofabrication and testing of a fully cellular nerve graft. *Biofabrication*, *5*(4), 045007.

169. Lozano, R., Stevens, L., Thompson, B. C., Gilmore, K. J., Gorkin, R., 3rd, Stewart, E. M., in het Panhuis, M., Romero-Ortega, M., & Wallace, G. G. (2015). 3D printing of layered brain-like structures using peptide modified gellan gum substrates. *Biomaterials*, *67*, 264–273.

170. Duan, B., Hockaday, L. A., Kang, K. H., & Butcher, J. T. (2013). 3D bioprinting of heterogeneous aortic valve conduits with alginate/gelatin hydrogels. *Journal of biomedical materials research. Part A*, *101*(5), 1255–1264.

171. Duan, B., Kapetanovic, E., Hockaday, L. A., & Butcher, J. T. (2014). Three-dimensional printed trileaflet valve conduits using biological hydrogels and human valve interstitial cells. *Acta biomaterialia*, *10*(5), 1836–1846.

172. Markstedt, K., Mantas, A., Tournier, I., Martínez Ávila, H., Hägg, D., & Gatenholm, P. (2015). 3D Bioprinting Human Chondrocytes with Nanocellulose-Alginate Bioink for Cartilage Tissue Engineering Applications. *Biomacromolecules*, *16*(5), 1489–1496.

173. Kesti, M., Eberhardt, C., Pagliccia, G., Kenkel, D., Grande, D., Boss, A., & Zenobi-Wong, M. (2015). Bioprinting: Bioprinting Complex Cartilaginous Structures with Clinically Compliant Biomaterials *(Adv. Funct. Mater. 48/2015). Advanced Functional Materials*, *25(48)*, *7397–7397*.

174. Yue, Z., Liu, X., Coates, P. T., & Wallace, G. G. (2016). Advances in printing biomaterials and living cells: implications for islet cell transplantation. *Current opinion in organ transplantation*, *21*(5), 467–475.

175. Seol, Y. J., Kang, H. W., Lee, S. J., Atala, A., & Yoo, J. J. (2014). Bioprinting technology and its applications. *European journal of cardio-thoracic surgery : official journal of the European Association for Cardio-thoracic Surgery*, *46*(3), 342–348.

176. Ozbolat, I. T., Peng, W., & Ozbolat, V. (2016). Application areas of 3D bioprinting. *Drug discovery today*, *21*(8), 1257–1271.

177. Hölzl, K., Lin, S., Tytgat, L., Van Vlierberghe, S., Gu, L., & Ovsianikov, A. (2016). Bioink properties before, during and after 3D bioprinting. *Biofabrication*, *8*(3), *032002*.

178. Mironov, V., Visconti, R. P., Kasyanov, V., Forgacs, G., Drake, C. J., & Markwald, R. R. (2009). Organ printing: tissue spheroids as building blocks. *Biomaterials*, *30*(12), 2164–2174.

179. Mehesz, A. N., Brown, J., Hajdu, Z., Beaver, W., da Silva, J. V., Visconti, R. P., Markwald, R. R., & Mironov, V. (2011). Scalable robotic biofabrication of tissue spheroids. *Biofabrication*, *3*(2), 025002.

180. Ozbolat I. T. (2015). Bioprinting scale-up tissue and organ constructs for transplantation. *Trends in biotechnology*, *33*(7), 395–400.

181. Ozbolat, Ibrahim T.; Chen, Howard; Yu, Yin (2014). Development of 'Multi-arm Bioprinter' for hybrid biofabrication of tissue engineering constructs. *Robotics and Computer-Integrated Manufacturing, 30(3), 295–304.*

182. Liu, W., Heinrich, M. A., Zhou, Y., Akpek, A., Hu, N., Liu, X., Guan, X., Zhong, Z., Jin, X., Khademhosseini, A., & Zhang, Y. S. (2017). Extrusion Bioprinting of Shear-Thinning Gelatin Methacryloyl Bioinks. *Advanced healthcare materials*, *6*(12), 10.1002/adhm.201601451.

183. Saunders, Rachel Elizabeth; Derby, Brian (2014). Inkjet printing biomaterials for tissue engineering: bioprinting. *International Materials Reviews, 59(8), 430–448.*

184. Lee, W., Debasitis, J. C., Lee, V. K., Lee, J. H., Fischer, K., Edminster, K., Park, J. K., & Yoo, S. S. (2009). Multi-layered culture of human skin fibroblasts and keratinocytes through three-dimensional freeform fabrication. *Biomaterials*, *30*(8), 1587–1595.

185. Derby, B. (2010). Inkjet Printing of Functional and Structural Materials: Fluid Property Requirements, Feature Stability, and Resolution. *Annual Review of Materials Research, 40(1), 395–414.*

186. Sun, J., Ng, J. H., Fuh, Y. H., San Wong, Y., Loh, H. T. & Xu, Q. (2009). Performance characterization of drop-on-demand micro-dispensing system with multi-printheads *Microsyst. Technol., 15, 1437–1448.*

187. Lee, W., Debasitis, J. C., Lee, V. K., Lee, J. H., Fischer, K., Edminster, K., Park, J. K., & Yoo, S. S. (2009). Multi-layered culture of human skin fibroblasts and keratinocytes through three-dimensional freeform fabrication. *Biomaterials*, *30*(8), 1587–1595.

188. Jang, D., Kim, D., & Moon, J. (2009). Influence of fluid physical properties on ink-jet printability. *Langmuir : the ACS journal of surfaces and colloids*, *25*(5), 2629–2635.

189. Lee, W., Debasitis, J. C., Lee, V. K., Lee, J. H., Fischer, K., Edminster, K., Park, J. K., & Yoo, S. S. (2009). Multi-layered culture of human skin fibroblasts and keratinocytes through three-dimensional freeform fabrication. *Biomaterials*, *30*(8), 1587–1595.

190. Faulkner-Jones, A., Fyfe, C., Cornelissen, D. J., Gardner, J., King, J., Courtney, A., & Shu, W. (2015). Bioprinting of human pluripotent stem cells and their directed

differentiation into hepatocyte-like cells for the generation of mini-livers in 3D. *Biofabrication*, *7*(4), 044102.

191. Gurkan, U. A., El Assal, R., Yildiz, S. E., Sung, Y., Trachtenberg, A. J., Kuo, W. P., & Demirci, U. (2014). Engineering anisotropic biomimetic fibrocartilage microenvironment by bioprinting mesenchymal stem cells in nanoliter gel droplets. *Molecular pharmaceutics*, *11*(7), 2151–2159.

192. Schuurman, W., Khristov, V., Pot, M. W., van Weeren, P. R., Dhert, W. J. A., & Malda, J. (2011). Bioprinting of hybrid tissue constructs with tailorable mechanical properties. *Biofabrication, 3(2), 021001.*

193. Afanasenkau, D., Kalinina, D., Lyakhovetskii, V., Tondera, C., Gorsky, O., Moosavi, S., Pavlova, N., Merkulyeva, N., Kalueff, A. V., Minev, I. R., & Musienko, P. (2020). Rapid prototyping of soft bioelectronic implants for use as neuromuscular interfaces. *Nature biomedical engineering*, *4*(10), 1010–1022.

194. Kuss, M. A., Harms, R., Wu, S., Wang, Y., Untrauer, J. B., Carlson, M. A., & Duan, B. (2017). Short-term hypoxic preconditioning promotes prevascularization in 3D bioprinted bone constructs with stromal vascular fraction derived cells. *RSC Advances, 7(47), 29312–29320.*

195. Xie, Z., Gao, M., Lobo, A. O., & Webster, T. J. (2020). 3D Bioprinting in Tissue Engineering for Medical Applications: The Classic and the Hybrid. *Polymers*, *12(8), 1717.*

196. Kang, H.-W., Lee, S. J., Ko, I. K., Kengla, C., Yoo, J. J., & Atala, A. (2016). A 3D bioprinting system to produce human-scale tissue constructs with structural integrity. *Nature Biotechnology, 34(3), 312–319.*

197. Khalil, S., and Sun, W., (2007). Biopolymer Deposition for Freeform Fabrication of Hydrogel Tissue Constructs. *Materials Science and Engineering: C, 27(3) 469-478.*

198. Chang, R., Nam, J., and Sun, W., (2008). Effects of Dispensing Pressure and Nozzle Diameter on Cell Survival from Solid Freeform fabrication–based Direct Cell Writing. *Tissue Engineering Part A, 14(1) 41-48.*

199. Cao, Y., Zhou, L., Wang, X., (2009). MicroPen Direct-Write Deposition of Polyimide. *Microelectronic Engineering, 86(10) 1989-1993.*

200. Li, M., Tian, X., Schreyer, D. J., (2011). Effect of Needle Geometry on Flow Rate and Cell Damage in the dispensing-based Biofabrication Process. *Biotechnology Progress, 27(6) 1777-1784.*

201. Martanto, W., Baisch, S. M., Costner, E. A., (2005). Fluid Dynamics in Conically Tapered Microneedles. *AIChE Journal, 51(6) pp. 1599-1607.*

202. Blaeser, A., Duarte Campos, D. F., Puster, U., Richtering, W., Stevens, M. M., & Fischer, H. (2015). Controlling Shear Stress in 3D Bioprinting is a Key Factor to Balance Printing Resolution and Stem Cell Integrity. *Advanced Healthcare Materials, 5(3), 326–333.*

203. N. Paxton, W. Smolan, T. Bock, F. Melchels, J. Groll, T. Jungst, (2017). Proposal to assess printability of bioinks for extrusion-based bioprinting and evaluation of rheological properties governing bioprintability. *Biofabrication 9 044107.*

204. M. Li, X. Tian, J.A. Kozinski, X. Chen, D.K. Hwang, (2015). Modeling mechanical cell damage in the bioprinting process employing a conical needle. *J. Mech. Med. Biol. 15 1550073,*

205. Chang, R., Nam, J., & Sun, W. (2008). Effects of dispensing pressure and nozzle diameter on cell survival from solid freeform fabrication-based direct cell writing. *Tissue engineering. Part A*, *14*(1), 41–48.

206. Nair, K., Gandhi, M., Khalil, S., Yan, K. C., Marcolongo, M., Barbee, K., & Sun, W. (2009). Characterization of cell viability during bioprinting processes. *Biotechnology journal*, *4*(8), 1168–1177.

207. Liu, W., Heinrich, M. A., Zhou, Y., Akpek, A., Hu, N., Liu, X., Guan, X., Zhong, Z., Jin, X., Khademhosseini, A., & Zhang, Y. S. (2017). Extrusion Bioprinting of Shear-Thinning Gelatin Methacryloyl Bioinks. *Advanced healthcare materials*, *6*(12), 10.1002/adhm.201601451.

208. Cidonio, G., Glinka, M., Dawson, J.I., & Oreffo, R.O.C. (2019). The cell in the ink: Improving biofabrication by printing stem cells for skeletal regenerative medicine. *Biomaterials, (), S0142961219302200.*

209. Polymer Properties Data. Flow Properties of Polymers. Time-Independent Fluids. (2015). Polymer data base. https://polymerdatabase.com/polymer%20physics/Viscosity2.html

210. Malvern Instruments Worldwide (2016). *A Basic Introduction to Rheology* (PDF). https://cdn.technologynetworks.com/TN/Resources/PDF/WP160620BasicIntroRheology.pdf

211. Xu, C., Zhang, M., Huang, Y., Ogale, A., Fu, J., & Markwald, R. R. (2014). Study of Droplet Formation Process during Drop-on-Demand Inkjetting of Living Cell-Laden Bioink. *Langmuir, 30(30), 9130–9138.*

212. L. Ouyang, R. Yao, Y. Zhao, W. Sun, (2016). Effect of bioink properties on printability and cell viability for 3D bioplotting of embryonic stem cells, *Biofabrication 8, 035020,*

213. Hölzl, K., Lin, S., Tytgat, L., Van Vlierberghe, S., Gu, L., & Ovsianikov, A. (2016). Bioink properties before, during and after 3D bioprinting. *Biofabrication, 8*(3), 032002.

214. Osti, G., Wolf, F., and Philippi, P., (2009). Spreading of liquid drops on acrylic surfaces. *Proceedings of the 20th International Congress of Mechanical Engineering, International Congress of Mechanical Engineering, Gramado, RS, Brazil.*

215. Chang, B., Nave, G., and Jung, S., (2012). Drop Formation from a Wettable Nozzle. *Communications in Nonlinear Science and Numerical Simulation, 17(5) 2045-2051*

216. Li, Q., and Lewis, J. A., (2003). Nanoparticle Inks for Directed Assembly of Three-Dimensional Periodic Structures. *Advanced Materials, 15(19) 1639-1643.*

217. Smay, J. E., Gratson, G. M., Shepherd, R. F., (2002). Directed Colloidal Assembly of 3D Periodic Structures. *Advanced Materials, 14(18) 1279-1283.*

218. Vozzi, G., Previti, A., De Rossi, D., (2002). Microsyringe-Based Deposition of Two-Dimensional and Three- Dimensional Polymer Scaffolds with a Well-Defined Geometry for Application to Tissue Engineering, *Tissue Engineering, 8(6) 1089-1098*

219. Choi, I. H., & Kim, J. (2016). A pneumatically driven inkjet printing system for highly viscous microdroplet formation. *Micro and Nano Systems Letters, 4(1).*

220. Wang, J., and Shaw, L. L., (2005). Rheological and Extrusion Behavior of Dental Porcelain Slurries for Rapid Prototyping Applications. *Materials Science and Engineering: A, 397(1) 314-321.*

221. Cao, Y., Zhou, L., Wang, X., (2009). MicroPen Direct-Write Deposition of Polyimide. *Microelectronic Engineering, 86(10) 1989-1993.*

222. Li, B., Clark, P. A., and Church, K., (2007). Robust direct-write dispensing tool and solutions for micro/meso- scale manufacturing and packaging. *ASME 2007 International Manufacturing Science and Engineering Conference, Anonymous American Society of Mechanical Engineers, pp. 715-721.*

223. Stanley, M., (1995) Modeling Axisymmetric Flows Dynamics of Films, Jets, and Drops. *Academic Press, San Diego.*

224. Bos, F., Wolfs, R., Ahmed, Z., (2016). Additive Manufacturing of Concrete in Construction: Potentials and Challenges of 3D Concrete Printing. *Virtual and Physical Prototyping, 11(3) 209-225.*

225. Jin, Y., Zhao, Z., Danyang, and Huang, Y., (2018) Study of Extrudability and Standoff Distance Effect during Nanoclay. *Enabled Direct Printing, 1(2) 123-134.*

226. Li, B., Clark, P. A., and Church, K., (2007), Robust direct-write dispensing tool and solutions for micro/meso- scale manufacturing and packaging, *ASME 2007 International Manufacturing Science and Engineering Conference, Anonymous American Society of Mechanical Engineers, pp. 715-721.*

227. S. Sakai, K. Hirose, K. Taguchi, Y. Ogushi, and K. Kawakami, (2009). An injectable, in situ enzymatically gellable, gelatin derivative for drug delivery and tissue engineering, *Biomaterials, 30 (20), 3371–3377.*

228. X. Z. Shu, Y. Liu, Y. Luo, M. C. Roberts, and G. D. Prestwich, (2002). Disulfide Cross-Linked Hyaluronan Hydrogels. *Biomacromolecules, v3(6), 1304–1311.*

229. Darr & Calabro, A. (2009). Synthesis and characterization of tyramine-based hyaluronan hydrogels. *J. Mater. Sci. Med., 20(1), 33–44.*

230. Kurisawa, M., Chung, J. E., Yang, Y. Y., Gao, S. J., & Uyama, H. (2005). Injectable biodegradable hydrogels composed of hyaluronic acid-tyramine conjugates for drug delivery and tissue engineering. *Chem. Commun., 4312-4314.*

231. Sanmartín-Masiá, E., Poveda-Reyes, S., & Gallego, G. (2017). Extracellular matrix-inspired gelatin/hyaluronic acid injectable hydrogels. *Int. J. Polym. Mater. Po., 66(6), 280-88.*

232. Becker, J., Lu, L., Runge, M.B., Zeng, H., Yaszemski, M.J., & Dadsetan, M. (2015) Nanocomposite bone scaffolds based on biodegradable polymers and hydroxyapatite, *Journal of Biomedical Materials Research 103 2549-2557.*

233. Isikli, C., Hasirci, V., & Hasirci, N. (2012). Co-culture in cartilage tissue engineering. *Journal of Tissue Engineering and Regenerative Medicine, 6, 135–143.*

234. Bohidar, H. B. (1998). Hydrodynamic properties of gelatin in dilute solutions. *International Journal of Biological Macromolecules, 23(1), 1–6.*

235. Baier Leach, J., Bivens, K. A., Patrick Jr., C. W., & Schmidt, C. E. (2003). Photocrosslinked hyaluronic acid hydrogels: Natural, biodegradable tissue engineering scaffolds. *Biotechnology and Bioengineering, 82(5), 578–589.*

236. Orme, N., M, R., & Phillips, R. (2016). Cell biology by the numbers. *In Choice Reviews Online Vol. 53, 53-4367-53–4367.*

237. Sidorenko, A., Krupenkin, T., Taylor, A., Fratzl, P., & Aizenberg, J. (2007). Reversible switching of hydrogel-actuated nanostructures into complex micropatterns. *Science (New York, N.Y.), 315*(5811), 487–490.

238. Kobayashi, S., Uyama, H., & Kimura, S. (2001). Enzymatic Polymerization. *Chemical Reviews, 101(12), 3793–3818.*

239. Park, K. M., Shin, Y. M., Joung, Y. K., Shin, H., & Park, K. D. (2010). In Situ Forming Hydrogels Based on Tyramine Conjugated 4-Arm-PPO-PEO via Enzymatic Oxidative Reaction. *Biomacromolecules, 11(3), 706–712.*

240. Baynton, K. J., Bewtra, J. K., Biswas, N., & Taylor, K. E. (1994). Inactivation of horseradish peroxidase by phenol and hydrogen peroxide: a kinetic investigation. *Biochimica et Biophysica Acta (BBA). Protein Structure and Molecular Enzymology, 1206(2), 272–278.*

241. Anghileri, A., Lantto, R., Kruus, K., Arosio, C., & Freddi, G. (2007). Tyrosinase-catalyzed grafting of sericin peptides onto chitosan and production of protein-polysaccharide bioconjugates. *Journal of biotechnology*, *127*(3), 508–519.

242. hen, T., Embree, H. D., Brown, E. M., Taylor, M. M., & Payne, G. F. (2003). Enzyme-catalyzed gel formation of gelatin and chitosan: potential for in situ applications. *Biomaterials*, *24*(17), *2831–2841.*

243. Yamamoto, H., Kuno, S., Nagai, A., Nishida, A., Yamauchi, S., & Ikeda, K. (1990). Insolubilizing and adhesive studies of water-soluble synthetic model proteins. *International journal of biological macromolecules*, *12*(5), *305–310.*

244. Jones, M. E., & Messersmith, P. B. (2007). Facile coupling of synthetic peptides and peptide-polymer conjugates to cartilage via transglutaminase enzyme. *Biomaterials*, *28*(35), *5215–5224.*

245. Hall, H., Baechi, T., & Hubbell, J. A. (2001). Molecular properties of fibrin-based matrices for promotion of angiogenesis in vitro. *Microvascular research*, *62*(3), *315–326.*

246. Teixeira, L. S., Feijen, J., van Blitterswijk, C. A., Dijkstra, P. J., & Karperien, M. (2012). Enzyme-catalyzed crosslinkable hydrogels: emerging strategies for tissue engineering. *Biomaterials, 33(5), 1281–1290.*

247. Sakurada, J., Sekiguchi, R., Sato, K., & Hosoya, T. (1990). Kinetic and molecular orbital studies on the rate of oxidation of monosubstituted phenols and anilines by horseradish peroxidase compound II. *Biochemistry*, *29*(17), 4093–4098.

248. Wang, X., Ao, Q., Tian, X., Fan, J., Tong, H., Hou, W., & Bai, S. (2017). Gelatin-Based Hydrogels for Organ 3D Bioprinting. *Polymers*, *9*(9), 401.

249. Irvine, S. A., Agrawal, A., Lee, B. H., Chua, H. Y., Low, K. Y., Lau, B. C., Machluf, M., & Venkatraman, S. (2015). Printing cell-laden gelatin constructs by free-form fabrication and enzymatic protein cross-linking. *Biomedical microdevices, 17(1), 16.*

250. Whulanza, Y., Arsyan, R., & Saragih, A. (2018). Characterization of hydrogel printer for direct cell-laden scaffolds. *AIP Conference Proceedings. 1933. 040002.*

251. Tong, A., Pham, Q. L., Abatemarco, P., Mathew, A., Gupta, D., Iyer, S., & Voronov, R. (2021). Review of Low-Cost 3D Bioprinters: State of the Market and Observed Future Trends. *SLAS technology, 26(4), 333–366.*

252. CELLINK (2021) *Bio X 3D bioprinter.* Acccessed on 20 September 2021 https://www.cellink.com/bioprinting/bio-x-3d-bioprinter/

253. Ostrovidov, S., Franck, P., Capiaumont, J., Dousset, B., & Belleville, F. (1998). Effects of H2O2 on the growth, secretion, and metabolism of hybridoma cells in culture. In vitro cellular & developmental biology. *Animal, 34(3), 259–264.*

254. Suzuki, Y. J., Forman, H. J., & Sevanian, A. (1997). Oxidants as stimulators of signal transduction. *Free radical biology & medicine, 22(1-2), 269–285.*

255. Herbert, J. M., Bono, F., & Savi, P. (1996). The mitogenic effect of H2O2 for vascular smooth muscle cells is mediated by an increase of the affinity of basic fibroblast growth factor for its receptor. *FEBS letters, 395(1), 43–47.*

256. Burdon, R. H., Alliangana, D., & Gill, V. (1995). Hydrogen peroxide and the proliferation of BHK-21 cells. *Free radical research, 23(5), 471–486.*

257. Burdon R. H. (1995). Superoxide and hydrogen peroxide in relation to mammalian cell proliferation. *Free radical biology & medicine, 18(4), 775–794.*

258. Gülden, M., Jess, A., Kammann, J., Maser, E., & Seibert, H. (2010). Cytotoxic potency of H2O2 in cell cultures: impact of cell concentration and exposure time. *Free radical biology & medicine, 49(8), 1298–1305.*

259. Ohguro, N., Fukuda, M., Sasabe, T., et al. (1999). Concentration dependent effects of hydrogen peroxide on lens epithelial cells. *British Journal of Ophthalmology 83:1064-1068.*

260. Suchaoin, W., & Chanvorachote, P. (2012). Caveolin-1 attenuates hydrogen peroxide-induced oxidative damage to lung carcinoma cells. *Anticancer research, 32(2), 483–490.*

261. Tochigi, M., Inoue, T., Suzuki-Karasaki, M., Ochiai, T., Ra, C., & Suzuki-Karasaki, Y. (2013). Hydrogen peroxide induces cell death in human TRAIL-resistant melanoma through intracellular superoxide generation. *International Journal of Oncology, 42, 863-872.*

262. Wang, D., Wang, Y., Xu, S., Wang, F., Wang, B., Han, K., Sun, D., & Li, L. (2016). Epigallocatechin-3-gallate Protects against Hydrogen Peroxide-Induced Inhibition of Osteogenic Differentiation of Human Bone Marrow-Derived Mesenchymal Stem Cells. *Stem Cells International. 2016. 1-10.*

263. Ramanauskiene, K., & Stelmakiene, A., & Majiene, D. (2015). Assessment of Lemon Balm (Melissa officinalis L.) Hydrogels: Quality and Bioactivity in Skin Cells. *Evidence-Based Complementary and Alternative Medicine. 2015.*

264. Holbrook, N. J., & Ikeyama, S. (2002). Age-related decline in cellular response to oxidative stress: links to growth factor signaling pathways with common defects. *Biochemical pharmacology, 64(5-6), 999–1005.*

265. Miyoshi, N., Oubrahim, H., Chock, P. B., & Stadtman, E. R. (2006). Age-dependent cell death and the role of ATP in hydrogen peroxide-induced apoptosis and necrosis. *Proceedings of the National Academy of Sciences of the United States of America, 103(6), 1727–1731.*

266. Whang, W. K., Park, H. S., Ham, I., Oh, M., Namkoong, H., Kim, H. K., Hwang, D. W., Hur, S. Y., Kim, T. E., Park, Y. G., Kim, J. R., & Kim, J. W. (2005). Natural compounds,fraxin and chemicals structurally related to fraxin protect cells from oxidative stress. *Experimental & molecular medicine, 37(5), 436–446.*

267. Lisanti, M. P., Martinez-Outschoorn, U. E., Lin, Z., Pavlides, S., Whitaker-Menezes, D., Pestell, R. G., Howell, A., & Sotgia, F. (2011). Hydrogen peroxide fuels aging, inflammation, cancer metabolism and metastasis: the seed and soil also needs "fertilizer". *Cell cycle (Georgetown, Tex.), 10(15), 2440–2449.*

268. Frippiat, C., Chen, Q. M., Zdanov, S., Magalhaes, J. P., Remacle, J., & Toussaint, O. (2001). Subcytotoxic H2O2 stress triggers a release of transforming growth factor-beta

1, which induces biomarkers of cellular senescence of human diploid fibroblasts. *The Journal of biological chemistry, 276(4), 2531–2537.*

269. Frippiat, C., Dewelle, J., Remacle, J., & Toussaint, O. (2002). Signal transduction in H2O2-induced senescence-like phenotype in human diploid fibroblasts. *Free radical biology & medicine, 33(10), 1334–1346.*

270. Dimri, G. P., Lee, X., Basile, G., Acosta, M., Scott, G., Roskelley, C., Medrano, E. E., Linskens, M., Rubelj, I., & Pereira-Smith, O. (1995). A biomarker that identifies senescent human cells in culture and in aging skin in vivo. *Proceedings of the National Academy of Sciences of the United States of America, 92(20), 9363–9367.*

271. Kiyoshima, T., Enoki, N., Kobayashi, I., Sakai, T., Nagata, K., Wada, H. ... Sakai, H. (2012). Oxidative stress caused by a low concentration of hydrogen peroxide induces senescence-like changes in mouse gingival fibroblasts. *International Journal of Molecular Medicine, 30, 1007-1012.*

272. Burdon, R. H., Gill, V., & Alliangana, D. (1996). Hydrogen peroxide in relation to proliferation and apoptosis in BHK-21 hamster fibroblasts. *Free radical research, 24(2), 81–93.*

273. Wiese, A. G., Pacifici, R. E., & Davies, K. J. (1995). Transient adaptation of oxidative stress in mammalian cells. *Archives of biochemistry and biophysics, 318(1), 231–240.*

274. Brenner, S., Gülden, M., Maser, E., & Seibert, H. (2010). Lasting effect of preceding culture conditions on the susceptibility of C6 cells to peroxide-induced oxidative stress. Toxicol. Vitro doi:10.1016/j.tiv.2010.06.005.

275. Leist, M., Raab, B., Maurer, S., Rösick, U., & Brigelius-Flohé, R. (1996). Conventional cell culture media do not adequately supply cells with antioxidants and thus facilitate peroxide-induced genotoxicity. *Free Radic. Biol. Med. 21:297–306*

276. Sasaki, K., Bannai, S., & Makino, N. (1998). Kinetics of hydrogen peroxide elimination by human umbilical vein endothelial cells in culture. *Biochim. Biophys. Acta 1380:275–288*

277. Andrae, U., Singh, J., & Ziegler-Skylakakis, K. (1985). Pyruvate and related α-ketoacids protect mammalian cells in culture against hydrogen peroxide-induced cytotoxicity. *Toxicol. Lett. 28:93–98*

278. Carballal, S., Radi, R., Kirk, M. C., Barnea, S., Freeman, B. A., & Alvarez, B. (2003). Sulfenic acid formation in human serum albumin by hydrogen peroxide and peroxinitrite. *Biochemistry 42:9906–9914*

279. Yu, C. J., Ko, C. J., Hsieh, C. H., Chien, C. T., Huang, L. H., Lee, C. W., & Jiang, C. C. (2014). Proteomic analysis of osteoarthritic chondrocyte reveals the hyaluronic acid-regulated proteins involved in chondroprotective effect under oxidative stress. *Journal of proteomics, 99, 40–53*

280. Yoon, B., Kim, Y.-H., Lee, J.-S., Hong, H.-D., Rhee, Y. K., Cho, C.-W., Kim, Y.-C., & Lee, O.-H. (2013). Protective Effect of Ferments of Hot-water Extract Mixture from Rhodiola sachalinensis and Red Ginseng on Oxidative Stress-induced C2C12 Myoblast. *The Korean Journal of Food And Nutrition. 26.*

281. Nakanishi, T., Tsujii, M., Asano, T., Iino, T., & Sudo, A. (2020). Protective Effect of Edaravone Against Oxidative Stress in C2C12 Myoblast and Impairment of Skeletal Muscle Regeneration Exposed to Ischemic Injury in Ob/ob Mice. *Frontiers in Physiology, 10(), 1596–.*

282. Yoshikawa, M., & Hosokawa, M., & Miyashita, K., & Fujita, T., & Nishino, H., & Hashimoto, T. (2020). Fucoxanthinol attenuates oxidative stress-induced atrophy and loss in myotubes and reduces the triacylglycerol content in mature adipocytes. *Molecular Biology Reports. 47.*

283. Li, J., Yang, Q., Han, L., Pan, C., Lei, C., Chen, H., & Lan, X. (2020). C2C12 Mouse Myoblasts Damage Induced by Oxidative Stress Is Alleviated by the Antioxidant Capacity of the Active Substance Phloretin. *Frontiers in Cell and Developmental Biology, 8(), 541260–.*

284. Kim H, Lee KI, Jang M, Namkoong S, Park R, Ju H, et al. (2016) Conessine Interferes with Oxidative Stress-Induced C2C12 Myoblast Cell Death through Inhibition of Autophagic Flux. *PLOS ONE 11(6): e0157096.*

285. Lee, J.-H., Jung, M.-H., Lee, Y.-H., Shin, Y., Kim, H.-S., Schreiber, J., Kim, T.-J. (2013). Inhibited Apoptosis of C2C12 Myoblasts by a Eupatorium chinense var. simplicifolium Root Extract. Bioscience, *Biotechnology and Biochemistry, 77(10), 2134–2136.*

286. Hongpaisan, J., & Roomans, G. M. (1999). Retaining ionic concentrations during in vitro storage of tissue for microanalytical studies. *Journal of Microscopy. 193 (3): 257–267.*

287. Sato, Y., Yamada, S., Takeda, S., Hattori, N., Nakamura, K., Tanaka, H., Mizuno, M., Hori, M., & Kodera, Y. (2018). Effect of Plasma-Activated Lactated Ringer's Solution on Pancreatic Cancer Cells In Vitro and In Vivo. *Annals of Surgical Oncology. 25 (1): 299–307.*

288. Esen, Z., Dikici, B., Duygulu, O., & Dericioglu, A. F. (2013). Titanium–magnesium based composites: Mechanical properties and in-vitro corrosion response in Ringer's solution. *Materials Science and Engineering: A. 573: 119–126.*
289. Rodríguez Fernández, J. (2021). Development of biomimetic injectable hydrogels for hepatic cell culture. pp 61-62.
290. Ozbolat, I.T. and Yu, Y. (2013). Bioprinting toward organ fabrication: challenges and future trends. *IEEE Trans. Biomed. Eng. 60,691–699*
291. Suntornnond, R., An, J., & Chua, C. K. (2017). Roles of support materials in 3D bioprinting—Present and future. *Int. J. Bioprinting 3(1), 83–86.*
292. Shapira, A., Noor, N.,. Asulin, M,. & Dvir, T. (2018). Stabilization strategies in extrusion-based 3D bioprinting for tissue engineering. *Applied Physics Reviews, 5(4), 041112*
293. Klouda, L. & Mikos, A. G. (2008). Thermoresponsive hydrogels in biomedical applications. *Eur. J. Pharm. Biopharm. 68(1), 34–45.*
294. Ratima, S., Jia, A. & Kai, C. C. (2017). Bioprinting of thermoresponsive hydrogels for next generation tissue engineering: A review. *Macromol. Mater. Eng. 302(1), 1600266.*
295. Dumortier, G., Grossiord, J. L., Agnely, F., & Chaumeil, J. C. (2006). A review of poloxamer 407 pharmaceutical and pharmacological characteristics. *Pharm. Res. 23(12), 2709–2728.*
296. Malikmammadov, E., Tanir, T. E., Kiziltay, A., Hasirci, V., & Hasirci, N. (2018). PCL and PCL-based materials in biomedical applications. Journal of biomaterials science. Polymer edition, 29(7-9), 863–893.
297. Woodruff, M. A. & Hutmacher, D. W. (2010). The return of a forgotten polymer—Polycaprolactone in the 21st century. *Prog. Polym. Sci. 35(10), 1217–1256.*
298. Lee, J. M., & Yeong, W. Y. (2016). Design and Printing Strategies in 3D Bioprinting of Cell-Hydrogels: A Review. *Advanced healthcare materials, 5(22), 2856–2865.*
299. LeRoux, M. A., Guilak, F., & Setton, L. A. (1999). Compressive and shear properties of alginate gel: effects of sodium ions and alginate concentration. *Journal of biomedical materials research, 47(1), 46–53.*
300. Carrow, JK, Kerativitayanan, P., Jaiswal, M.K., Lokhande, G., & Gaharwar, AK. (2015). Polymers for bioprinting. *In: Yoo JJ, Atala A, eds. Essentials of 3D Biofabrication and Translation. Academic Press; 229-248.*
301. Kang, H.W., Lee, S., Ko, I. et al. (2016). A 3D bioprinting system to produce human-scale tissue constructs with structural integrity. *Nat Biotechnol 34, 312–319*

302. Aydin, L, Kucuk, S, & Kenar, H. (2020). A universal self-eroding sacrificial bioink that enables bioprinting at room temperature. *Polym Adv Technol. 31: 1634– 1647*
303. Dranseikiene, D., Schrüfer, S., Schubert, D.W. et al. (2020). Cell-laden alginate dialdehyde–gelatin hydrogels formed in 3D printed sacrificial gel. *J Mater Sci: Mater Med 31, 31.*
304. Ahlfeld, T., Köhler, T., Czichy, C., Lode, A., & Gelinsky, M. (2018). A Methylcellulose Hydrogel as Support for 3D Plotting of Complex Shaped Calcium Phosphate Scaffolds. *Gels, 4(3), 68.*
305. Schütz, K., Placht, A. M., Paul, B., Brüggemeier, S., Gelinsky, M., & Lode, A. (2017). Three-dimensional plotting of a cell-laden alginate/methylcellulose blend: towards biofabrication of tissue engineering constructs with clinically relevant dimensions. *Journal of tissue engineering and regenerative medicine, 11(5), 1574–1587.*
306. Lemos, F. O., Florentino, R. M., Lima Filho, A., Dos Santos, M. L., & Leite, M. F. (2019). Inositol 1,4,5-trisphosphate receptor in the liver: Expression and function. *World journal of gastroenterology, 25(44), 6483–6494.*
307. Tamaddon, M., Gilja, H., Wang, L., Oliveira, J.M, Sun, X., Tan, R., & Liu, C. (2020). Osteochondral scaffolds for early treatment of cartilage defects in osteoarthritic joints: from bench to clinic. *Biomaterials Translational 1(1), 3-17.*
308. Kilian, D., Ahlfeld, T., Akkineni, A.R. et al. (2020). 3D Bioprinting of osteochondral tissue substitutes – in vitro-chondrogenesis in multi-layered mineralized constructs. *Sci Rep 10, 8277.*
309. Berruto, M., Delcogliano, M., de Caro, F., Carimati, G., Uboldi, F., Ferrua, P., Ziveri, G., & De Biase, C. F. (2014). Treatment of large knee osteochondral lesions with a biomimetic scaffold: results of a multicenter study of 49 patients at 2-year follow-up. *Am J Sports Med. 42, 1607-1617.*
310. Nagarajan, Muralidharan; Benjakul, Soottawat; Prodpran, Thummanoon; Songtipya, Ponusa (2013). Effects of bleaching on characteristics and gelling property of gelatin from splendid squid (Loligo formosana) skin. Food Hydrocolloids, 32(2), 447–452.
311. Hongyue Chen,Jing Qin andYi Hu. (2019). Efficient Degradation of High-Molecular-Weight Hyaluronic Acid by a Combination of Ultrasound, Hydrogen Peroxide, and Copper Ion. Molecules 2019, 24(3), 617
312. Chang, K. L., Tai, M. C., & Cheng, F. H. (2001). Kinetics and products of the degradation of chitosan by hydrogen peroxide. Journal of agricultural and food chemistry, 49(10), 4845–4851.

313. Mubarok, W., Qu, Y., & Sakai, S. (2021). Influence of Hydrogen Peroxide-Mediated Cross-Linking and Degradation on Cell-Adhesive Gelatin Hydrogels. ACS Applied Bio Materials, 4(5), 4184–4190.